HOLLOW STRUCTURAL SECTIONS IN FLEXURE

HOLLOW STRUCTURAL SECTIONS IN FLEXURE

by

Janardan Prasad, B.Sc. (Hons.)

A Thesis

Submitted to the Faculty of Graduate Studies

in Partial Fulfilment of the Requirements

for the Degree

Master of Engineering

McMaster University

1972

MASTER OF ENGINEERING
(Civil Engineering)

McMASTER UNIVERSITY
Hamilton, Ontario

TITLE: HOLLOW STRUCTURAL SECTIONS IN FLEXURE

AUTHOR: Janardan Prasad, B.Sc. (Hons.) (Banaras Hindu University)

SUPERIVSOR: Dr. Robert M. Korol

NUMBER OF PAGES: xii, 146

SCOPE AND CONTENTS:

A research programme is presented for assessing the capability of Hollow Structural Sections for design in flexure. This investigation is the continuation of earlier work on the topic which provided guidelines primarily for rectangular sections with relatively low flange slenderness. The present work attempts to relate the tube slenderness and yield strength to the rotation capacity and moment resistance of round sections subjected to bending moment. Also an attempt is made to establish similar guidelines for rectangular sections with relatively high flange slenderness.

An experimental programme on 16 different sections was performed to evaluate the moment-curvature relationship which is of fundamental importance in flexural design. The occurrence of local buckling in compression flange and the consequent reduction in moment resistance is the critical factor which separates the sections into the categories governed by allowable stress or plastic method of design.

An attempt is made to develop an analytical method to determine the critical buckling stress for round sections subjected to pure moment in the inelastic range.

The experimental results are compared with the analytical predictions. Finally a design criterion to separate the sections into the design categories is established.

ACKNOWLEDGEMENTS

I wish to express my deepest gratitude to Dr. R. M. Korol for his advice and patience during the course of this thesis work. Also, I would like to thank Mr. Larry Ife for his time spent in discussions concerning this problem.

This investigation was made possible through the financial assistance of Comite International pour le Developpement et l'etude de la Construction Tubulaire (CIDECT) with direct motivation of the Steel Company of Canada, to whom I extend my sincere thanks.

TABLE OF CONTENTS

		Page
CHAPTER 1	INTRODUCTION	
	1.1 Preliminary Remarks	1
	1.2 Design Methods and Limitations	2
	1.3 Literature Review	5
	1.4 Current Work	8
CHAPTER 2	ANALYTICAL FORMULATION OF TUBE-TYPE BEAMS	11
	2.1 Introduction	11
	2.2 Prediction of the Moment-Curvature and Load-Deflection Relationship	11
	2.2.1 Elastic Analysis	11
	2.2.2 Plastic Analysis	12
	2.3 Inelastic Instability of Tubular Beams in Pure Bending	17
	2.3.1 The Co-ordinate System and Basic Assumptions	18
	2.3.2 Plasticity Considerations	19
	2.3.3 Equilibrium Considerations	24
	2.3.4 Computational Procedure and Results	37
CHAPTER 3	EXPERIMENTAL PROGRAM	54
	3.1 Testing Material	54
	3.2 Material Properties	54
	3.3 Preparation for Testing of Beam	55
	3.4 Testing Arrangement	57
	3.5 Testing Procedure	58

		Page
CHAPTER 4	EXPERIMENTAL RESULTS AND DISCUSSION	78
	4.1 Preliminaries	78
	4.2 Performance of Rectangular Sections	78
	4.2.1 Design Criteria	80
	4.2.2 Design Supplement on the Basis of Minimum Guaranteed Strength	81
	4.3 Performance of Round Sections	81
	4.3.1 Comparison Between Theoretical and Experimental Buckling	83
	4.3.2 Limitations of the Theory	84
	4.3.3 Design Criteria	85
	4.3.4 Comparison with CSA Specifications	87
	4.3.5 Comparison with Other Relevant Work	88
CHAPTER 5	CONCLUSIONS AND SUGGESTIONS FOR FURTHER RESEARCH	118
	5.1 Rectangular Sections	118
	5.2 Round Sections	118
	5.3 Suggestions for Further Research	120
APPENDIX 1	DISPLACEMENT EQUATIONS	122
APPENDIX 2	DESCRIPTION OF COMPUTER PROGRAM FOR EVALUATION OF LIMITING D/T RATIOS	129
	A.2.1 Introduction	129
	A.2.2 Designations	130
	A.2.3 Flow-charts	133
	A.2.4 Computer Program	137
BIBLIOGRAPHY		143

LIST OF FIGURES

Figure	Title	Page
1.1	Stress-Strain Relationship	10
1.2	Moment-Curvature Relationship	10
2.1	Simple Span Beam	43
2.2	Two Span Beam	43
2.3	Deflection at Collapse	44
2.4	Load Deflection Curve - Two Span Beam	44
2.5	Cylindrical Shell under Bending	45
2.6	Displacement Co-ordinates	46
2.7	Stub Columns after Test	47
2.8	Idealised Stress-Strain Relationships	48
2.9	Theoretical Results	53
3.1	Hollow Structural Section	60
3.2	Typical Stress-Strain Curve	60
3.3	Coupon Test Results	62
3.4	Bearing Surface of HSS on Load Points	68
3.5	Details of Loading - Simple Span	69
3.6	Details of Loading - Two Span	70
3.7	Details of Test Arrangement - Two Span Beam	71
3.8	Simple Span Test - HSS 6.625 O.D.X 0.156	72
3.9	Simple Span Test - HSS 10.75 O.D.X 0.219	74
3.10	Two Span Test - HSS 4.5 O.D.X 0.156	76
4.1	Results of Test No. (1a)	90
4.2	Results of Test No. (2a)	91

Figure	Title	Page
4.3	Results of Test No. (3a)	92
4.4	Results of Test No. (4a)	93
4.5	Results of Test No. (5a)	94
4.6	Results of Test No. (6a)	95
4.7	Results of Test No. (7a)	96
4.8	Results of Test No. (8a)	97
4.9	Design Criteria	99
4.10	Rotation Capacities	100
4.11	Design Curves; σ_{0G} = 55 KSI	103
4.12	Design Curves; σ_{0G} = 50 KSI	104
4.13	Results of Test No. (1b)	105
4.14	Results of Test No. (2b)	106
4.15	Results of Test No. (3b)	107
4.16	Results of Test No. (4b)	108
4.17	Results of Test No. (5b)	109
4.18	Results of Test No. (6b)	110
4.19	Results of Test No. (7b)	111
4.20	Results of Test No. (8b)	112
4.21	Two Span Beam - Test No. (1c)	113
4.22	Two Span Beam - Test No. (2c)	114
4.23	Design Criteria; σ_{0G} = 42 KSI	116
4.24	Design Criteria; σ_{0G} = 52 KSI	117

LIST OF TABLES

Table	Title	Page
2.1	Stability Criterion - Coarse Grid (8 terms)	49
2.2	Stability Criterion - Medium Grid (8 terms)	50
2.3	Stability Criterion - Fine Grid (8 terms)	51
2.4	Stability Criterion - Fine Grid (12 terms)	51
2.5	Theoretical Design Criteria	52
3.1	Material Properties Obtained From Tensile Coupons	61
4.1	Test Data - Rectangular Sections	98
4.2	Moment Ratios	102
4.3	Test Data - Round Sections	115
5.1	Limiting b/t Ratios for Rectangular Sections	121
5.2	Limiting D/t Ratios for Round Sections	121a

NOMENCLATURE

A_1, A_{12}, A_{13} A_2, A_{21}, A_{23} A_3, A_{31}, A_{32}	Plasticity coefficients
a_n	Constant coefficient of (n + 1)th term in the deflection function
B	Width of rectangular HSS
B_e	Axial rigidity (elastic) = $Et/(1 - \mu_e^2)$
B_p	Axial rigidity (plastic) = $Et/(1 - \mu_p^2)$
b	Flat flange width
D	Outside diameter of round HSS
D_e	Bending rigidity (elastic)= $\frac{Et^3}{12(1 - \mu_e^2)}$
D_p	Bending rigidity (plastic) = $\frac{Et^3}{12(1 - \mu_p^2)}$
E	Modulus of elasticity
E_{st}	Strain-hardening modulus
E_T	Tangent modulus
E_s	Secant modulus
F	A scalar function
f	Shape factor
K	Curvature
K_p	Elastic limit curvature based on an idealised elastic-plastic material
K_b	Total curvature at the inset of buckling
K_L	Maximum curvature at the level of M_p

k	Index in Ramberg-Osgood stress-strain relationship
L	Length of the tube
M	Applied moment
M_0	Yield moment
M_p	Plastic moment
M_u	Ultimate moment
M_x, M_y	Bending moment resultants on the shell element along x and y directions respectively
M_{xy}, M_{yx}	Twisting moments
M'_x, M'_y, M'_{xy}	Increments in M_x, M_y, M_{xy}, etc.
m	Number of longitudinal half waves
$\frac{m\pi R}{L}$	Buckle half wave-length parameter
N	Number of elements into which the cross-section of the tube is divided to perform numerical integration
N_x, N_y	Normal stress resultants along x and y directions respectively
N_{xy}, N_{yx}	Shear stress resultants
N'_x, N'_y, N'_{xy}	Increments in N_x, N_y, N_{xy}, etc.
n	An integar
P	Total load applied
P_e	Computed load to produce the specified deflection on the basis of elastic analysis
P_0	Yield load
P_u	Ultimate load
P_p	$= P_u - P_e$

p	Number of terms considered in the deflection function
Q, Q', Q''	Functional notations
q	An integar
q_1, q_2, etc.	Expressions in stability criterion
q'_{11}, q'_{12}, etc.	Expressions in stability criterion
R	Mean radius of the tube
R_x, R_y	Radii of curvature along x and y directions respectively
t	Thickness of the tube or rectangular section
u, v, w	Displacement co-ordinates along x, y and z directions respectively
x, y, z, θ	Co-ordinate system
Y, Y_1, Y_2	Expressions in stability criterion
α	$= \frac{3}{\sigma_i^2}(1 - E_T/E_s)$
α_1, α_2, etc.	Expressions in stability criterion
β_{11}, β_{12}, etc.	Elements of the determinant obtained by the stability criterion
γ	Shear strain
γ^{oct^p}	Plastic octahedral shear strain
δ	Deflection
δ_u	Deflection at $P = P_u$
δ_{2u}	Deflection at $P = P_u$, at point 2
δ_{2e}	Deflection at $P = P_e$, at point 2
δ_{2p}	$= \delta_{2u} - \delta_{2e}$
δ_0	Deflection at $P = P_0$
ϕ	Rotation

ϕ_H	Hypothetical elastic rotation
Φ	Loading function in plastic region
$d\Phi$	Increment in Φ
Ω	A functional notation
∇^4	Operator $(\frac{\partial^2}{\partial x^2} + 2\frac{\partial^2}{\partial x \partial \theta} + \frac{\partial^2}{\partial \theta^2})^2$
ε_x, ε_y	Normal strains along x and y directions respectively
ε'_x, ε'_y, γ'	Increments in ε_x, ε_y and γ respectively
ε_c	Critical buckling strain in bending (along x-direction)
ε_{max}	Maximum bending strain (along x-direction)
ε^e_{ij}	Elastic part of the strain tensor
ε^p_{ij}	Plastic part of the strain tensor
ε_i	Incipient strain
σ_0	Yield strength
σ_x, σ_y	Normal stresses along x and y directions respectively
σ_{xy}, τ	Shear stress
$\sigma_{0.7}$	Stress point on the Ramberg-Osgood stress-strain curve when $E_s = 0.7\ E$
σ_c	Critical buckling stress in compression
σ_{cb}	Critical buckling stress in bending
σ_p	Proportionality limit
χ'_x, χ'_y	Increments in curvature along x and y directions respectively
χ'_{xy}	Increment in twist

σ_x''	Trial value of σ_x for a given value of ε_x
ε_x''	Computed value of ε_x for the value of σ_x''
$\delta\sigma_x''$	Increment in σ_x''
$\delta\varepsilon_x''$	Increment in ε_x''
Δ	Determinant notation
Θ_b	Rotation capacity at the inset of buckling
Θ	Actual rotation capacity

CHAPTER 1

INTRODUCTION

1.1 Preliminary Remarks

The present day construction in steel mainly consists of the use of conventional rolled shapes such as wide flange or I-sections. The introduction of hollow structural sections in this segment of the industry has some definite advantages over the conventional shapes; a few of the pluses relate to fireproofing, corrosion-resistance and aesthetic appearance. In Canada, they are manufactured by the Steel Company of Canada, Limited and are available in rectangular, square and round shapes.

At present the costs[30] of steel office buildings and reinforced concrete buildings - both in the 25-storey range - are so close that a 5% difference in cost would definitely favour the less expensive type. In estimating the cost of steel construction, two general items of cost are of major importance: the steel members used including detailing, fabrication, erection and painting; and the cost of protecting steel from fire. A considerable advantage of reinforced concrete construction over steel is the adequacy of meeting fireproofing requirements. In a number of structures such as columns the extra thickness of concrete necessary to protect the reinforcing steel contributes to the strength of the structure, whereas in the case of steel, the fireproof coating is, in fact, a penalty due to its dead weight. Replacing the conventional shapes by hollow structural sections will eventually result in a reduced amount of fireproofing due to their comparatively small area of exposure. An example illustrating the use of

HSS to reduce cost of fireproofing is the U.S. Steel Building in Pittsburg. The design makes use of the inside space of the hollow structural sections for circulating water. This provision considerably reduces the initial cost of the heating system of the building and of course, the very important factor of fireproofing.

As stated above, since the area of exposure of hollow structural sections is comparatively less than that of the conventional shapes, the provision of corrosion resistance will result in comparatively lower cost.

The use of this new shape has introduced a new phase of aesthetic appearance in steel construction as observed in a number of completed structures such as Ontario Place and Sheridan College (which makes use of the untampered surface).

The design of a member in most structures is governed, either by direct stresses, bending stresses, or a combination of both which are induced by the specified load of occupancy. As a column, the rectangular or round hollow structural sections are definitely superior to the conventional shapes due to their substantial torsional rigidities. This torsional rigidity also plays its role in the beam behaviour since lateral buckling is rarely significant. For the design of compression or tension members the present day methods are considered to be adequate. The beam behaviour of hollow structural sections definitely needs to be investigated and the current work is confined to this area.

1.2 Design Methods and Limitations

The elastic method of design is based on the concept of a specified safety factor against nominal yielding of the most highly stressed fibres. For the detailed design employing HSS this method is adequate if the yield stress is reached without premature local buckling. Allowable stress design

which is based solely on a yield point criterion does not give a consistent margin of safety against failure, however. Present day codes[1, 2] attempt in part to take into account properties of the cross-section and continuity of the structure but still fall short of complete consistency.

Plastic design proposes to base the design on the actual load carrying capacity of the structure which usually renders the elastic method to be conservative. In building design working load is specified according to occupancy criteria. In general, it is a consistent percentage of the ultimate load. The ultimate load is realised only if the members undergo plastic deformation at a number of sections without significant local buckling. Such a condition could produce a significant reduction in bending moment resistance. This process is generally referred to as the redistribution of moments and formation of "plastic hinges".

Thus two necessary conditions must be satisified in plastic design:

(a) Redistribution of moments in an indeterminate structure when the plastic moment M_p is reached at the section of the first and subsequent hinges before collapse.

(b) Maintenance of the resisting moment M_p at a critical section until sufficient additional sections have yielded to form a mechanism.

When the plastic moment M_p is reached at the first hinge of an indeterminate structure, it is assumed that the relative rotations of the segments meeting the hinge can occur until sufficient additional sections have yielded to form a mechanism. This rotation for which the plastic moment needs to be maintained is called the "rotation capacity".

On the basis of the requirement of rotation capacity and yielding the cross-sections can be classified as follows:

(a) Plastic Design Sections - Sections which are capable of satisfying the minimum rotation requirement and the development and maintenance

of the fully pastic moment.

(b) Allowable Stress Design Sections

(i) Compact Sections - Sections which are capable of attaining the computed plastic moment without necessarily satisfying the minimum rotation requirement.

(ii) Non-compact Sections - Sections which are capable of attaining the computed yield moment M_o defined as that moment in which yielding of the outermost fibre is initiated.

(c) Reduced Stress Sections - Sections which buckle locally before they reach the computed yield moment.

The actual stress-strain curve* for cold-formed steel is shown in Figure 1.1. This curve may be idealised in two ways:

(a) Using bilinear segments with elastic modulus E and strain-hardening modulus E_{st}.

(b) Fitting a modified** Ramberg-Osgood[26] type of stress-strain relationship to the experimental curve.

For practical purposes the bilinear segment idealisation is often convenient whereas for theoretical determination of local buckling either idealisation may be used depending upon convenience of a mathematical formulation.

The simple plastic theory assumes the bilinear segments of the stress-strain curve with strain-hardening modulus $E_{st} = 0$, and the moment at the section remains constant after attaining a stress of $\pm \sigma_o$ in all elements of the section for all further increases in curvature. This assumed behaviour neglects the additional moment capacity due to the effect of strain-hardening but it is normally on the safe side and is often quite convenient for design purposes.

*In this investigation stress at yielding is generally based on a 0.5% total strain value.

**Even digit exponents will be permitted within the limitations necessary for the correctness of detailed computations.

Figure 1.2 shows a nondimensional plot of moment M/M_p vs curvature K/K_p. Curves (1), (2), (3) and (4) are based upon the simple plastic theory, the bilinear idealisation of the stress-strain curve, the Ramberg-Osgood stress-strain relationship and the experimentally observed moment-curvature relationship respectively for a compact section.

1.3 Literature Review

The ASCE "Commentary of Plastic Design in Steel"[2] assumes, for A36 steel beams designed by the plastic design method, that unloading does not occur until the plastic rotation (the total rotation minus the rotation at M_p) is at least three times the hypothetical rotation ϕ_H calculated by an elastic analysis with $M = M_p$. This is equivalent to the requirement that the minimum plastic rotation has to be at least three times the hypothetical rotation ϕ_H. The work done by Hudoba[3] on HSS recommends the minimum plastic rotation to be at least four times the hypothetical rotation ϕ_H and it is concluded that this value of minimum rotation requirement is satisfactory in plastic design of HSS beams.

A rational attempt has been made by Hudoba[3] for the determination of flange slenderness ratio b/t of rectangular HSS for the requirements of plastic design.

No successful attempts appear to have been made in the past to relate theoretically the local buckling of round tubular beams in the inelastic range, in pure bending.

In the elastic range the bending of circular tubes was first attempted by Brazier[4]. According to his theory the elastic curvature produced in the initially straight cylinder produces the well known phenomenon of the flattening of cross-sections of curved tubes under bending. The cross-section becomes more and more oval in shape until a point is reached at which the resistance to bending starts to decrease. Subsequently collapse

takes place. The critical buckling stress computed by Brazier is given by:

$$\sigma_{cb} = \frac{2}{9}\left(\frac{1}{1-\mu^2}\right)^{1/2} E$$

where μ is Poisson's ratio and E is the modulus of elasticity.

Donnell[5] in his investigation of compression and bending of cylindrical shells realised that, in the small deflection theory adopted by Brazier, the second order terms neglected, increase considerably with large deflections. The type of failure assumed by Brazier does take place in comparatively thick tubes especially those stressed beyond the yield point. It was concluded by Donnell that either the oval type (Brazier) or the small wave type (Donnell) is more or less an independent type of failure. In actual tubes failure is produced by whichever shape requires the least load. For design purposes Donnell recommends an empirical value of critical buckling stress in compression given by:

$$\sigma_c = E\,\frac{(0.6\ t/R - 10^{-7}\ R/t)}{(1 + 0.004\ E/\sigma_o)}$$

and the buckling stress in bending may rise to 1.4 times the value given above.

Donnell's classical work on the topic evolves two distinguished theories:

(a) Theory on assumption of perfect initial shape and infinitesimal displacements known as Small Deflection Theory.

(b) Theory considering initial displacement and finite deflections known as Large Deflection Theory.

These theories were quite difficult to work out and further simplifications and modifications were taken by Batdorf[8,9].

Flügge[6] investigated the problem under combined bending and compression in the elastic range and calculated an interaction curve for a particular radius thickness ratio given by:

$$[(1/12)(t^2/R^2) = 10^{-6}]$$

for a particular longitudinal buckle half wave-length parameter ($\frac{m\pi R}{L} = 1$). For this case the ratio between the maximum critical stress for bending alone was 1.3 times the critical stress for pure compression. The ratio of 1.3 was cited by Timoshenko[7] without a qualifying statement as to the assumed buckle half wave-length and has been a general rule ever since.

The paper of Suer ,Harris, Skene and Benjamin[10] deals with pressurized and unpressurized cylinders subjected to bending. A statistical analysis was made to fit the experimental results of Donnell[5], Imperial[11], Lundquist[12], Mossman and Robinson[13], and Peterson[14] and it was concluded that there is not a uniform ratio between the buckling coefficients over the complete range of D/t ratio. For low values of D/t the critical buckling stress in bending was about 60% greater than that for pure compression and this difference decreased with increasing D/t ratio to a value of about 25% for large D/t.

Seide and Weingarten[15] used the small deflection theory of Donnell modified by Batdorf. In their investigation it was clear that the critical buckling stress varied with longitudinal buckle half wave-length parameter $\frac{m\pi R}{L}$ for elastic buckling of a thin cylinder under bending. Also, it had a unique minima at a certain value of $\frac{m\pi R}{L}$. It was also pointed out that for thinner cylinders (D/t > 200) there was no significant difference between critical buckling stress either in bending or in compression (the critical buckling stress value in compression is for a moderately long cylinder).

For $\frac{m\pi R}{L} = 1$ the computations of Siede and Weingarten were fairly close to that of Flügge.

Yao[16] investigated the problem on the basis of oval type failure using Donnell's large deflection theory modified by Batdorf. He derived the (elastic) stability criterion on the principle of minimum potential energy. An elaborate comparison of existing theories (Brazier, Seide and Weingarten, and Yao) was made in this paper and for D/t ratio < 80, the large deflection theory gave slightly smaller values of critical buckling stress as compared to the small deflection theory.

Gerard[17, 18] formulated the stability theory for thin shells in the inelastic range, using the fundamental hypothesis of mechanics of plasticity. Employing small deflection theory with the modification of Batdorf he adopted the deformation theory of plasticity which utilized total stress-strain relations. Critical buckling stress coefficients for compression, radial pressure and torsion were derived. The theory took into account the total stress-strain history at the point considered which is basically a function of tangent modulus E_T and secant modulus E_s.

The bending experiments performed by Khaliq and Schilling[19] involved behaviour in the inelastic range and a limiting value of D/t ratio was recommended to attain the fully plastic moment. Premature local buckling as related to geometrical parameters was also described by Schilling[20].

1.4 Current Work

The present investigation is a study of the behaviour of HSS subjected to moment gradients and constant moment regimes. As mentioned earlier, the work done by Hudoba[3] provides a reasonable guideline for the design of rectangular HSS in the range of compact sections in allowable stress and plastic design. However, needs for further investigations were noted to

correlate the behaviour of rectangular HSS with flats of higher slenderness ratio than the compact section range. A number of such rectangular HSS were, therefore, included in the study. The present guidelines for design in the plastic range employing round sections still fall short of complete consistency and, therefore, a rational attempt is made to relate the tube slenderness ratio D/t to the rotation capacity of round HSS beams. Finally the analytical predictions are compared with the results of a series of experiments.

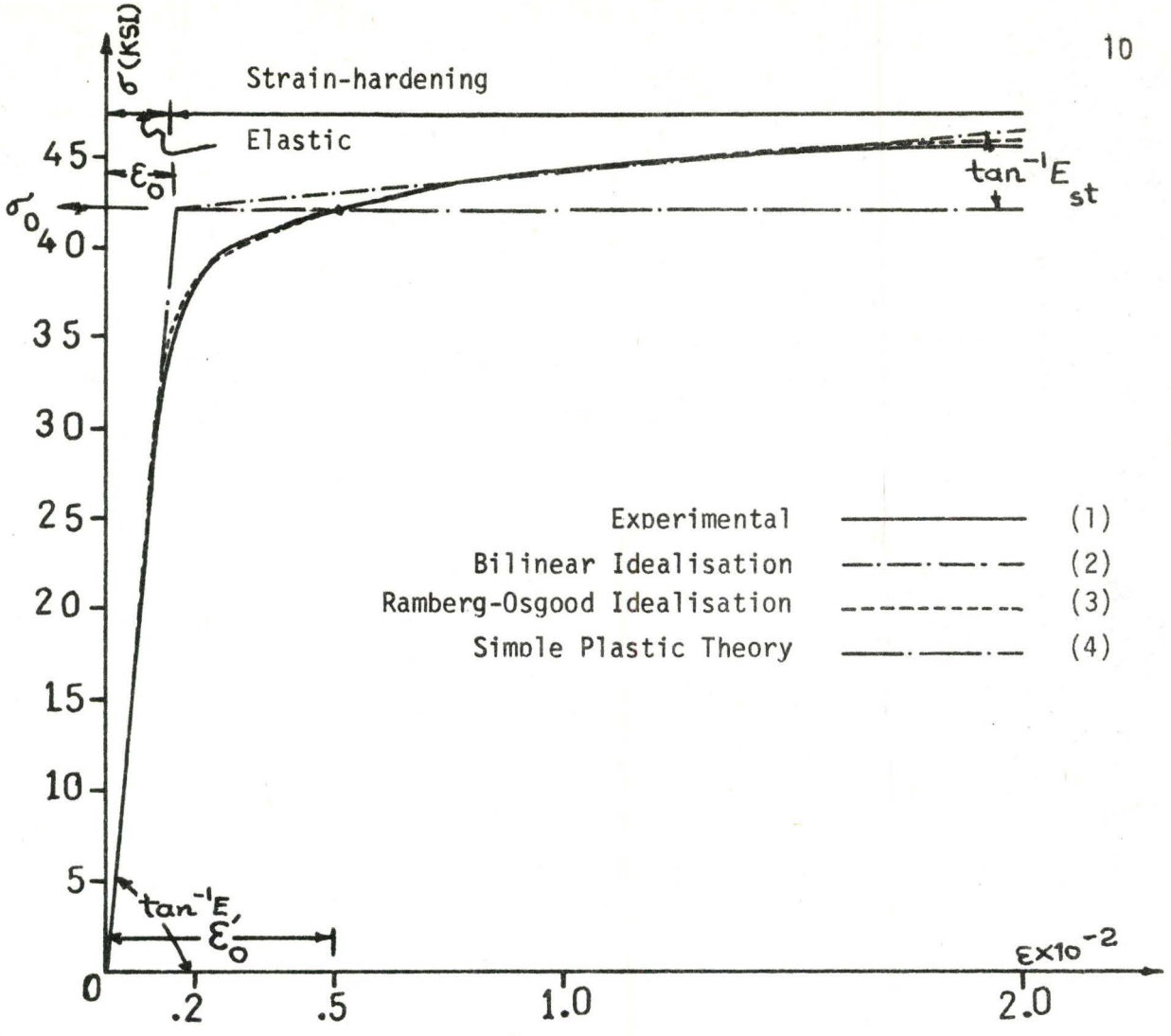

FIGURE 1.1 Stress-Strain Relationship

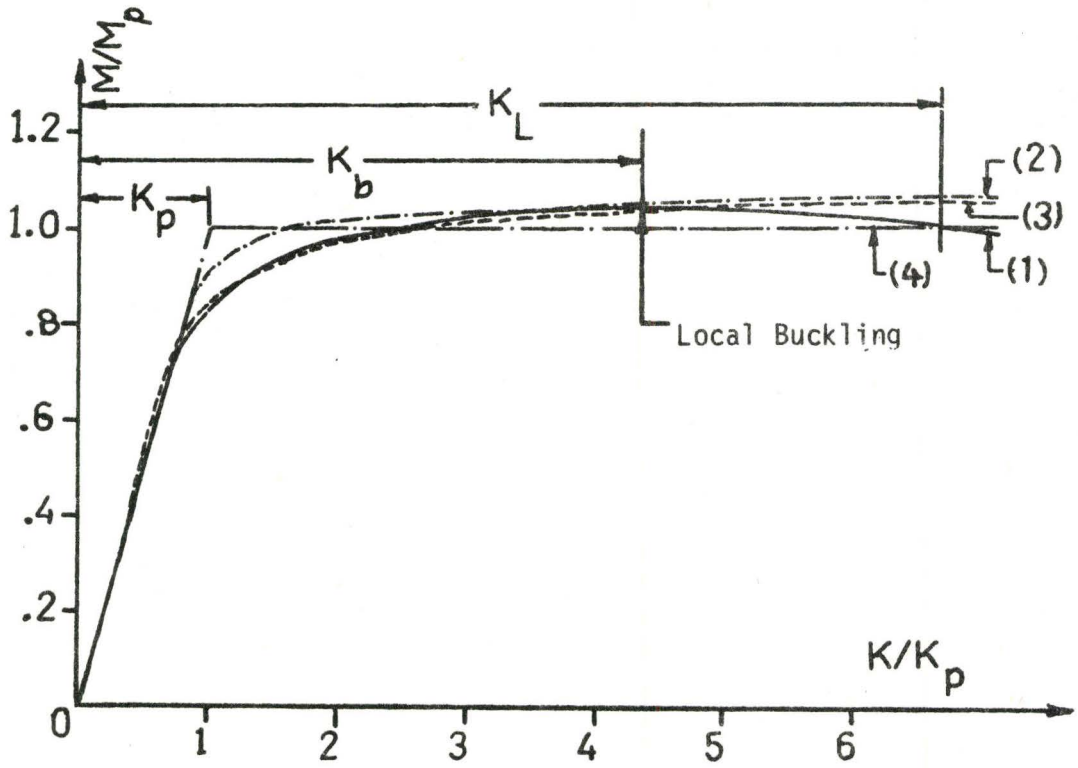

FIGURE 1.2 Moment-Curvature Relationship

CHAPTER 2

ANALYTICAL FORMULATION OF TUBE-TYPE BEAMS

2.1 Introduction

The theoretical work associated with HSS specially applied to tubes is divided in the following sections:

(a) prediction of moment curvature relations and associated load-deflection relationships,

(b) determination of tube slenderness ratios D/t to separate round sections according to the design categories stated earlier which control yielding and rotational requirements.

The reader is referred to Hudoba[3] for the theoretical treatment of rectangular and square HSS.

2.2 Prediction of the Moment-curvature and Load-deflection Relationships

In the experimental program two types of beams were investigated:

(a) a simply supported beam with simulated two point loading so that the central portion of the beam is subjected to constant moment.

(b) a two span beam symmetrical about the central support in which each span is loaded at two points and such that the first plastic hinge forms at the middle support. The stresses at the load points were computed to be in the elastic range during the formation of this hinge. The exterior support conditions were simple.

An attempt will be made to analyse these two cases.

2.2.1 Elastic Analysis

The elastic moments were calculated for a designed loading condition for a simply supported beam shown in Figure 2.1 and two span beam shown in

Figure 2.2. The total load on the beam was P(KIPS) to simulate two point loading. For the two span beam the loading conditions were designed such that the negative moment at the middle support was approximately 2.43 times the maximum positive moment in the span. The maximum positive moment was developed at one of the loading points in each span which is hereafter called the Major Load Point.

2.2.2 Plastic Analysis

(a) Moment Curvature Relationship

The moment curvature relationship was calculated using bilinear segments of the stress-strain curve and for this purpose the computer program compiled by Hudoba[3] was used. A comparison is made between the values obtained by the two idealisations of stress-strain curve (the bilinear one and the Ramberg-Osgood type) in Figure 1.2. It is obvious that there is no significant difference and either idealisation may be used for this purpose.

(b) Load Deflection Relationship

Simple Span Beam

The deflection δ of a simply supported beam (at centre) with simulated two point loading can be related to the corresponding curvature K as follows:

$$\delta = (a^2/3 + ab + b^2/2)K$$

This expression is based on the assumption that the plastic hinge occurs at midspan and the conventional slope deflection equations are used[28].

Two Span Beam

The same method can be applied to the two-span beam to find the deflection at collapse. Since the spans and loading conditions are symmetrical about the middle support as shown in Figure 2.2(a), the process can be simplified to that of evaluating deflection of a propped cantilever as given in Figure 2.3(a). The point loads P_1 and P_2 can be related to the total load P as follows:

$$P_1 = P(a + b - d)/(2b)$$

$$P_2 = P(d - a)/(2b)$$

For simplification simple plastic theory will be used. Figure 2.3(b) shows the mechanism to be formed at collapse under the total collapse load P_u which is evaluated by statics as:

$$P_u = \frac{2(2L - a)}{a(L - d)} M_p$$

To make use of the slope deflection equations, the following convention is adopted.

(a) Actual moments are to be considered and clockwise end moments are positive.

(b) Deflection is positive downwards.

(c) Clockwise rotations at the ends are positive.

(d) Hinge rotations at the ends are positive.

The slope deflection equations using these conventions can be written for a member AB as follows:

$$\phi_{AB} = \frac{\delta}{L} + \frac{L}{6EI}\left[2(M_{AB} - M^F_{AB}) - (M_{BA} - M^F_{BA})\right]$$

$$\phi_{BA} = \frac{\delta}{L} + \frac{L}{6EI}\left[2(M_{BA} - M^F_{BA}) - (M_{AB} - M^F_{AB})\right]$$

where δ is the deflection of B relative to A, ϕ_{AB} and ϕ_{BA} are the rotations at the ends A and B of the member AB respectively, and M^F_{AB} and M^F_{BA} are the fixed-end bending moments which would be produced at the ends of the member if it were subjected to the same loading but both ends were held clamped in position and direction.

Figure 2.3(c) shows the freebody diagram of the mechanism and it can be observed that:

$$M_{12} = -M_p,\ M_{21} = -M_p,\ M_{23} = +M_p,\ M_{32} = 0$$

$$M^F_{23} = -P_2 \frac{bc^2}{(b + c)^2} = -\frac{P_u}{2} \frac{(d - a)c^2}{(L - a)^2}$$

$$M^F_{32} = +P_2 \frac{b^2c}{(b + c)^2} = +\frac{P_u}{2} \frac{(d - a)bc}{(L - a)^2}$$

Figure 2.3(d) shows the deformation pattern.

Let δ_{2e} = the elastic deflection of point 2,

and δ_{2u} = deflection of point 2 at collapse. Then,

$$\phi_{23} = -\frac{\delta_{2u}}{L - a} + \frac{L - a}{6EI}(2M_p - 2M^F_{23} + M^F_{32})$$

$$\phi_{32} = -\frac{\delta_{2u}}{L - a} + \frac{L - a}{6EI}(-M_p - 2M^F_{32} + M^F_{23})$$

The hinge rotations can be related to the end rotations as follows:

$$\psi_1 = -\varphi_{12}$$

$$\psi_2 = \phi_{21} - \phi_{23}$$

On the assumption that hinge 2 is formed later than hinge 1, that is, $\psi_2 = 0$

$$\delta_{2u} = \frac{M_p}{6EIL}\left[(2L - 3a)(L - a) + \frac{c(d - a)(2c + b)(2L - a)}{a(L - d)}\right]$$

It can be shown that

$$P_u = \frac{170}{9}(M_p/L)$$

$$\delta_{2u} = (0.047M_pL^2)/(EI) = (0.00249P_uL^3)/(EI)$$

for $a = 0.3L$, $b = 0.5L$, $c = 0.2L$ and $d = 0.4L$

To find the load-deflection curve, it can be assumed that the deflection is purely governed by elastic theory initially and is given by:

$$\delta_{2e} = (0.00193P_eL^3)/(EI)$$

where P_e is the elastic limit load in the sense of a unit shape factor for the section.

It can also be assumed that in the plastic range the slope of the load deflection curve is the same as that of a similar simple span beam. The plastic deflection for point 2 in the interval of $P_e < P < P_u$ is given by:

$$\frac{0.00675(P-P_e)L^3}{EI}$$

The limiting plastic deflection δ_{2p} is therefore given by:

$$\delta_{2p} = [0.00675P_pL^3/(EI)]$$

where $P_e + P_p = P_u$

Thus $\delta_{2u} = \delta_{2e} + \delta_{2p}$

After simplification,

$$P_e = 0.885P_u$$

$$P_p = 0.115P_u$$

$$\delta_{2e} = 0.687\delta_{2u}$$

$$\delta_{2p} = 0.313\delta_{2u}$$

The yield load obtained by elastic analysis, P_o, on the basis of $(M_p/M_o) = 1.30$, can be related to the ultimate load P_u as:

$$P_o = 0.502P_u$$

The considerable difference between P_e and P_o makes it obvious that this load deflection relationship gives a rough picture of the actual deflection. The form of the exact relationship reflects a gradual transition from P_o to P_u as shown in Figure 2.4. An idealised elastic-plastic material response is implied by this curve.

It is of interest to see whether the method given here will predict the actual load deflection relationship with a sufficient degree of accuracy. Although the agreement between the theory based on the idealised behaviour and the experimental results is considered adequate, the effect of residual stresses, stress concentrations and the gradual plastification of the cross-section have been neglected in the theory.

2.3 Inelastic Instability of Tubular Beams in Pure Bending

For theoretical purposes the round HSS can be approximated by thin-walled cylindrical shells. In addition the stability criterion can be determined by one of the two basic approaches. These involve:

(a) a small deflection theory with a wave type of deformation at failure (Donnell's theory modified by Batdorf[8]), or

(b) a large deflection theory incorporating an oval type of failure (Donnell's revised theory modified by Batdorf[9] and Yao[16]).

A further modification can be included to account for the inelastic range.

Seide and Weingarten[15] made use of small deflection theory in the elastic range in which the stability criterion ultimately resulted in the solution of an eighth-order differential equation. A typical small wave type of deflection function was assumed and solved by the approximate method

of Galerkin satisfying the stability criterion.

It is decided, therefore, to adopt a method similar to that of Seide and Weingarten taking into account the inelastic behaviour of the material for a thin circular cylinder with simply supported ends and subjected to constant bending moments at the ends. Stress concentrations and residual stresses inherent to HSS are to be neglected.

2.3.1 The Co-ordinate System and Basic Assumptions

Figure 2.5(a) and (b) show the co-ordinate system adopted for a point on the cylindrical shell where x, y, and z are the distanced measured along longitudinal, circumferential and radial directions respectively. The origin of x-axis is taken to be one of the ends of the cylindrical segment under consideration. The y-co-ordinate is measured clockwise along the centroidal circumference beginning at the intersection of the vertical with the centroidal circumference. The centroidal radius of the cylinder, R, and the inclination θ of the point with respect to the vertical can be related to the co-ordinate y as $y = R\theta$. The y co-ordinate is the distance measured from the median surface to the point considered in the radial direction, positive outwards.

Figure 2.5(c) shows the freebody diagram of an element of the shell under a state of plane stress. N_x^* and N_y^* are the forces acting per unit length along the x and y directions respectively; N_{xy}, N_{yx} are shear forces per unit length. M_x and M_y are corresponding bending moments. Before proceeding further, the following assumptions are made to simplify the problem:

(a) all points lying on a normal to the middle surface before loading do so after loading.

(b) the distance z of a point from the middle surface may be considered as unaffected by the deformation of the shell and the stresses.

---

* N_x and N_y are positive in compression.

(c) The plane cross-sections of the cylinder remain plane after bending.

Consequently,

$$\varepsilon_x = \varepsilon_c \cos\theta \qquad (1)$$

where ε_c is the maximum compressive strain in the x-direction at a section and ε_x is the strain at that section and angle θ from the vertical. Figures 2.5(b) and 2.5(d) reflect this assumption geometically.

Furthermore, the condition of plane stress provides

$$N_z = 0$$

$$M_z = 0$$

$$N_{xz} = N_{zx} = N_{yz} = N_{zy} = 0$$

$$M_{xz} = M_{zx} = M_{yz} = M_{zy} = 0$$

This assumption evidently simplifies the problem to that of plane stress and plane strain.

The displacement of the midsurface of a shell element is defined by u, v and w which are related to x, y and z directions respectively. These quantities are shown in Figure 2.6.

2.3.2 Plasticity Considerations

When a body is stressed beyond its elastic limit the strain at a point of the body may be considered to consist of two parts viz. elastic

and plastic strains. This may be expressed in tensor notation as:

$$\varepsilon_{ij} = \varepsilon^{e}_{ij} + \varepsilon^{p}_{ij}$$

The elastic strain tensor ε^{e}_{ij} and stress tensor σ^{e}_{ij} have a unique relationship prescribed by the generalised Hooke's Law. There are mainly two theories which provide a relationship between the plastic strain tensor ε^{p}_{ij} and the stress tensor σ_{ij}.

(a) Incremental Theory[21, 22]

The derivation of the stress-strain relationship by this theory is based on the following assumptions:

(i) the total work done on the plastic strains must be positive,

(ii) the increment of the stress tensor and the increment of strain tensor have a linear relationship (such as Prandtl-Reuss equation),

(iii) the yield surface is convex and changes continuously during the plastic deformation process, and

(iv) the loading surface at the loading point has only one normal.

The stress-strain relationship may be expressed as:

$$d\varepsilon^{p}_{ij} = F\left(\frac{\partial \Phi}{\partial \sigma_{ij}}\right)\left(\frac{\partial \Phi}{\partial \sigma_{k\ell}}\right) d\sigma_{k\ell} \qquad \text{for } d\Phi > 0 \qquad (2a)$$

$$d\varepsilon^{p}_{ij} = 0 \qquad \text{for } d\Phi < 0 \qquad (2b)$$

where Φ is the loading function and F is a scalar function.

(b) Deformation Theory[23]

The plastic stress-strain relationship based on this theory has the general form of:

$$\varepsilon^p_{ij} = (\tfrac{1}{2} G_p)\, S_{ij} \qquad \text{for } d\Phi > 0 \tag{3a}$$

$$d\varepsilon^p_{ij} = 0 \qquad \text{for } d\Phi < 0 \tag{3b}$$

where G is a scalar function and can be interpreted as the plastic shear modulus. Equation (3a) also applies to the case:

$$(\tfrac{1}{2}\gamma^{oct^p}) = (\tfrac{1}{2}G_p)\tau_{oct}$$

where γ^{oct^p} is the plastic part of the octahedral shearing strain introduced by Nadai[23].

Lee[24], in his investigation of cylindrical shells subjected to compression, reported that the results which the two types of theories yield differ greatly for many of the problems of inelastic buckling of plates and shells. The available results agree best with predictions obtained by using the deformation theory.

Therefore, the deformation theory will be used for the problem under investigation. To attain the fully plastic moment a major portion of the tube section undergoes substantial plastic deformation and hence Poisson's ratio μ for the material will be assumed to be 0.5. This value is derived from the principle of incompressibility.

For the octahedral shear law the stress and strain intensities can be defined as follows:

$$\sigma_i = (\sigma_x^2 + \sigma_y^2 - \sigma_x\sigma_y + 3\tau^2)^{1/2} \tag{4a}$$

$$\varepsilon_i = \frac{2}{3} (\varepsilon_x^2 + \varepsilon_y^2 + \varepsilon_x\varepsilon_y + \gamma^2/4)^{1/2} \tag{4b}$$

where x and y subscripts have been dropped from τ and γ.

With the assumption that the principal axes of stress and strain coincide, the secant modulus E_s can be defined as:

$$E_s = \sigma_i/\varepsilon_i \tag{4c}$$

Thus the following simplified two-dimensional stress strain relations are obtained

$$\varepsilon_x = (\sigma_x - \tfrac{1}{2}\sigma_y)/E_s$$

$$\varepsilon_y = (\sigma_y - \tfrac{1}{2}\sigma_x)/E_s$$

$$\gamma = 3\tau/E_s$$

When buckling occurs the displacements vary slightly from their values before buckling, the resulting strain variations arise partly from variations of the middle surface strains and partly due to bending strains. These resulting variations have been considered by Stowell[25]. Using the assumption that no part of the shell is unloaded, Stowell has derived the variations of the moments during the buckling process. The variations of middle surface forces are derived from this work by Gerard[17] and are as follows:

$$N_x' = B_p[A_1\varepsilon_x' + \tfrac{1}{2}A_{12}\varepsilon_y' - \tfrac{1}{2}A_{13}\gamma'] \tag{5a}$$

$$N_y' = B_p[A_2\varepsilon_y' + \tfrac{1}{2}A_{21}\varepsilon_x' - \tfrac{1}{2}A_{23}\gamma'] \tag{5b}$$

$$N'_{xy} = (B_p/2)[A_2\gamma' - \tfrac{1}{2}A_{31}\varepsilon'_x - \tfrac{1}{2}A_{32}\varepsilon'_y] \tag{5c}$$

$$M'_x = -D_p[A_2\chi'_x + \tfrac{1}{2}A_{12}\chi'_y - \tfrac{1}{2}A_{13}\chi'_{xy}] \tag{5d}$$

$$M'_y = -D_p[A_2\chi'_y + \tfrac{1}{2}A_{21}\chi'_x - \tfrac{1}{2}A_{23}\chi'_{xy}] \tag{5e}$$

$$M'_{xy} = -(D_p/2)[A_3\chi'_{xy} - \tfrac{1}{2}A_{32}\chi'_x - \tfrac{1}{2}A_{32}\chi'_y] \tag{5f}$$

where B_p and D_p are axial and bending rigidities respectively for a fully plastic plate element. Their values are as follows: $B_p = 4E_s t/3$ and $D_p = E_s t^3/9$. ε'_x, ε'_y are midsurface normal strain variations with respect to x and y directions respectively and γ' is the midsurface shear strain variation. χ'_x, χ'_y are changes in curvature with respect to x and y directions while χ'_{xy} is the change in twist.

Furthermore, the plasticity coefficients A_1, A_2, etc. are defined by Gerard[17] as follows:

$$A_1 = 1 - \alpha\sigma_x^2/4 \tag{6a}$$

$$A_2 = 1 - \alpha\sigma_y^2/4 \tag{6b}$$

$$A_3 = 1 - \alpha\tau^2 \tag{6c}$$

$$A_{21} = A_{12} = 1 - \alpha\sigma_x\sigma_y/2 \tag{6d}$$

$$A_{31} = A_{13} = \alpha\sigma_x\tau \tag{6e}$$

$$A_{32} = A_{23} = \alpha\sigma_y\tau \tag{6f}$$

where $\alpha = \frac{3}{\sigma_i^2}(1 - E_t/E_s)$

and σ_i is given by equation (4a).

In the elastic region $\alpha = 0$ and, therefore, $A_1 = A_2 = A_3 = A_{12} = A_{21} = A_{21} = 1$, and $A_{13} = A_{23} = A_{32} = 0$. By replacing the axial and bending rigidities of the fully plastic plate by

$$B_e = \frac{Et}{(1 - \mu_e^2)}$$

and $$D_e = \frac{Et^3}{12(1 - \mu_e^2)}$$

respectively, the equations (5a) to (5f) reduce to the familiar relations for the elastic plate.

2.3.3 Equilibrium Considerations

Donnell's small deflection theory as modified by Batdorf[8] consists of three equilibrium equations:

$$\partial N_x'/\partial x + \partial N_{xy}'/\partial y = 0 \tag{7a}$$

$$\partial N_y'/\partial y + \partial N_{xy}'/\partial x = 0 \tag{7b}$$

$$\begin{aligned} &-(\partial^2 M_x'/\partial x^2) - 2(\partial^2 M_{xy}'/\partial x\,\partial y) - (\partial^2 M_y'/\partial y^2) + (N_y'/R_y) \\ &\quad + N_x(\partial^2 w/\partial x^2) + 2N_{xy}(\partial^2 w/\partial x\,\partial y) + N_y(\partial^2 w/\partial y^2) = 0 \end{aligned} \tag{7c}$$

Gerard introduced a new term (N_x'/R_x) in equation (7c) which may be neglected for cylindrical shells since R_x will tend to infinity.

For a cylinder in pure bending $\sigma_y = 0$, $\tau = 0$, $R_y = R$ and $y = R\theta$.

Hence from equation (4a)

$$\sigma_i = \sigma_x$$

Now from equations (4c) and (1)

$$\sigma_x = E_s \varepsilon_c \cos\theta$$

Thus $N_x = E_s t \varepsilon_c \cos\theta$,

$$N_y = 0 \tag{8a}$$

and $N_{xy} = 0$

Making use of equations (6a) to (6f),

$$A_1 = \frac{1}{4} + \frac{3}{4}\frac{E_t}{E_s} \tag{8b}$$

$$A_2 = A_3 = A_{12} = A_{21} = 1 \tag{8c}$$

$$A_{31} = A_{13} = A_{23} = A_{32} = 0 \tag{8d}$$

The middle surface strain variations and changes in curvature that occur during buckling of a cylindrical shell are related to the displacements as follows:

$$\varepsilon_x' = \frac{\partial u}{\partial x} \tag{9a}$$

$$\varepsilon_y' = \frac{\partial v}{\partial y} + \frac{w}{R} \tag{9b}$$

$$\gamma' = \frac{1}{2}\left[\frac{\partial u}{\partial y} + \frac{\partial v}{\partial x}\right] \tag{9c}$$

$$\chi_x' = \frac{\partial^2 w}{\partial x^2} \tag{9d}$$

$$\chi_y' = \frac{\partial^2 w}{\partial y^2} \tag{9e}$$

$$\chi_{xy}' = \frac{\partial^2 w}{\partial x \partial y} \tag{9f}$$

Using equations (5a) to (5f) and (9a) to (9f) the equilibrium equations (7a) to (7c) can be simplified as follows:

$$A_1\left(\frac{\partial^2 u}{\partial x^2}\right) + \frac{1}{4R^2}\frac{\partial^2 u}{\partial \theta^2} + \frac{3}{4R}\frac{\partial^2 v}{\partial x \partial \theta} + \frac{1}{2R}\frac{\partial w}{\partial x} = 0 \tag{10a}$$

$$\frac{1}{R^2}\frac{\partial^2 v}{\partial \theta^2} + \frac{1}{4}\frac{\partial^2 v}{\partial x^2} + \frac{3}{4R}\frac{\partial^2 u}{\partial x \partial \theta} + \frac{1}{R^2}\frac{\partial w}{\partial \theta} = 0 \tag{10b}$$

$$Y + \frac{1}{2}\frac{\partial u}{\partial x} + \frac{1}{R}\frac{\partial v}{\partial \theta} + \frac{w}{R} = 0 \tag{10c}$$

where $Y = Y_1 + Y_2$ and

$$Y_1 = \frac{Rt^2}{12}\left[A_1\frac{\partial^4 w}{\partial x^4} + \frac{2}{R^2}\frac{\partial^4 w}{\partial x^2 \partial \theta^2} + \frac{1}{R^4}\frac{\partial^4 w}{\partial \theta^4}\right]$$

$$Y_2 = \frac{3}{4}\,\varepsilon_c\, R\,\cos\theta\,\frac{\partial^2 w}{\partial x^2}$$

Equations (10a) to (10c) constitute a basic set of equilibrium equations for the inelastic instability of thin cylindrical shells in pure bending. Making use of these equations the stability criterion can be reduced to a function of the radial displacement w, and after solving for w the longitudinal displacements u and v can be computed to trace out the exact profile of deformations.

The detailed steps are traced out in Appendix 1 to arrive at the following basic equation for the evaluation of buckling load.

$$\begin{aligned}
Q(w) = {} & \alpha_1 \frac{\partial^8 w}{\partial x^8} + \frac{\alpha_2}{R^2}\,\frac{\partial^8 w}{\partial x^6\,\partial\theta^2} + \frac{\alpha_3}{R^4}\,\frac{\partial^8 w}{\partial x^4\partial\theta^4} + \frac{\alpha_4}{R^6}\,\frac{\partial^8 w}{\partial x^2\partial\theta^6} \\
& + \frac{\alpha_5}{R^8}\,\frac{\partial^8 w}{\partial\theta^8} + \frac{\alpha_6}{R}\,\frac{\partial^7 w}{\partial x^6\partial\theta} + \frac{\alpha_7}{R^3}\,\frac{\partial^7 w}{\partial x^4\partial\theta^3} + \frac{\alpha_8}{R^5}\,\frac{\partial^7 w}{\partial x^2\partial\theta^5} \\
& + \frac{\alpha_9}{R^7}\,\frac{\partial^7 w}{\partial\theta^7} + \alpha_{10}\frac{\partial^6 w}{\partial x^6} + \frac{\alpha_{11}}{R^2}\,\frac{\partial^6 w}{\partial x^4\partial\theta^2} \\
& + \frac{\alpha_{12}}{R^4}\,\frac{\partial^6 w}{\partial x^2\partial\theta^4} + \frac{\alpha_{13}}{R^6}\,\frac{\partial^6 w}{\partial\theta^6} + \frac{\alpha_{14}}{R}\,\frac{\partial^5 w}{\partial x^4\partial\theta} \\
& + \frac{\alpha_{15}}{R^3}\,\frac{\partial^5 w}{\partial x^2\partial\theta^3} + \alpha_{16}\frac{\partial^4 w}{\partial x^4} + \frac{\alpha_{17}}{R^2}\,\frac{\partial^4 w}{\partial x^2\partial\theta^2} \\
& + \frac{\alpha_{18}}{R}\,\frac{\partial^3 w}{\partial x^2\partial\theta} + \alpha_{19}\frac{\partial^2 w}{\partial x^2} = 0
\end{aligned} \tag{11}$$

where $\alpha_1, \alpha_2, \ldots, \alpha_{18}, \alpha_{19}$ are variable coefficients involving the geometrical parameters and material properties of the cylinder, and are obtained as follows:

$$\alpha_1 = A_1^2 \tag{12a}$$

$$\alpha_2 = 4A_1^2 \tag{12b}$$

$$\alpha_3 = 10A_1 - 4 \tag{12c}$$

$$\alpha_4 = 4A_1 \tag{12d}$$

$$\alpha_5 = 1 \tag{12e}$$

$$\alpha_6 = \frac{1}{R} \frac{\partial A_1}{\partial \theta} [4(2A_1 - 1) + A_1/(A_1 - 1/4)] \tag{12f}$$

$$\alpha_7 = \frac{1}{R} \frac{\partial A_1}{\partial \theta} \frac{(2A_1 + 1)}{(A_1 - 1/4)} \tag{12g}$$

$$\alpha_8 = \frac{3}{R(A_1 - 1/4)} \frac{\partial A_1}{\partial \theta} \tag{12h}$$

$$\alpha_9 = - \frac{2}{R(A_1 - 1/4)} \frac{\partial A_1}{\partial \theta} \tag{12i}$$

$$\alpha_{10} = \frac{1}{R^2} \left[\frac{\partial^2 A}{\partial \theta^2} \left\{ 4A_1 - 2 + \frac{A_1}{2(A_1 - 1/4)} \right\} - \frac{1}{4(A_1 - 1/4)^2} \left(\frac{\partial A_1}{\partial \theta} \right)^2 \right] + 9A_1 \varepsilon_c \cos\theta / t^2 \tag{12j}$$

$$\alpha_{11} = 9(4A_1 - 2)\varepsilon_c \cos\theta/t^2 + \frac{1}{R^2}\frac{\partial^2 A_1}{\partial\theta^2}\left[6 + \frac{(1 - A_1)}{(A_1 - 1/4)}\right] \tag{12k}$$

$$\alpha_{12} = 9\varepsilon_c \cos\theta/t^2 + \frac{1}{R^2}\frac{1}{(A_1 - 1/4)}\left[\frac{3}{(A_1 - 1/4)}\left(\frac{\partial A_1}{\partial\theta}\right)^2 - \frac{3}{2}\frac{\partial^2 A_1}{\partial\theta^2}\right] \tag{12ℓ}$$

$$\alpha_{13} = -\frac{1}{R^2(A_1 - 1/4)}\left[\frac{\partial^2 A_1}{\partial\theta^2} - \frac{2}{(A_1 - 1/4)}\left(\frac{\partial A_1}{\partial\theta}\right)^2\right] \tag{12m}$$

$$\alpha_{14} = \frac{4}{R^3}\left[\frac{\partial^3 A_1}{\partial\theta^3} + \frac{1}{(A_1 - 1/4)}\frac{\partial A_1}{\partial\theta}\left\{\frac{1}{(A_1 - 1/4)}\left(\frac{\partial A_1}{\partial\theta}\right)^2 - 2\frac{\partial^2 A_1}{\partial\theta^2}\right\}\right] + \frac{9\varepsilon_c}{Rt^2}\left[\frac{\partial A_1}{\partial\theta}\frac{1}{(A_1 - 1/4)}\cos\theta - 4(2A_1 - 1)\sin\theta\right] \tag{12n}$$

$$\alpha_{15} = -\frac{9\varepsilon_c}{Rt^2}\left[4\sin\theta + 2\frac{\partial A_1}{\partial\theta}\frac{1}{(A_1 - 1/4)}\cos\theta\right] \tag{12o}$$

$$\alpha_{16} = -\frac{9(4A_1 - 2)\varepsilon_c}{R^2t^2}\cos\theta + \frac{1}{R^4}\frac{\partial^4 A_1}{\partial\theta^4} + \frac{1}{R^2(A_1 - 1/4)}\left[\frac{\partial^2 A_1}{\partial\theta^2} - \frac{2}{(A_1 - 1/4)}\left(\frac{\partial A_1}{\partial\theta}\right)^2\right]\left[\frac{9\varepsilon_c}{2t^2}\cos\theta - \frac{1}{R^3}\frac{\partial^2 A_1}{\partial\theta^2}\right] - \frac{2}{R^2}\frac{\partial A_1}{\partial\theta}\frac{1}{(A_1 - 1/4)}\left[\frac{1}{R^2}\frac{\partial^3 A_1}{\partial\theta^3} + \frac{9\varepsilon_c}{2t^2}\sin\theta\right] + \frac{12(A_1 - 1/4)}{R^2t^2} \tag{12p}$$

$$\alpha_{17} = -\frac{54\varepsilon_c \cos\theta}{R^2t^2} + \frac{1}{(A_1 - 1/4)} \frac{9\varepsilon_c}{R^2t^2} \cos\theta \left[2 \left(\frac{\partial A_1}{\partial \theta}\right)^2 \frac{1}{(A_1 - 1/4)} - \frac{\partial^2 A_1}{\partial \theta^2}\right] + \frac{54\varepsilon_c}{R^2t^2} \frac{1}{(A_1 - 1/4)} \frac{\partial A_1}{\partial \theta} \sin\theta \tag{12q}$$

$$\alpha_{18} = \frac{9\varepsilon_c}{R^3t^2} \left[4 \sin\theta + \frac{1}{(A_1 - 1/4)} \; 2 \sin\theta \left(\frac{\partial^2 A_1}{\partial \theta^2}\right) - \frac{4}{(A_1 - 1/4)} \left(\frac{\partial A_1}{\partial \theta}\right)^2 \sin\theta + 6 \frac{\partial A_1}{\partial \theta} \cos\theta \;\right] \tag{12r}$$

$$\alpha_{19} = \frac{9\varepsilon_c}{R^4t^2} \frac{\cos\theta}{(A_1 - 1/4)} \left[\; (A_1 - 1/4) + \frac{\partial^2 A_1}{\partial \theta^2} - \frac{2}{(A_1 - 1/4)} \left(\frac{\partial A_1}{\partial \theta}\right)^2 - 2 \frac{\partial A_1}{\partial \theta} \tan\theta\right] \tag{12s}$$

For the elastic case, Donnell's stability criterion as modified by Batdorf can be written as:

$$D_e \nabla^4 w + \frac{Et}{R^2} \nabla^{-4} \frac{\partial^4 w}{\partial x^4} + t(\sigma_{cb} \cos\theta) \frac{\partial^2 w}{\partial x^2} = 0 \tag{13}$$

If Poisson's ratio μ_e in equation (13) is replaced by 0.5 and σ_{cb} by $E\varepsilon_c$, equation (13) reduces to the form

$$D_p \nabla^4 w + \frac{Et}{R^2} \nabla^{-4} \frac{\partial^4 w}{\partial x^4} + tE\varepsilon_c \cos\theta \frac{\partial^2 w}{\partial x^2} = 0 \tag{14}$$

It is verified that equation (11) reduces to equation (14) when the coefficients $\alpha_1, \alpha_2, \ldots\ldots, \alpha_{18}, \alpha_{19}$ etc. in equations (12a) to

(12s) are modified to apply to the elastic case by substituting

$$E_T = E_S = E,\ A_1 = 1,$$

and $$\frac{\partial A_1}{\partial \theta} = \frac{\partial^2 A_1}{\partial \theta^2} = \frac{\partial^3 A_1}{\partial \theta^3} = \frac{\partial^4 A_1}{\partial \theta^4} = 0$$

A suitable solution for the deflection function 'w' to satisfy the stability criterion which fulfills the conditions appropriate to simple support of the cylinder ends by bulkheads rigid in their own plane but free to warp out of their plane can be assumed as follows:

$$w = \sin \frac{m\pi x}{L} \sum_{n=0}^{\infty} a_n \cos n\theta \qquad (15)$$

To fit this solution to the stability criterion which eventually means to find the coefficients $a_0, a_1, a_2, \ldots, a_n \ldots$ etc., Galerkin's approximate method[27] can be used. A direct solution does not appear to be tractable.

In practice, the number of terms used in the deflection function are limited. Based on five significant figure accuracy of the buckling coefficient, Seide and Weingarten[15] have established in their solution of elastic buckling that the number of terms used varies from 12 to 51 for D/t ratios of 200 to 2000. Therefore, it is assumed that only 'p' terms need to be considered, that is,

$$w = \sin \frac{m\pi x}{L} \sum_{n=0}^{(p-1)} a_n \cos n\theta \qquad (16)$$

Then the equations for coefficients $a_0, a_1, \ldots, a_{p-2}, a_{p-1}$, etc. are given by

$$\int_0^{2\pi} \int_0^{L} Q'(w) \sin \frac{m\pi x}{L} \cos q\theta \, dx d\theta = 0 \qquad (17)$$

$$q = 0, 1, 2, \ldots, (p-1)$$

where $Q'(w)$ represents the stability criterion, equation (11), after substituting the assumed deflection function w i.e. expression (15).

It is interesting to note that the various terms of equation (11) involve only even derivatives with respect to x, that is,

$$\frac{\partial^2}{\partial x^2}, \frac{\partial^4}{\partial x^4}, \frac{\partial^6}{\partial x^6}, \frac{\partial^8}{\partial x^8}$$

etc., and the integration of equation (17) in x will simply yield a constant coefficient

since $$\int_0^{L} \sin^2 \frac{m\pi x}{L} \, dx = \frac{L}{2} .$$

Therefore, equation (17) reduces to the form:

$$\int_0^{2\pi} Q''(w) \cos q\theta \, d\theta = 0 \qquad (18)$$

$$q = 0, 1, 2, \ldots, (p-1)$$

where $$Q''(w) = \frac{Q'(w)}{\sin(m\pi x/L)} = \Omega$$

where Ω is purely a function of θ.

It can be observed that the coefficients α_1, α_2, . . . α_{18}, α_{19}, etc. in equations (12a) to (12s) are generally functions of θ and are dependent upon the stress-strain relationship. Since simple plastic theory or an idealised bilinear stress-strain curve does not satisfy stress continuity requirements over the full range of strain, a continuous stress-strain relationship such as that of Ramberg-Osgood[26] can be used.

On further simplification, equation (18), after substituting appropriate expressions for $Q''(w)$, reduces to the form:

$$\sum_{j=1}^{19} \int_0^{2\pi} \alpha_j q_j \cos q\theta \, d\theta = 0 \qquad (19)$$

$$q = 0, 1, 2, \ldots, (p-1)$$

where the coefficients q_j in equation (19) are given by

$$q_1 = \left(\frac{m\pi}{L}\right)^8 \Sigma a_n \cos n\theta \qquad (20a)$$

$$q_2 = \left(\frac{m\pi}{L}\right)^6 \left(\frac{n}{R}\right)^2 \Sigma a_n \cos n\theta \qquad (20b)$$

$$q_3 = \left(\frac{m\pi}{L}\right)^4 \left(\frac{n}{R}\right)^4 \Sigma a_n \cos n\theta \qquad (20c)$$

$$q_4 = \left(\frac{m\pi}{L}\right)^2 \left(\frac{n}{R}\right)^6 \Sigma a_n \cos n\theta \qquad (20d)$$

$$q_5 = \left(\frac{n}{R}\right)^8 \Sigma a_n \cos n\theta \qquad (20e)$$

$$q_6 = \left(\frac{m\pi}{L}\right)^6 \left(\frac{n}{R}\right) \Sigma a_n \sin n\theta \qquad (20f)$$

$$q_7 = \left(\frac{m\pi}{L}\right)^4 \left(\frac{n}{R}\right)^3 \Sigma\ a_n \sin n\theta \tag{20g}$$

$$q_8 = \left(\frac{m\pi}{L}\right)^2 \left(\frac{n}{R}\right)^5 \Sigma\ a_n \sin n\theta \tag{20h}$$

$$q_9 = \left(\frac{n}{R}\right)^7 \Sigma\ a_n \sin n\theta \tag{20i}$$

$$q_{10} = -\left(\frac{m\pi}{L}\right)^6 \Sigma\ a_n \cos n\theta \tag{20j}$$

$$q_{11} = -\left(\frac{m\pi}{L}\right)^4 \left(\frac{n}{R}\right)^2 \Sigma\ a_n \cos n\theta \tag{20k}$$

$$q_{12} = -\left(\frac{m\pi}{L}\right)^2 \left(\frac{n}{R}\right)^4 \Sigma\ a_n \cos n\theta \tag{20ℓ}$$

$$q_{13} = -\left(\frac{n}{R}\right)^6 \Sigma\ a_n \cos n\theta \tag{20m}$$

$$q_{14} = -\left(\frac{m\pi}{L}\right)^4 \left(\frac{n}{R}\right) \Sigma\ a_n \sin n\theta \tag{20n}$$

$$q_{15} = -\left(\frac{m\pi}{L}\right)^2 \left(\frac{n}{R}\right)^3 \Sigma\ a_n \sin n\theta \tag{20o}$$

$$q_{16} = \left(\frac{m\pi}{L}\right)^4 \Sigma\ a_n \cos n\theta \tag{20p}$$

$$q_{17} = \left(\frac{m\pi}{L}\right)^2 \left(\frac{n}{R}\right)^2 \Sigma\ a_n \cos n\theta \tag{20q}$$

$$q_{18} = \left(\frac{m\pi}{L}\right)^2 \left(\frac{n}{R}\right) \Sigma\ a_n \sin n\theta \tag{20r}$$

$$q_{19} = -\left(\frac{m\pi}{L}\right)^2 \Sigma\ a_n \cos n\theta \tag{20s}$$

where the summation sign refers to summation for 'p' terms, that is,

$$\sum_{n=0}^{(p-1)}$$

Equation (19) cannot be directly integrated (using Ramberg-Osgood stress-strain relationship) since the derivatives of the plasticity coefficient, A_1, with respect to θ, are very crumbersome to be worked out mathematically. The only practical way to integrate equation (24) is by the technique of finite elements.

The system of equations obtained by integration of equation (19) is a homogeneous system of 'p' equation in 'p' unknowns, a_0, a_1, . . . , a_{p-2}, a_{p-1}, etc. as follows:

$$\begin{aligned}
&a_0 \beta_{11} + a_1 \beta_{12} + - - - - + a_{p-1} \beta_{1p} = 0 \\
&a_0 \beta_{21} + a_1 \beta_{22} + a_2 \beta_{23} + - - - - + a_{p-1} \beta_{2p} = 0 \\
&- \\
&- \\
&- \\
&a_0 \beta_{(p-1)} + a_1 \beta_{(p-1)2} + a_2 \beta_{(p-1)3} + - - - - \\
&\quad + a_{p-1} \beta_{(p-1)p} = 0 \\
&a_0 \beta_{p1} + a_1 \beta_{p2} + a_2 \beta_{p3} + - - - - + a_{p-1} \beta_{pp} = 0
\end{aligned} \tag{21}$$

Such a system of homogeneous linear equations has a non-trivial solution[27] in the case when the determinant formed by the coefficients of

$a_0, a_1, \ldots, a_{p-2}, a_{p-1}$ vanishes, that is,

$$\Delta = \begin{vmatrix} \beta_{11} & \beta_{12} & \cdots & \beta_{1(p-1)} & \beta_{1p} \\ \beta_{21} & \beta_{22} & \cdots & & \\ \cdots & \cdots & \cdots & \cdots & \cdots \\ \beta_{p1} & \beta_{p2} & \cdots & \beta_{p(p-1)} & \beta_{pp} \end{vmatrix} = 0 \qquad (22)$$

Equation (22) is of pth degree of certain function of stress-strain relationship and generally speaking, it would give p values of the critical buckling strain ε_c for a particular cylinder with a particular longitudinal buckle wave-length if the cylinder behaved elastically. Since the Ramberg-Osgood stress-strain relationship is non-linear the β's incorporate ε_c in a non-linear way through the parameter A_1. Reference is made to the α's which are incorporated in the $\beta_{11}, \beta_{12}, \ldots, \beta_{pp}$. The value of ε_c associated with the minimum buckling load is to be determined as described below.

If a unique solution of equation (21) does exist, the radial deflection function w can be determined and it will be of interest to observe the theoretical deformations. These can be obtained in equations (A-6)* and (A-10)* and solving for u and v respectively.

---

* These equations are worked out in Appendix 1.

2.3.4 Computational Procedure and Results

To obtain the condition of equation (22) one can solve the problem in one of two ways.

(i) Start with the assumed value of R and t and iterate the value of ε_c for a certain longitudinal buckle half wave-length.

(ii) With an assumed value of ε_c, t and longitudinal half buckle wave-length iterate for R.

The latter procedure was adopted in the actual computations since it was more convenient.

The strength characteristics of Round HSS, tested, were broadly of two types:

(a) Guaranteed 0.5% Strain Yield Strength = 42 KSI

(b) Guaranteed 0.5% Strain Yield Strength = 52 KSI

A short stub column for each of these two types was tested in compression in which yielding was followed by an axisymmetric mode of buckling. Figures 2.7(a) and 2.7(b) show the deformations in these stub columns after test. The following Ramberg-Osgood[26] type of stress-strain relationships were obtained by curves fitting to the experimental results. These are shown in Figures 2.8(a) and 2.8(b) respectively.

(a) For a Guaranteed Yield Strength of 42 KSI*

$$\frac{E\varepsilon}{37.75} = \frac{\sigma}{37.75} + \frac{3}{7}\left(\frac{\sigma}{37.75}\right)^{17} \qquad (23)$$

$E = 29500$ KSI

$\sigma_0 = 42.15$ KSI

$E_{st} = 250$ KSI

*Specimen taken from HSS 4.5 O.D. X 0.156

(b) For a Guaranteed Yield Strength of 52 KSI**

$$\frac{E\varepsilon}{49.10} = \frac{\sigma}{49.10} + \frac{3}{7}\left(\frac{\sigma}{49.10}\right)^{20} \tag{24}$$

$E = 29500$ KSI

$\sigma_0 = 52.93$ KSI

$E_{st} = 260$ KSI

A special computer programme was developed using this type of stress-strain relationship which solves for the condition of equation (22) at specific rotation or yield requirements and is discussed in Appendix 2. The purpose of the programme is to integrate numerically the various elements of equation (22) and to compute the resulting determinant. This method is applied to various values of buckle half wave-length parameters $\frac{m\pi R}{L}$ for temporarily fixed value of tube slenderness ratio D/t. The actual value of the D/t ratio for which buckling occurs at the preassigned rotation is then determined.

To illustrate the application of this procedure the evaluation of limiting D/t ratio for a plastic design section will be discussed.

For a given maximum strain ε_{max} of a section the curvature K associated with that section is given by:

$$K = 2\,\varepsilon_{max}/D \tag{25}$$

** Specimen taken from HSS 6.625 O. D. X 0.188

Hence if the critical strain at buckling is known, then some measure of the maximum curvature can be found from equation (25) when ε_c replaces ε_{max}. As will be evident from the test results, some reserve ductility is available without a significant reduction in bending moment capacity. Therefore, the theoretical D/t value associated with a given critical strain will be a conservative value unless other factors such as residual stresses and local bearing stresses are significant. Further discussion of these points is presented in Chapter 4.

If the rotation capacity of a section is based on the theoretical buckling curvature K_b then

$$\Theta_b = \frac{K_b}{K_p} - 1 \tag{26}$$

where K_p is the calculated elastic limit curvature based on an idealised elastic-plastic material and is given by

$$K_p = \frac{M_p}{EI}$$

Figure 1.2 illustrates the quantities defined above relative to a typical moment-curvature plot. The actual rotation capacity is Θ.

Hence

$$K_p = 2\sigma_0 \, f/(DE) \tag{27}$$

where f is the shape factor.

From earlier work[3] a hinge capacity, $\Theta = 4$ was proposed. Consequently, from equations (26) and (27),

$$K_b = 10\sigma_0 \, f/(DE)$$

that is,

$$\varepsilon_c = 5\sigma_0 \, f/E \tag{28}$$

For the stress-strain relationship given by equation (23), the determinants for various values of D/t ratio along with varying $\frac{m\pi R}{L}$ are tabulated for the aforesaid value of ε_c in Table 2.1, taking the first 8 terms of equation (19). The values of these determinants indicate two possibilities of solution;

(a) For $\frac{m\pi R}{L} \simeq 0.5$ to 1.5 a tube even with low D/t ratio of 20 buckles.

(b) A unique solution located in the range of $40 < D/t < 50$ and $6 < \frac{m\pi R}{L} < 10$, which to the right side of the table (increasing D/t ratio) gives an increasing set of negative arrays.

Because of non-linearity of the problem a unique solution does not appear to be possible. The range of solution given by (a) is rejected, however, on both physical grounds (half wave-lengths too high) and mathematical results. The values of the determinant in the range considered are non-regular. On the other hand in the category (b) the set of determinants is well-behaved and in the physically plausible range.

Therefore solution (b) will be taken as the region to predict the extent of buckling.

The problem then is to select the smallest value of D/t for a given buckling strain (or stress). This approach corresponds to finding the lowest eigenvalue of the determinant of coefficients for a conventional linear problem.

Table 2.2 shows the set of determinants under a closed array ($D/t \simeq 40 - 50$ and $\frac{m\pi R}{L} \simeq 6 - 10$) and concludes that the solution is located

at D/t $\simeq$ 46 - 48 and $\frac{m\pi R}{L} \simeq$ 7 - 9.0. A finer grid with 8 terms pin-points the values for which the determinant is zero more closely as in Table 2.3. As a check a few more terms of equation (19) are taken, which in this case, considered totals to 12 and Table 2.4 shows the set of determinants for this array. A minimum D/t of 47 with $\frac{m\pi R}{L} \simeq 8$ is evident. Consequently, for a plastic design section having stress characteristics given by equation (23) the limiting D/t ratio is 47. It is possible to locate even more accurate value of D/t ratio but for practical purposes the accuracy obtained is sufficient.

This procedure was repeated to classify the sections for various yielding and rotational requirements having stress-characteristics given by equations (23) and (24). The conclusion of these computations using 12 terms of equation (19) is presented in Table 2.5.

These results show that there is considerable difference for plastic design sections having different stress characteristics due to the considerable difference in the values of strain to be attained before buckling. For compact and non-compact sections in allowable stress design the difference is small since the strains to be attained before buckling are very near. In fact the limiting D/t ratio for a non-compact section is a lower bound since the computed yield moment M_0 is normally attained before the strain of 5000 μin/in occurs. For the stress characteristics given by equation (23) M_0 is attained at a strain of 2000 μin/in and this gives a predicted D/t ratio of 280. This value does not warrant much significance in the design of HSS, since the method does not take into account the stress concentrations on the loaded surface nor the geometrical imperfection which would be of importance.

Figure 2.9 is a plot of θ_b vs D/t for the strength characteristics given by equations (23) and (24). As evident from the plot, the variation

in yield strength generates a set of contours. Such contours can be used in design with modifications taking into account the experimental behaviour.

A comparison of these results with test data and the limitations implicit in the theory will be discussed in Chapter 4.

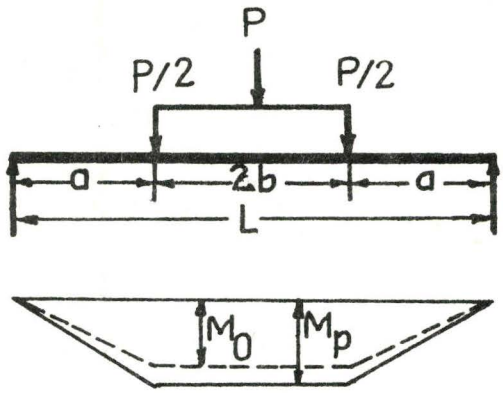

(a) loading

(b) bending moment distribution

FIGURE 2.1 Simple Span Beam

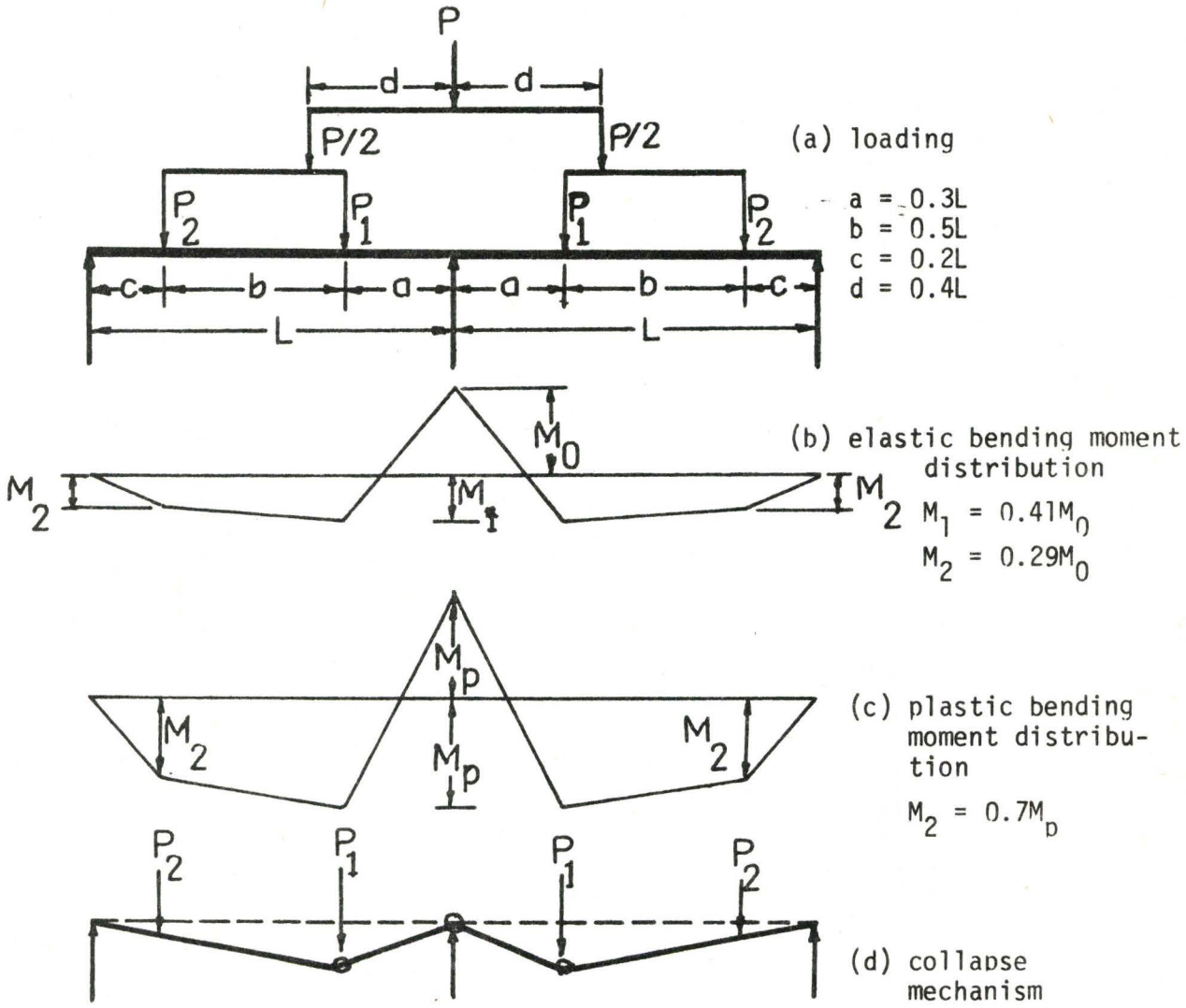

(a) loading

a = 0.3L
b = 0.5L
c = 0.2L
d = 0.4L

(b) elastic bending moment distribution

$M_1 = 0.41M_0$

$M_2 = 0.29M_0$

(c) plastic bending moment distribution

$M_2 = 0.7M_p$

(d) collapse mechanism

FIGURE 2.2 Two Span Beam

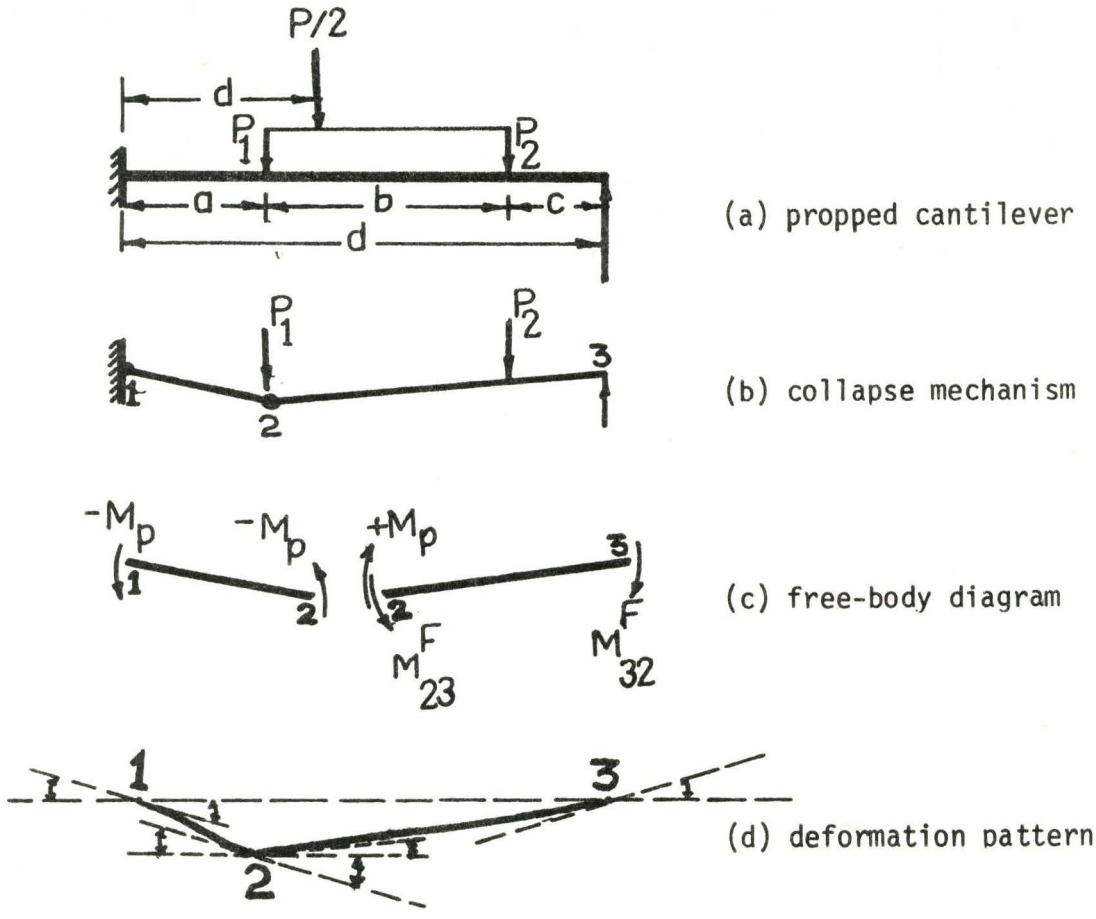

FIGURE 2.3 Deflection at Collapse

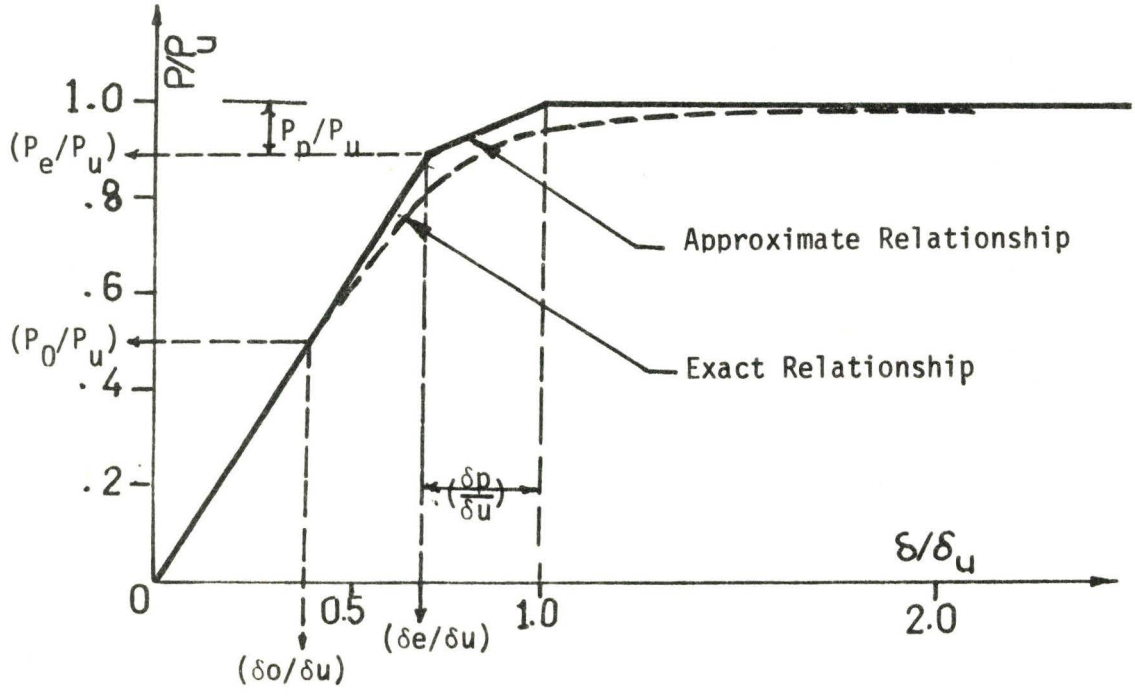

FIGURE 2.4 Load Deflection Curve - Two Span Beam

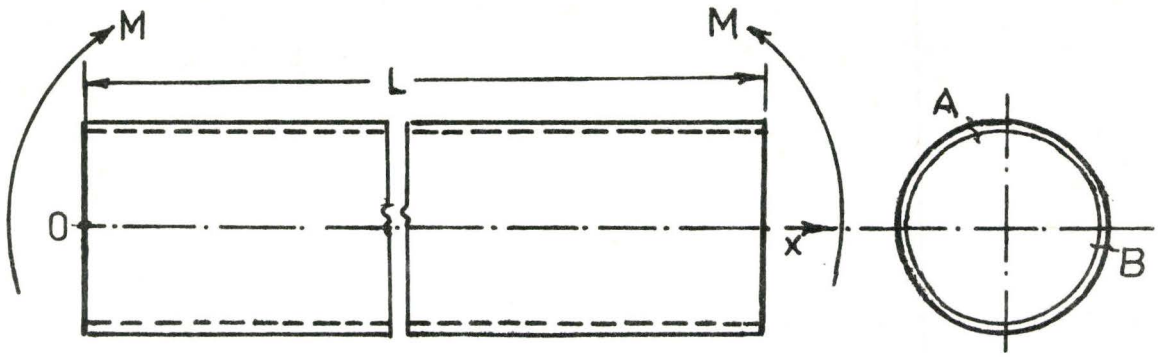

(a) x - co-ordinate

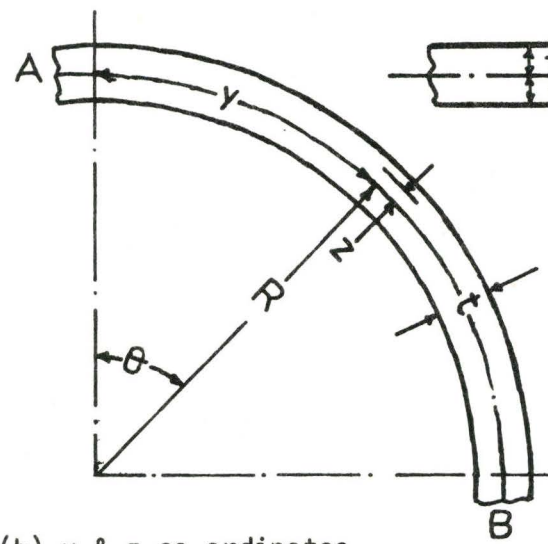

(b) y & z co-ordinates

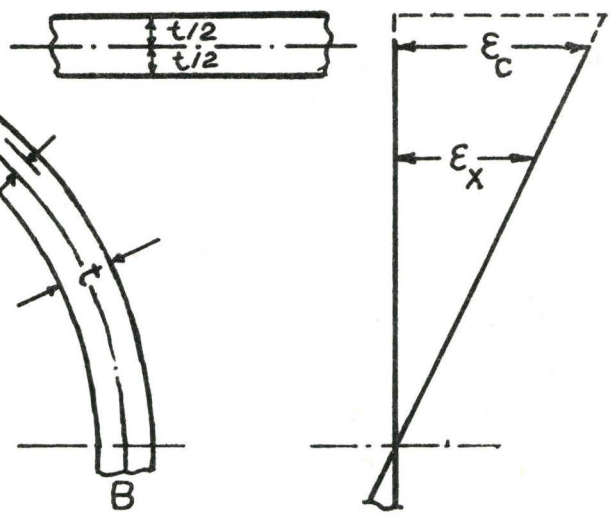

(d) strain distribution

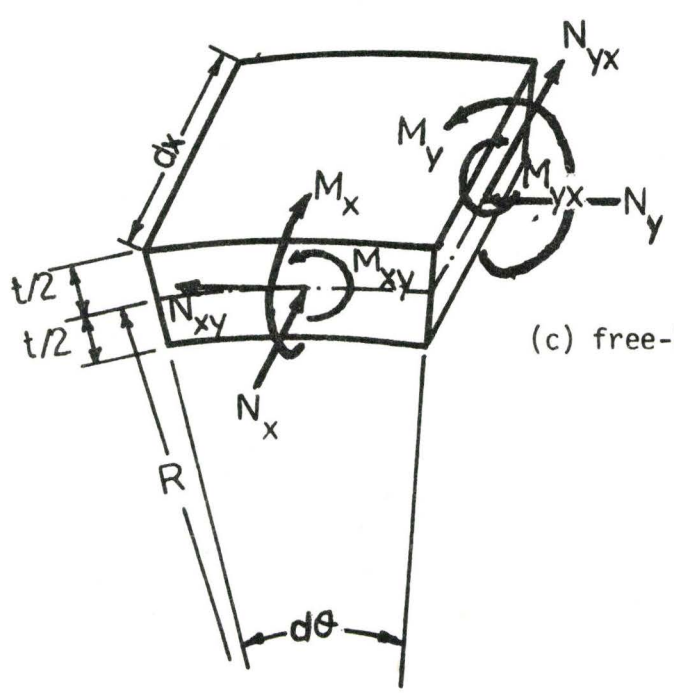

(c) free-body diagram

FIGURE 2.5 Cylindrical Shell Under Bending

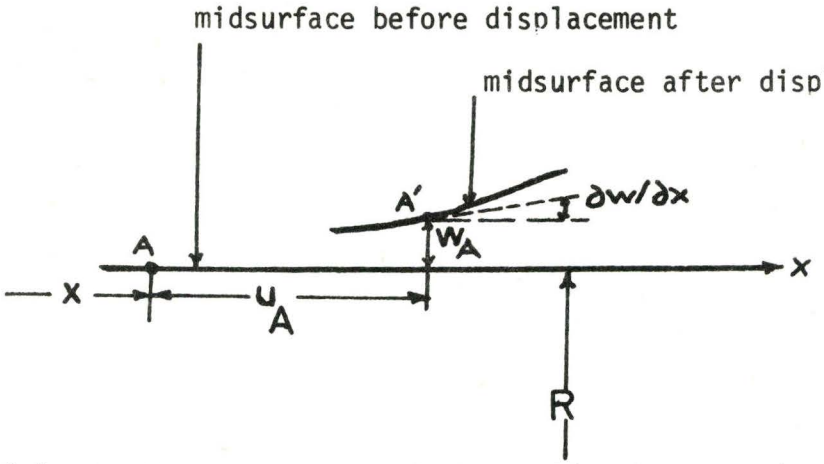

(a) displacement observed along midsurface x-axis

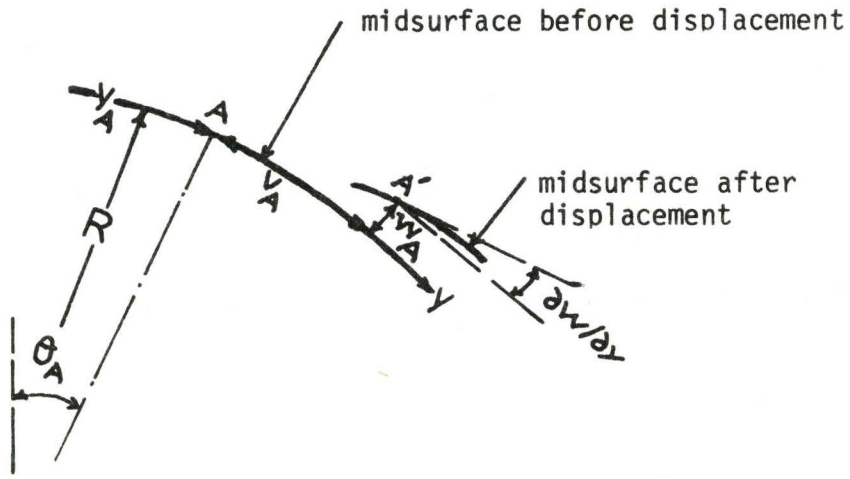

(b) displacement observed along midsurface circumference

FIGURE 2.6 Displacement Co-ordinates

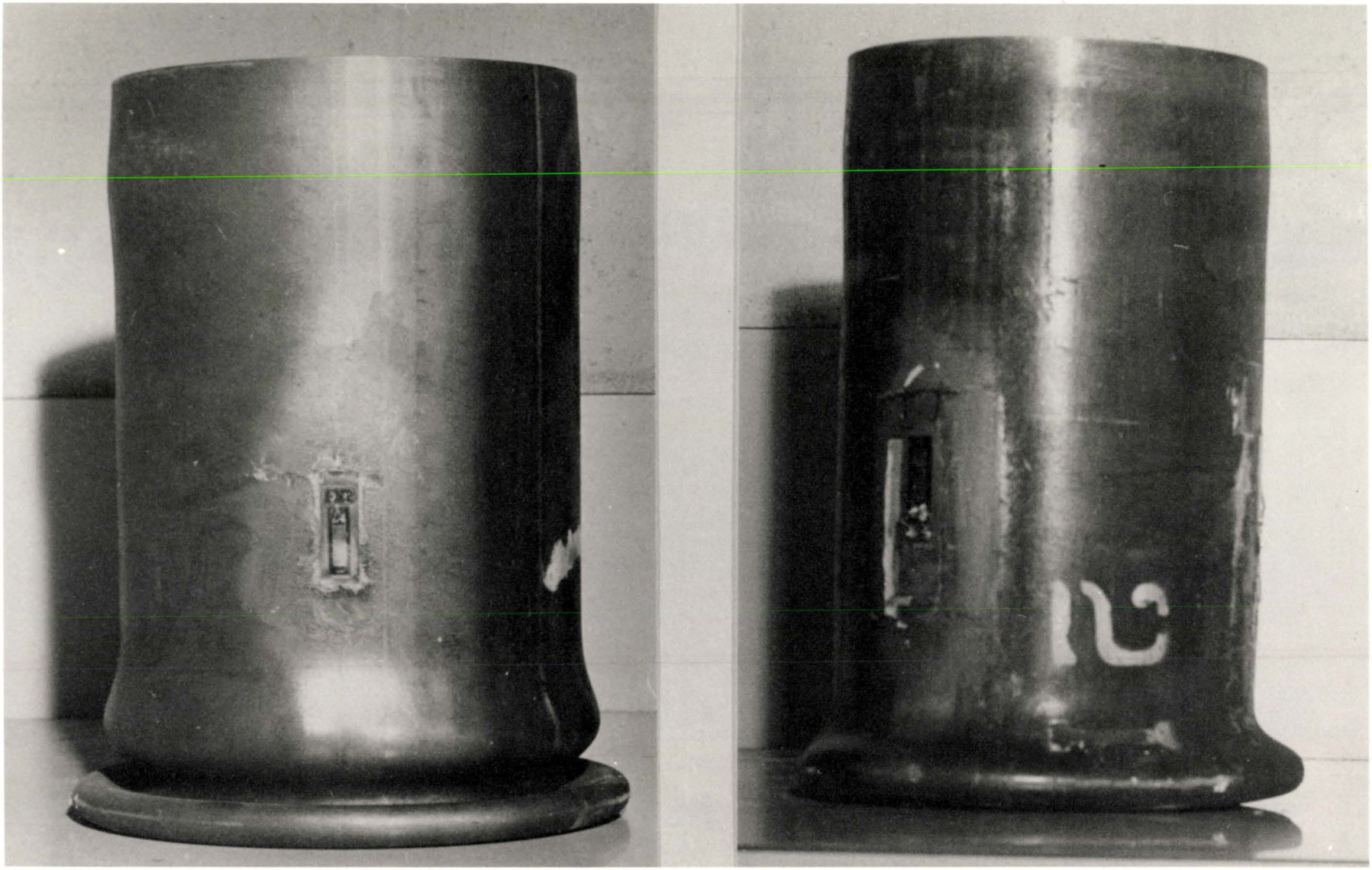

(a) HSS 6.625 O.D. X 0.188

(b) HSS 4.5 O.D. X 0.156

FIGURE 2.7 Stub Columns After Test

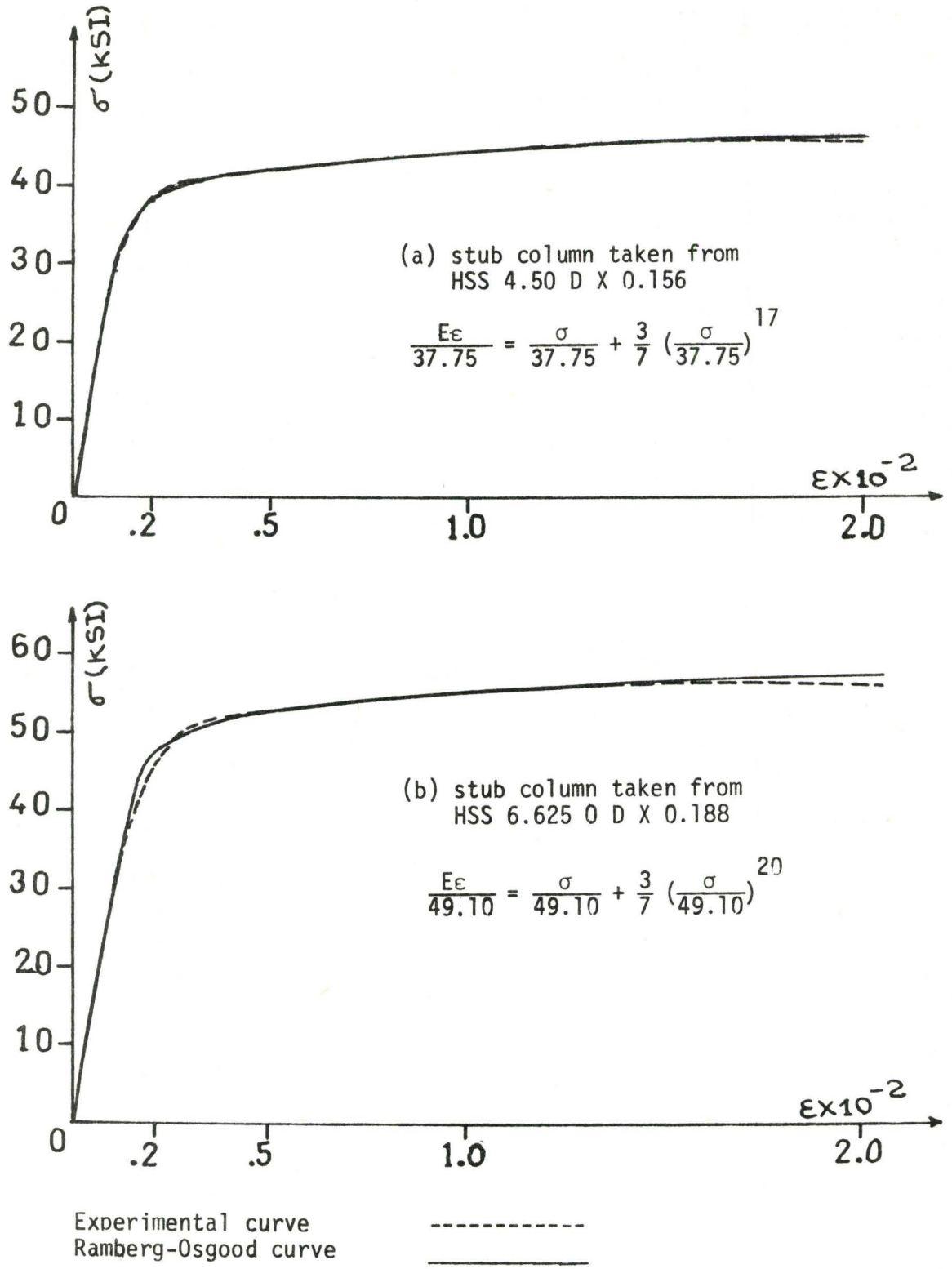

FIGURE 2.8 Idealised Stress-Strain Relationships

$\frac{m\pi R}{L}$ \ D/t	20	30	40	50	60	70	80
0.5	-2.1×10^{11}	1.9×10^{43}	3.4×10^{31}	2.0×10^{23}	8.3×10^{16}	4.6×10^{11}	1.3×10^{7}
1.0	1.5×10^{15}	1.9×10^{29}	4.0×10^{17}	2.8×10^{9}	1.4×10^{3}	9.1×10^{-3}	2.9×10^{-7}
1.5	4.2×10^{17}	2.9×10^{16}	2.6×10^{5}	3.4×10^{-3}	2.0×10^{-9}	2.2×10^{-14}	3.0×10^{-18}
2.0	4.3×10^{19}	3.9×10^{9}	1.1×10^{1}	7.0×10^{-6}	$8.7 \times .0^{-11}$	7.4×10^{-15}	2.4×10^{-18}
3.0	6.2×10^{22}	5.3×10^{11}	1.1×10^{4}	1.4×10^{-2}	2.3×10^{-7}	2.2×10^{-11}	6.9×10^{-15}
4.0	2.6×10^{25}	2.1×10^{14}	4.8×10^{6}	7.3×10^{0}	1.5×10^{-4}	1.7×10^{-8}	6.8×10^{-12}
6.0	2.7×10^{30}	1.1×10^{19}	1.5×10^{11}	1.2×10^{5}	1.1×10^{0}	2.5×10^{-6}	-4.6×10^{-8}
8.0	3.2×10^{35}	8.0×10^{23}	4.5×10^{15}	1.7×10^{9}	-1.2×10^{5}	-1.9×10^{1}	-8.8×10^{-3}
10.0	2.0×10^{40}	4.0×10^{28}	2.1×10^{12}	1.7×10^{12}	-1.7×10^{9}	-1.8×10^{5}	-2.4×10^{1}
12.0	3.7×10^{44}	7.0×10^{32}	3.8×10^{24}	9.0×10^{17}	-6.1×10^{12}	-8.3×10^{8}	-1.2×10^{4}
15.0	1.1×10^{50}	2.0×10^{38}	1.1×10^{30}	3.0×10^{23}	1.1×10^{18}	-4.1×10^{13}	-1.3×10^{10}
20.0	2.2×10^{57}	4.0×10^{45}	2.3×10^{37}	9.5×10^{30}	5.3×10^{25}	1.4×10^{21}	5.7×10^{16}

TABLE 2.1 Stability Criterion - Coarse Grid (8 terms)

$\frac{m\pi R}{L}$ \ D/t	40	42	44	46	48	50
6	1.5×10^{11}	9.9×10^{10}	4.7×10^{9}	2.5×10^{8}	1.5×10^{7}	1.2×10^{5}
6.5	1.8×10^{12}	8.3×10^{10}	4.1×10^{9}	2.2×10^{8}	1.3×10^{7}	7.3×10^{5}
7.0	2.4×10^{13}	9.2×10^{11}	3.9×10^{10}	1.6×10^{9}	5.4×10^{7}	-1.3×10^{6}
7.5	3.2×10^{14}	1.1×10^{13}	4.3×10^{11}	1.2×10^{10}	-1.5×10^{8}	-1.0×10^{8}
8.0	4.5×10^{15}	1.6×10^{14}	5.7×10^{12}	1.4×10^{11}	-6.4×10^{9}	-1.7×10^{9}
8.5	7.3×10^{16}	2.5×10^{15}	8.8×10^{13}	2.3×10^{12}	-6.5×10^{10}	-2.4×10^{10}
9.0	1.1×10^{18}	3.9×10^{16}	1.4×10^{15}	4.5×10^{13}	1.1×10^{11}	-2.3×10^{11}
10.0	2.1×10^{20}	8.0×10^{18}	3.2×10^{17}	1.3×10^{16}	4.6×10^{14}	1.7×10^{12}

TABLE 2.2 Stability Criterion - Medium Grid (8 terms)

TABLE 2.3 Stability Criterion - Fine Grid (8 terms)

$\frac{m\pi R}{L}$ \ D/t	46.0	46.5	47.0	47.5	48.0
7.5	1.2×10^{10}	6.8×10^{9}	2.1×10^{9}	3.9×10^{8}	-1.5×10^{8}
8.0	1.4×10^{11}	4.2×10^{10}	6.8×10^{9}	-4.4×10^{9}	-6.4×10^{9}
8.5	2.3×10^{12}	7.7×10^{11}	1.8×10^{11}	-1.5×10^{10}	-6.5×10^{10}
9.0	4.5×10^{13}	1.7×10^{13}	6.1×10^{12}	1.7×10^{12}	1.1×10^{11}

TABLE 2.4 Stability Criterion - Fine Grid (12 terms)

$\frac{m\pi R}{L}$ \ D/t	46.0	46.5	47.0	47.5	48.0
7.5	1.1×10^{20}	1.9×10^{19}	6.2×10^{18}	6.6×10^{17}	-2.5×10^{17}
8.0	1.3×10^{21}	2.7×10^{20}	3.0×10^{19}	-1.5×10^{19}	-1.5×10^{19}
8.5	2.9×10^{22}	6.9×10^{21}	1.1×10^{21}	-7.7×10^{19}	-2.1×10^{20}
9.0	6.9×10^{23}	2.4×10^{23}	5.9×10^{22}	1.2×10^{22}	4.4×10^{22}

TABLE 2.5 THEORETICAL DESIGN CRITERIA

(a) Stress-characteristics given by equation (23)

Buckling Parameters \ Category	Plastic Design	Allowable Stress Design	
		Compact	Non-Compact
ε_c	0.009310	0.007300	0.005000
σ_{cb}(ksi)	44.14	43.38	42.15
Θ_b	4.0	2.93	1.71
Limiting D/t Ratio	47	60	88

(b) Stress-characteristics given by equation (24)

Buckling Parameters \ Category	Plastic Design	Allowable Stress Design	
		Compact	Non-Compact
ε_c	0.011707	0.007500	0.005000
σ_{cb}	55.98	54.46	52.93
Θ_b	4.0	2.23	1.16
Limiting D/t Ratio	36	56	85

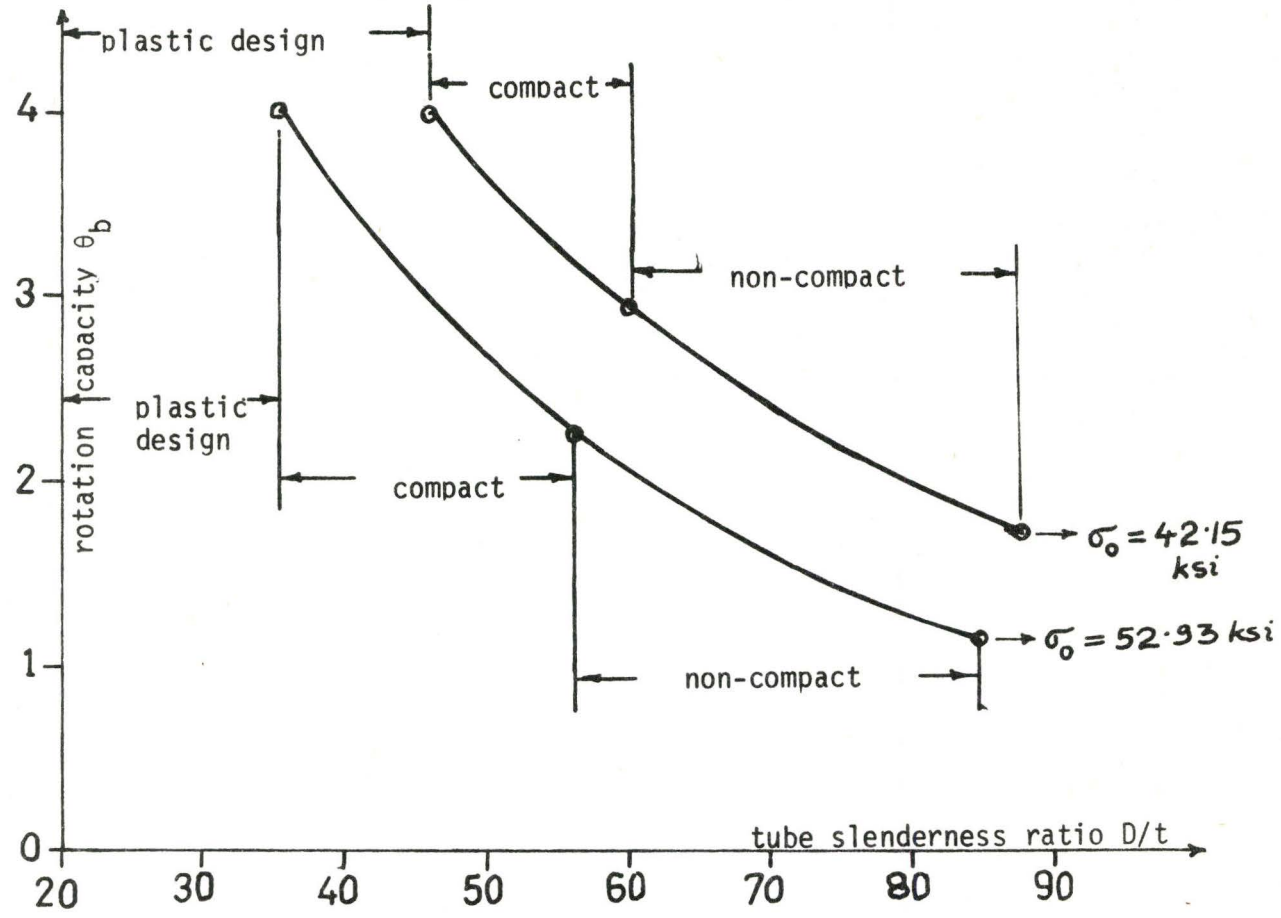

FIGURE 2.9 Theoretical Results

CHAPTER 3

EXPERIMENTAL PROGRAM

3.1 Testing Method

HSS are manufactured by the Steel Co. of Canada Ltd., suppliers of the test sections in two ways:

(a) Hot-forming if the periphery of the section does not exceed 16 inches, and

(b) Cold-forming if the periphery of the section exceeds 16 inches.

Most of the sections investigated were cold-formed. The round HSS for the test series were selected to provide a range of tube slenderness ratios, D/t, for plastic design, compact and non-compact categories. The rectangular sections selected were in the intermediate flange slenderness ratio, b/t, range.

The test sections are listed in Table 3.1 designated as HSS DXBXt if rectangular or HSS DXt if round as shown in Figure 3.1.

3.2 Material Properties

A typical stress-strain curve obtained from a tension test is shown in Figure 3.2. The yield stress σ_0 is the stress corresponding to a total strain of 0.5% which is easily obtained in routine spot checks in the steel industry. This stress usually corresponds closely to the constant stress at yielding and is close to the stress obtained by the conventional 0.2% offset strain method. The idealised bilinear stress-strain curve is given by the yield strength σ_0, the modulus of elasticity E and the strain-hardening modulus E_{st} obtained from the tension test. This data is used to predict the moment curvature and load-deflection relationships.

HSS material properties as concluded by Hudoba[3] do not vary significantly along the periphery of the cross-section and the material taken at right angles to the seam of the section represents a reasonable sample to assess the material properties. Therefore, the tensile coupons were cut accordingly (Figure 3.1) confirming to ASTM specification[29] A 370 - 65 (14). Strain gauges were mounted on both sides of the coupons to separate the bending effect.

Table 3.1 sumarizes the material properties of the coupons cut from each of the sections. Figure 3.3 shows the stress-strain curves for the material of each section.

The stub columns (2.3.4) tested to determine the material properties in compression were carefully machined with their lengths being about twice their corresponding outside diameters. Each cross-section was machined to an accuracy of $\pm$ 0.001 inch. Three strain gauges were mounted on each specimen 120° apart to check the uniformity of loading during the test.

These tests were performed on the hydraulic testing machine "Tinius Olsen" at a common constant slow strain rate of 100 micro-in/in/sec.

3.3 Preparation for Testing of Beam

(a) Mounting Strain-gauges

During the test series two types of electric strain gauges were used:

(i) EP-08-500BH-120 made by Micro-Measurment Co., Romulus, Michigan in which the specifications for the gauges were as follows:

Resistance in ohms - 120 $\pm$ 0.15%

Gage factor at 75°F - 2.055 $\pm$ 0.5%

Strain Limits - approximately 15%

(ii) HE-181B Budd Fineline TM Strain-gauges made by The Budd Co. Instruments Div., Phonexville, Pa., where the specifications for gauges were as follows:

Resistance in ohms - 120 $\pm$ 0.15%

Gage factor at 75°F - 2.04 $\pm$ 0.5%

Strain Limits - approximately 15%

For the gauge installation M-Bond AE - 10 adhesive was used. The surface preparation, the gauge preparation and installation were made as recommended in the Instruction Bulletin B-137 provided by Micro-Measurements Co., Michigan.

(b) Preparation of Test-apparatus

The load cells were calibrated in the 120 KIPS Tinius Olsen testing machine before each test. The calibration curves were linear and the drift was negligible. The load cells together with the electric strain gauges were connected to a switch and balance box unit which was connected to a strain indicator.

(c) Consideration of Bearing Surface of HSS on Load Points

For the rectangular HSS load was distributed on the surface through a 3" wide bearing plate with a roller as shown in Figure 3.4(a). This was considered satisfactory since the resulting stress concentration would not be too high. It was observed that application of load on the surface of the round HSS through the V-shaped blocks as shown in Figure 3.4(b) results in a considerable stress concentration. The effect is noticeable particularly with high D/t ratio and the subsequent punching of the surface produces a significant drop in the moment carrying capacity. The first four tests on round sections (as described in Chapter 4) were done using only

V-shaped block at each loading point. In the following six tests 3" to 6" wide circular plates taken from the test section itself were used to distribute the load onto the surface as shown in Figure 3.4(c). This device was considered satisfactory to provide a clearer representation of the actual moment carrying capacity of the round HSS.

3.4 Testing Arrangement

(a) Simple Span Beam

The test set up was designed to confirm computed shape factors of HSS as well as to assess the potential problem of local buckling in a pure moment domain. Figure 3.5 shows the overall experimental set up. This experiment was designed to simulate two-point loading on a simple span beam. Two equal vertical loads were applied with a hydraulic jack midway between load points onto the test section through a spreader beam. The load at midspan was measured by a load cell which was located between the jack and a ball and socket support seated on the spreader beam. The central part of the beam between the two load points was therefore subject to uniform moment. Electric resistance strain gauges were placed at midspan, having been mounted on the top and bottom flanges of the test HSS. At the load points the strain gauges were located only on the bottom. One of the strain gauges at midspan was placed at right angles to the direction of bending.

The moment curvature relationship was determined by monitoring the loads with the load cell and the strains by strain gauges.

The vertical deflection at midspan was measured by means of a dial gauge with an accuracy of $\pm$ 0.001 inches. Because the displacements were very large (usually to 10 inches), measurement of deflection was certainly accurate.

(b) Two Span Beam

The test set up was designed to study the effect of moment gradient or shear force on the moment carrying capacity and to assess the moment transfer principle inherent in plastic design. Such a statically indeterminate structure is shown in Figure 3.6. The spans and loading conditions were simulated about the middle support and were designed such that the negative moment at the middle support exceeds the positive moment in the span (Figure 2.2). As the load is increased the negative moment $-M_p$ is initiated over the middle support which must be maintained until $+M_p$ occurs at the major load points at which a mechanism is formed.

Electric strain gauges were mounted on the top flange of HSS at the middle support and on the bottom flanges of major load points. The base of the middle support was reinforced to prevent the settlement. Movement was checked with a precision dial gauge. Negligible displacement was recorded during testing with the conclusion being that the support was rigid. A load cell was placed at the middle support to determine the reaction, thereby making the force system experimentally determinate.

The details associated with this type of test are shown in Figure 3.7.

3.5 Testing Procedure

In the elastic range of the test, the hydraulic pressure was increased in increments to give predetermined elastic behaviour of HSS. The load was maintained at each of these values until all readings had been taken.

After yielding had occurred the midspan deflection was increased in increments to permit sufficient values for plotting a moment curvature relationship. The flow of hydraulic fluid to the ram was then terminated for a short stabilization period before readings were taken. The readings

of the electric strain gauges and dial gauge at midspan for the deflection were recorded for each increment of the load.

The section was deformed well into the yield zone to ensure a rotation from 4 to 8 times the rotation of the elastic limit. For most of the tests flange buckling predominated and the visual observations and measurements of the progression of yielding and local buckling were recorded. This monitoring extended into the unloading range using the above procedure as well.

The redistribution of moments for the two span beam was checked by the load cell at the middle support. The fairly constant readings of this load cell indicated the maintenance of the resisting negative plastic moment $-M_p$ at the interior support until $+M_p$ occurred in the spans. When considerable local buckling was observed at the middle support, the readings of the load cell decreased due to the reduced moment resistance at the section.

The deformations in the sections after completion of tests are shown in Figures 3.8 to 3.10.

---

* The jack used had a maximum travel of 6" only. After every 6" of deflection the jack was released and steel blocks were inserted between the jack and the spreader beam. Meanwhile the test beam was clamped to avoid any unloading.

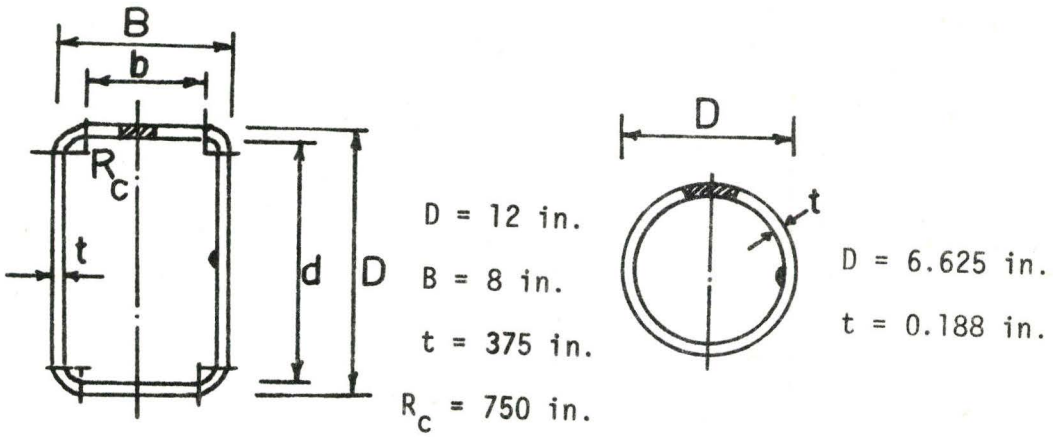

HSS - 12 X 8 X 0.375

HSS - 6.625 O.D.X 0.188

Location of Material for Tensile Coupons

(a) Rectangular

(b) Round

FIGURE 3.1 Hollow Structural Sections

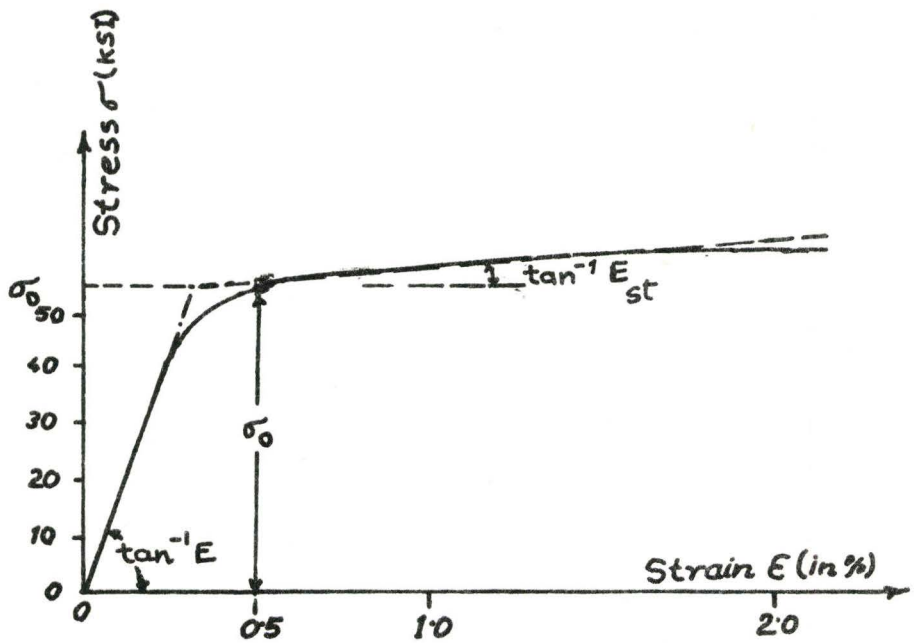

FIGURE 3.2 Typical Stress-Strain Curve

TABLE 3.1

Material Properties Obtained From Tensile Coupons

S.N.	HSS Designation	R_c (in)	σ_0 (ksi)	E_{st} (ksi)	Type of Span	Width of bearing plate if used (in)
1	12.0 X 8.0 X 0.375	0.750	62.5	360	Single	3
2	12.0 X 8.0 X 0.312	0.625	52.6	400	Single	3
3	8.0 X 8.0 X 0.250	0.500	58.0	420	Single	3
4	6.0 X 6.0 X 0.188	0.375	55.5	420	Single	3
5	10.0 X 10.0 X 0.312**	0.624	56.0	280	Single	3
6	8.0 X 6.0 X 0.188**	0.375	54.0	310	Single	3
7	7.0 X 7.0 X 0.188	0.375	57.0	380	Single	3
8	10.0 X 10.0 X 0.250	0.500	61.0	410	Single	3
9	4.5 O D X 0.156*	-	44.8	310	Single	-
10	4.5 O D X 0.156	-	44.8	310	Two	3
11	6.625 O D X 0.156	-	44.2	280	Single	-
12	6.625 O D X 0.188*	-	53.5	370	Single	-
13	20.0 O D X 0.250	-	54.4	290	Single	-
14	10.75 O D X 0.219	-	44.4	490	Single	6
15	10.75 O D X 0.219	-	44.4	490	Two	6
16	12.75 O D X 0.250	-	54.5	650	Single	6
17	14.0 O D X 0.250	-	43.2	400	Single	6
18	16.0 O D X 0.250	-	44.8	255	Single	6

Modulus of Elasticity = 29500 ksi

* These two sections were also tested as stub columns and their behaviour in compression is shown in Figure 2.8.

** The actual thickness of these sections was found to be 0.302 (No. 5) and 0.180 (No. 6) inch.

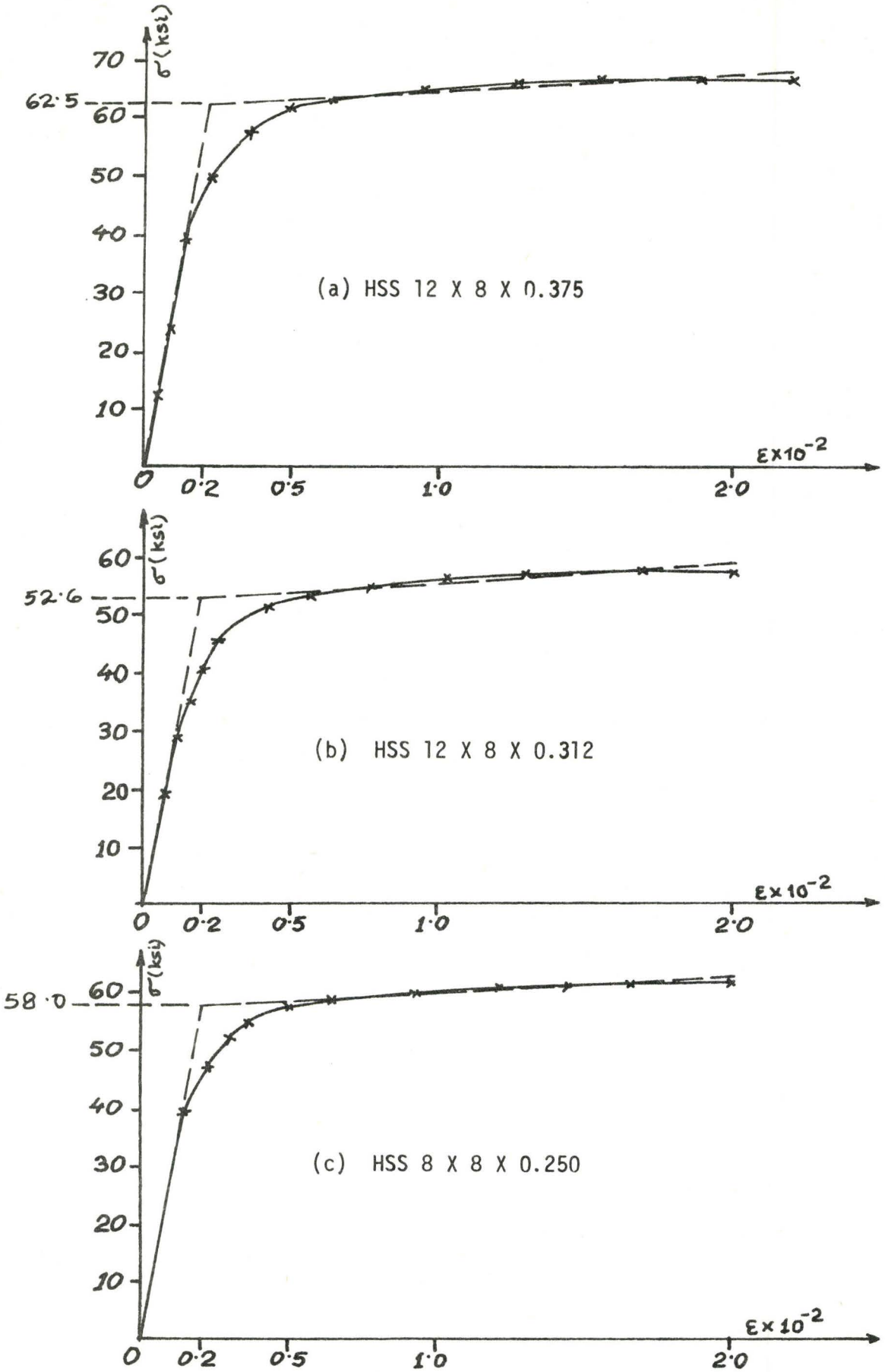

FIGURE 3.3 Coupon Test Results (continued)

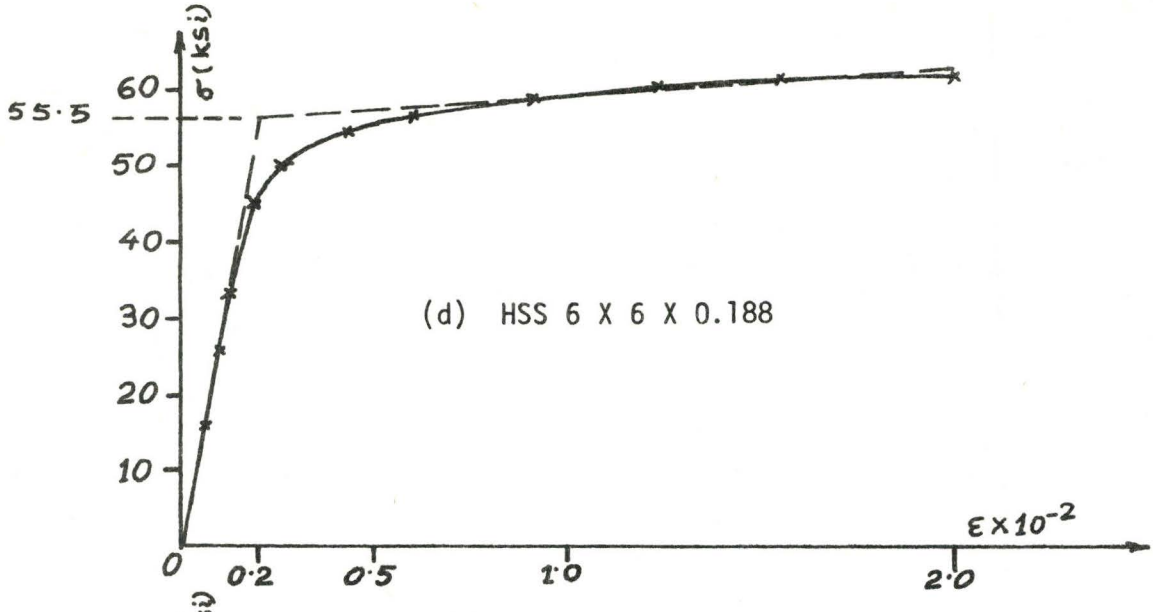

(d) HSS 6 X 6 X 0.188

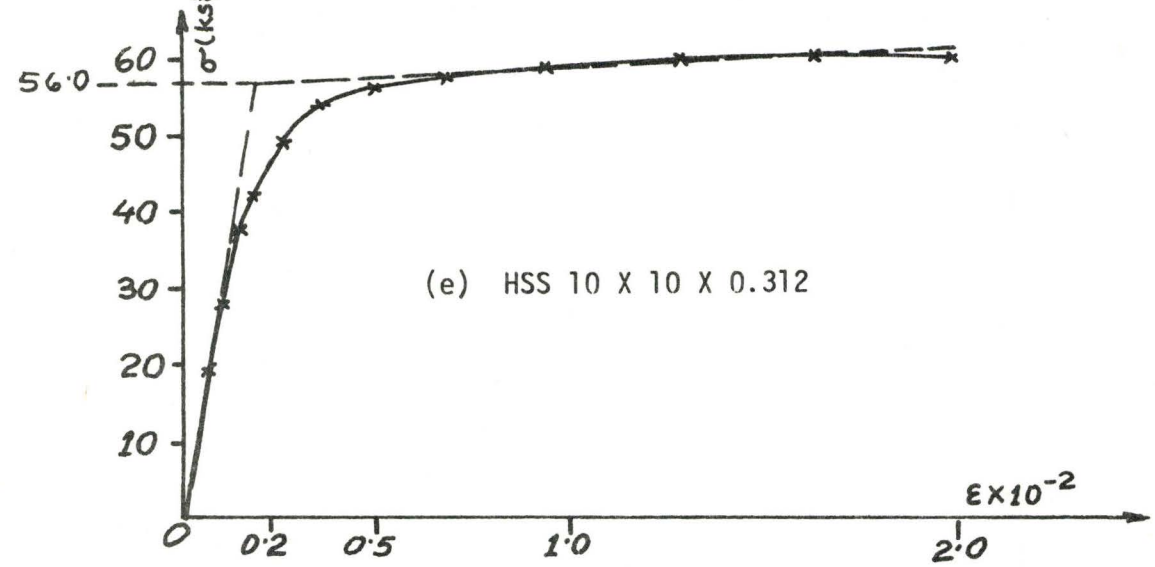

(e) HSS 10 X 10 X 0.312

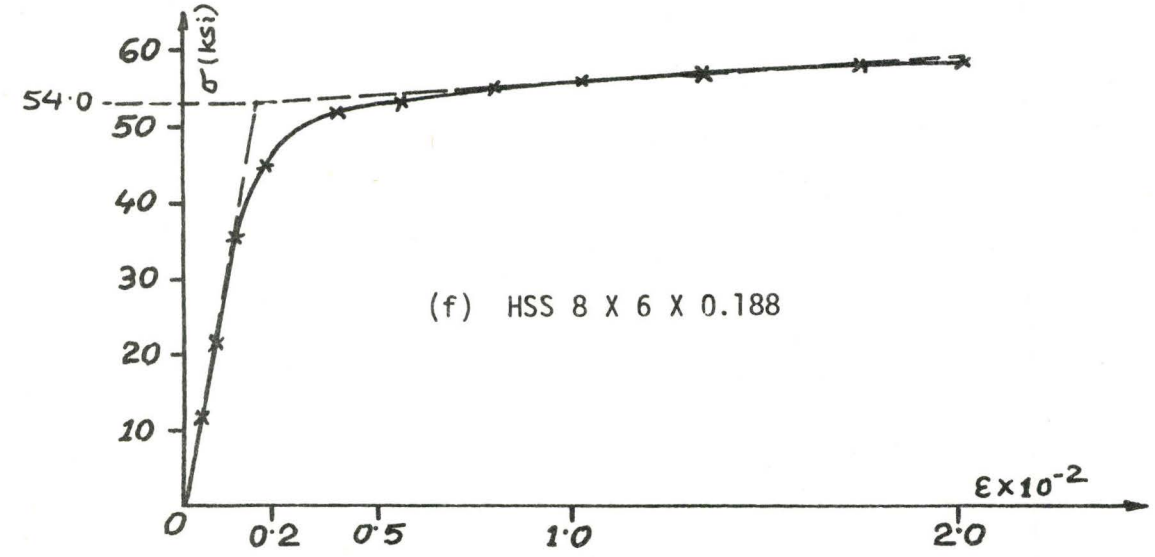

(f) HSS 8 X 6 X 0.188

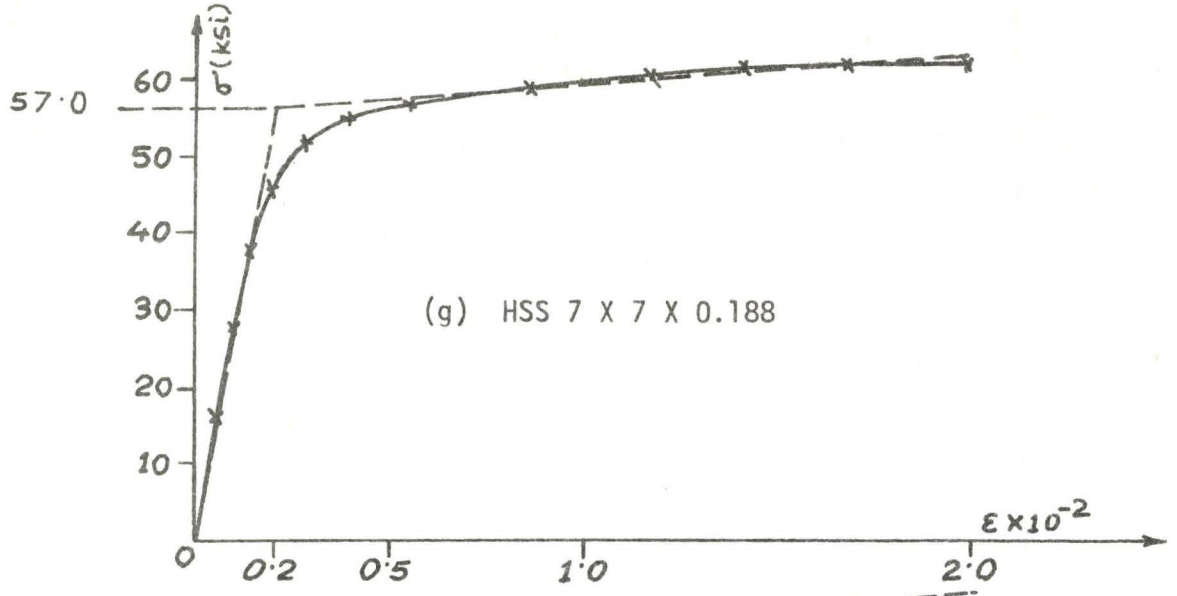

(g) HSS 7 X 7 X 0.188

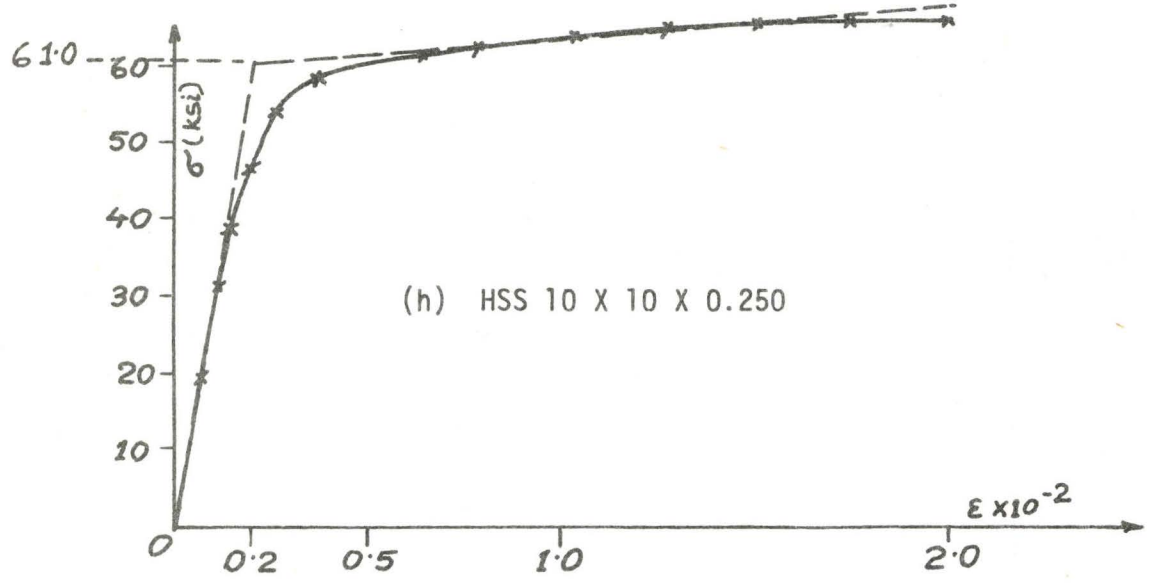

(h) HSS 10 X 10 X 0.250

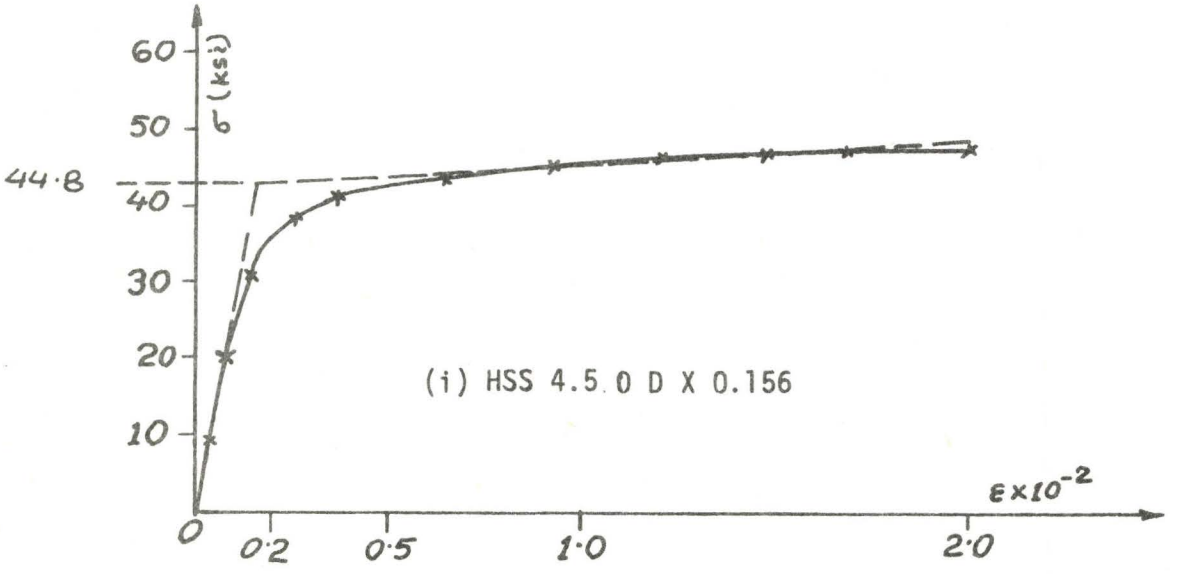

(i) HSS 4.5.0 D X 0.156

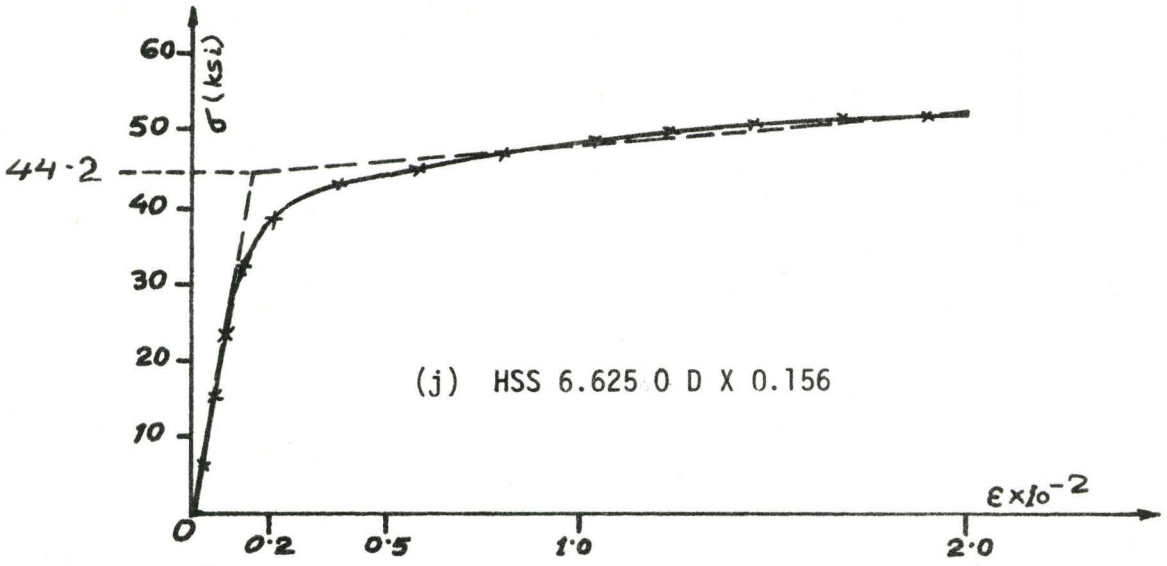

(j) HSS 6.625 0 D X 0.156

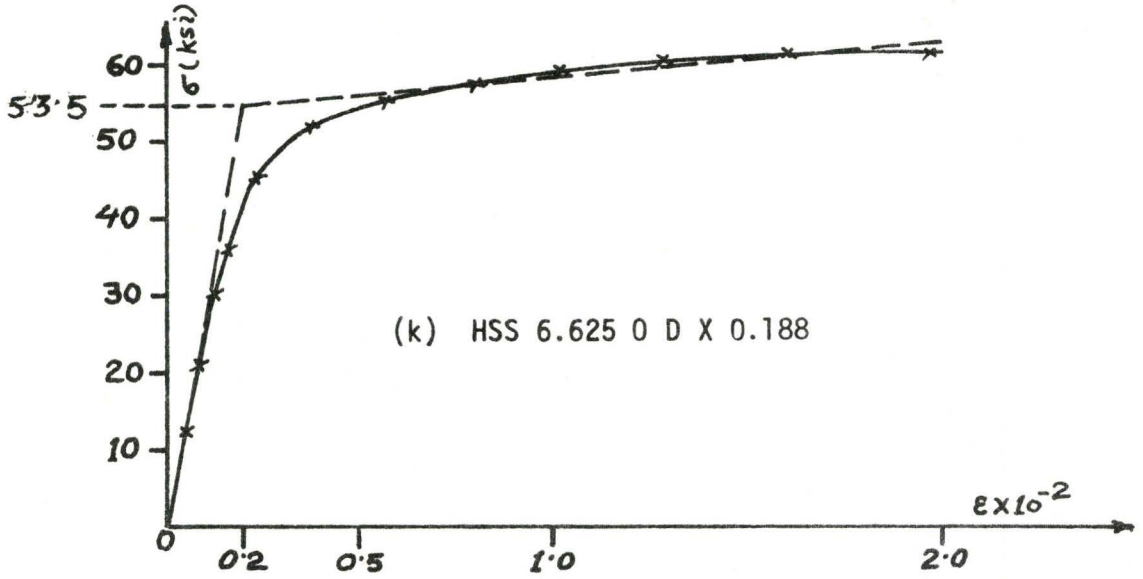

(k) HSS 6.625 0 D X 0.188

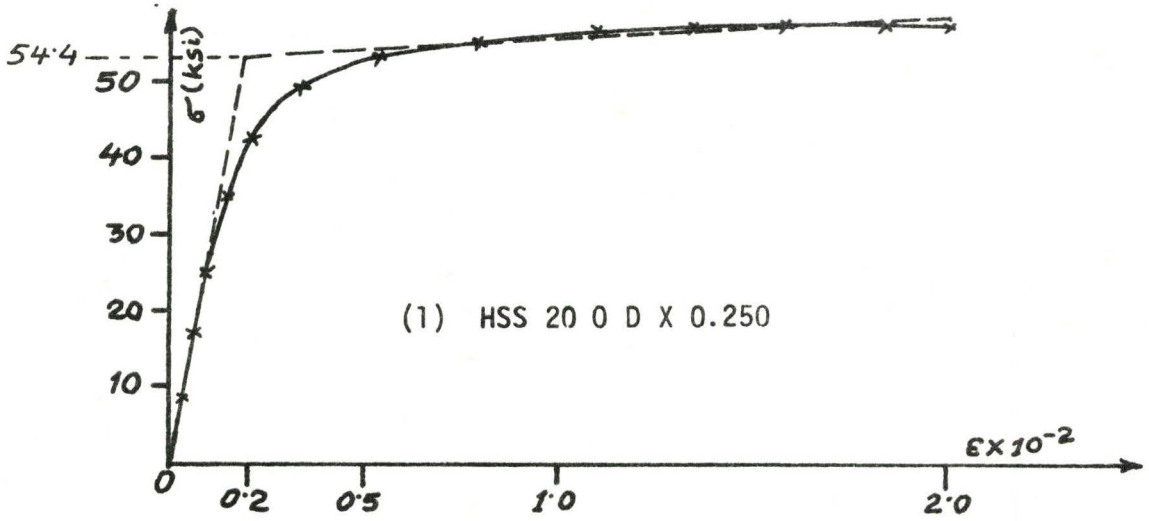

(l) HSS 20 0 D X 0.250

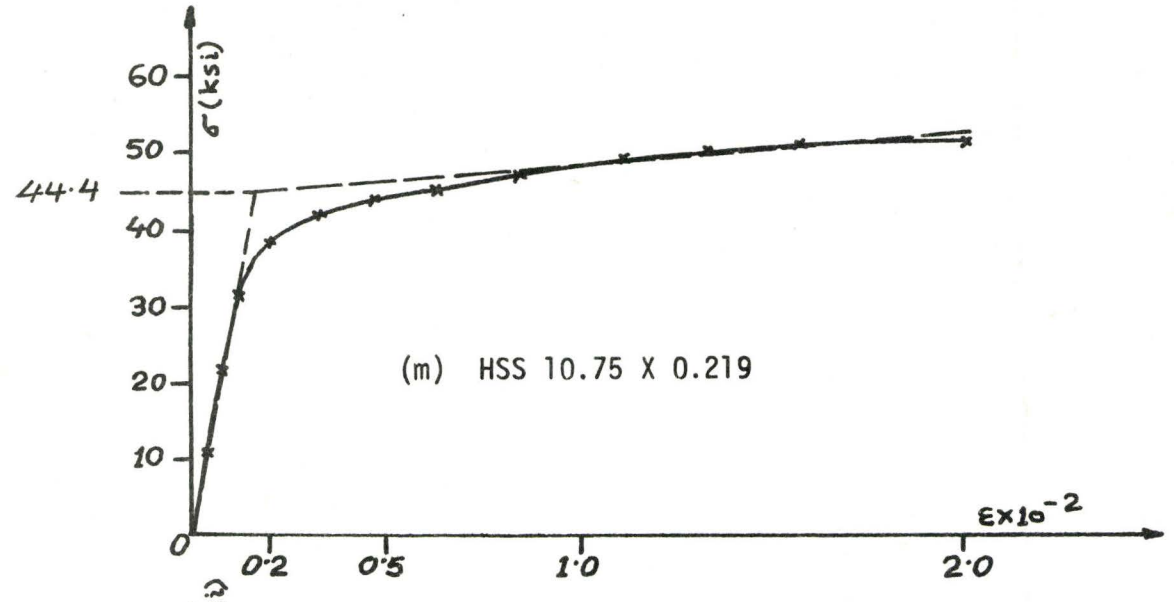

(m) HSS 10.75 X 0.219

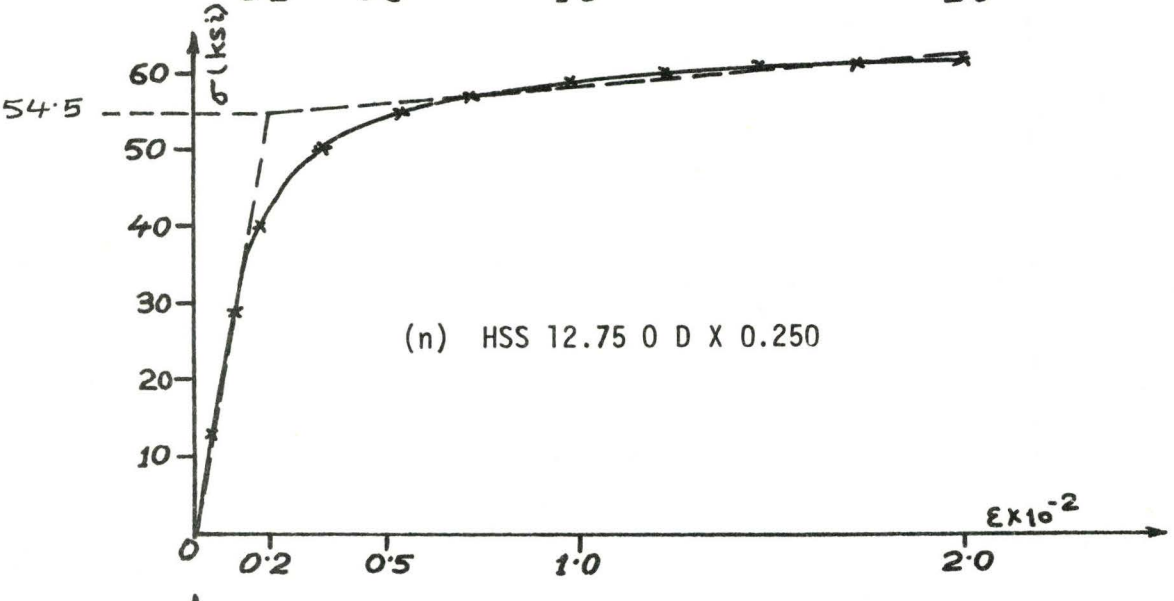

(n) HSS 12.75 O D X 0.250

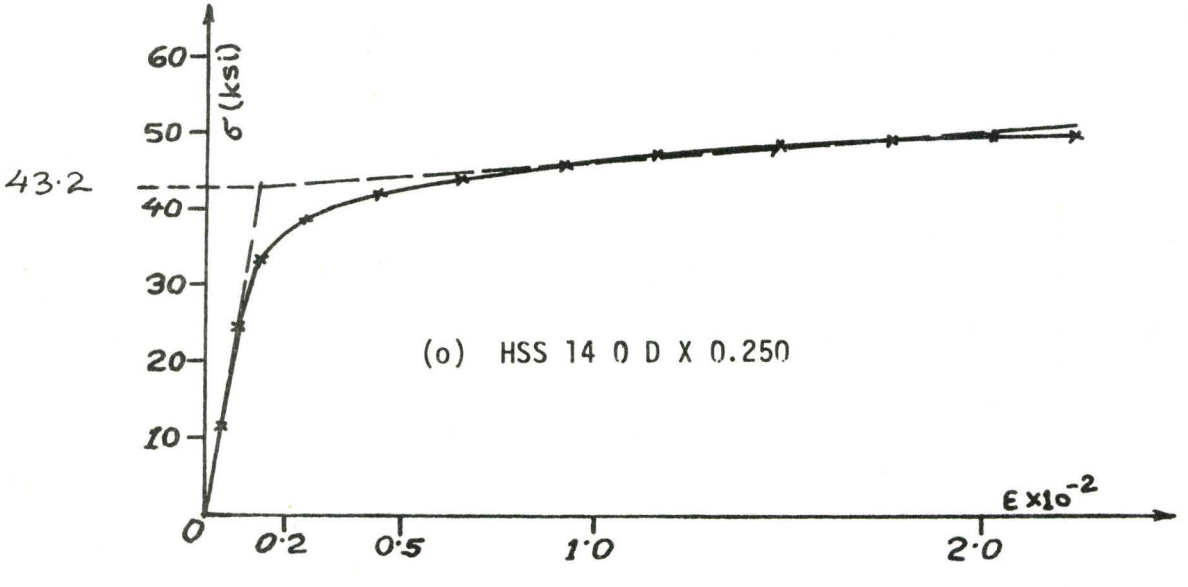

(o) HSS 14 O D X 0.250

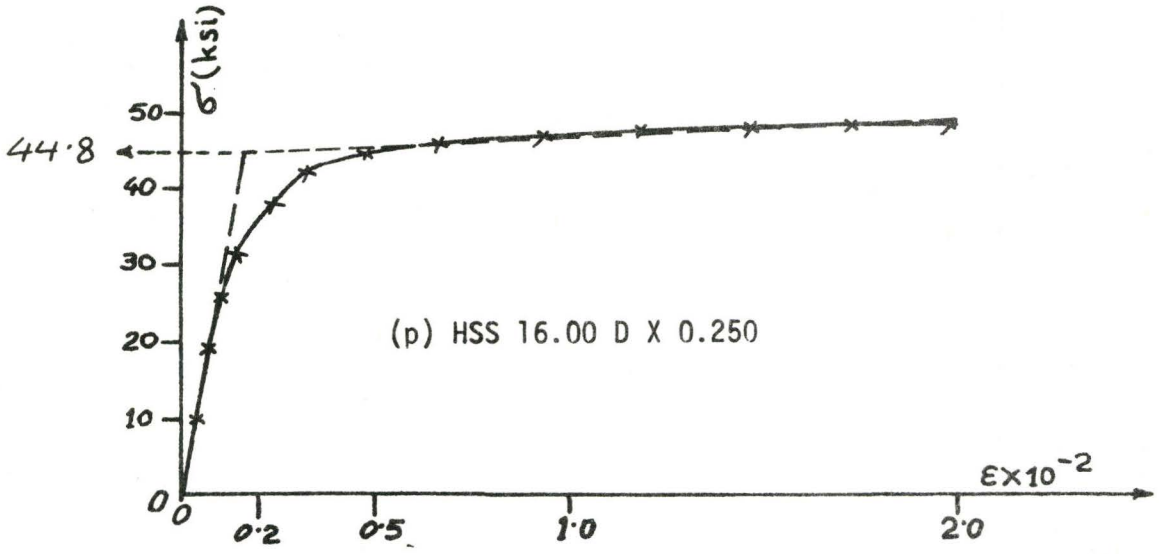

(p) HSS 16.00 D X 0.250

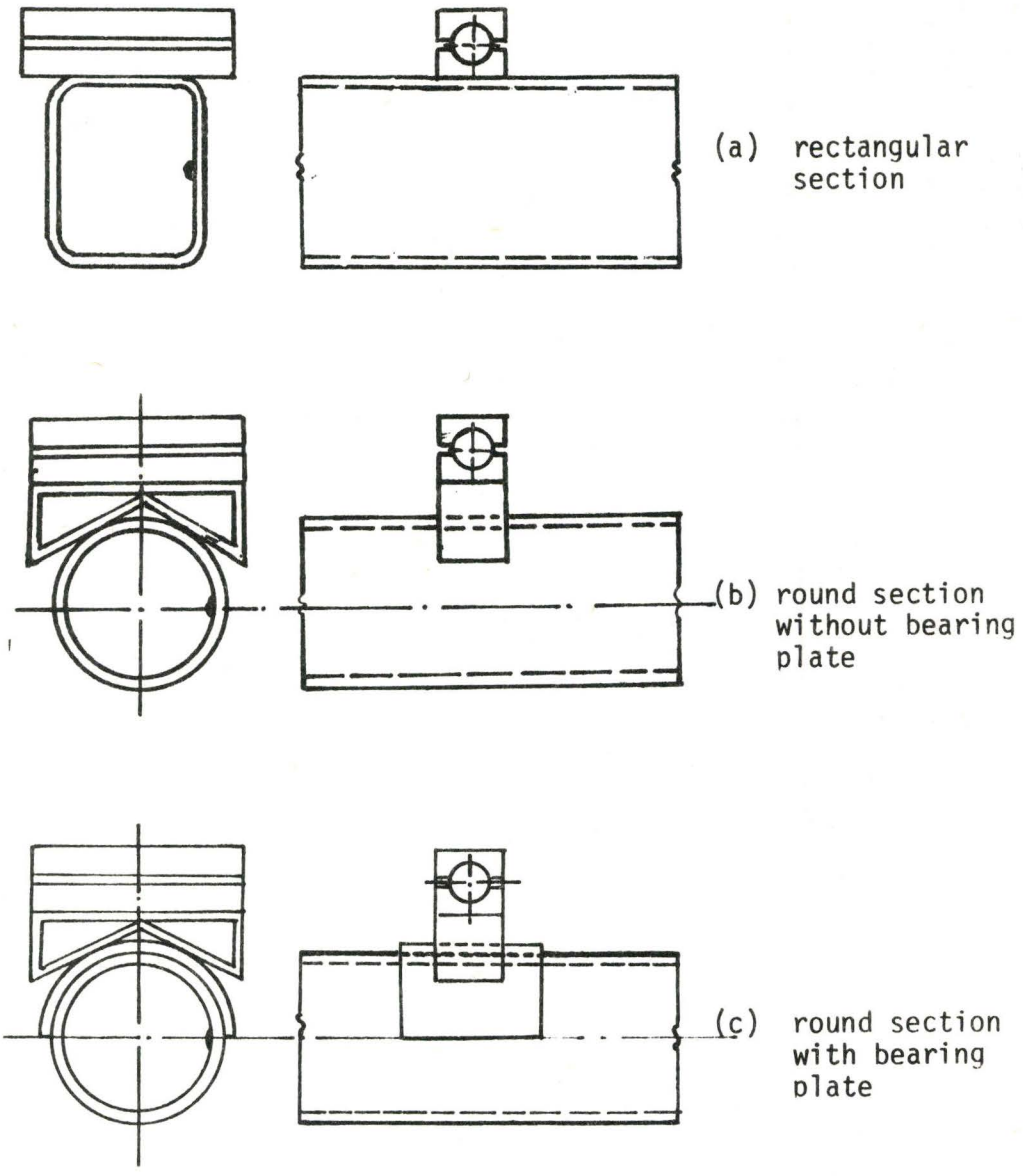

FIGURE 3.4 Bearing Surface of HSS on Load Points

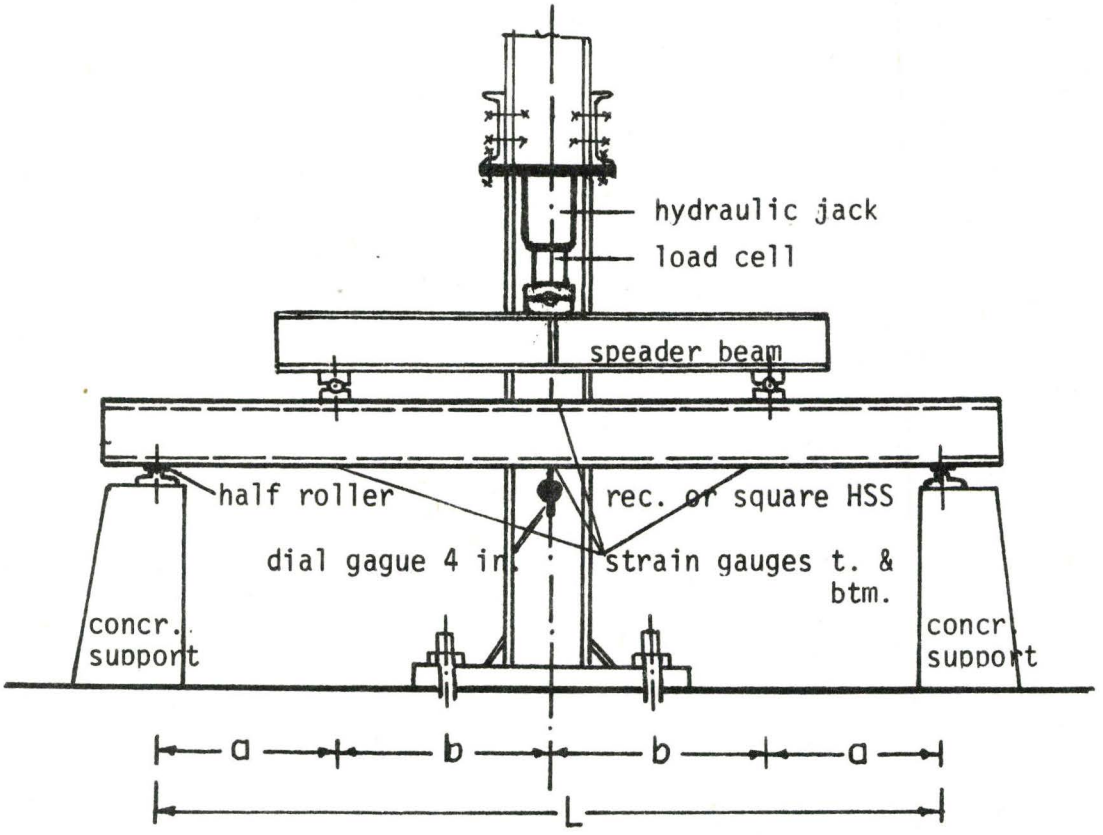

FIGURE 3.5 Details of Loading - Simple Span

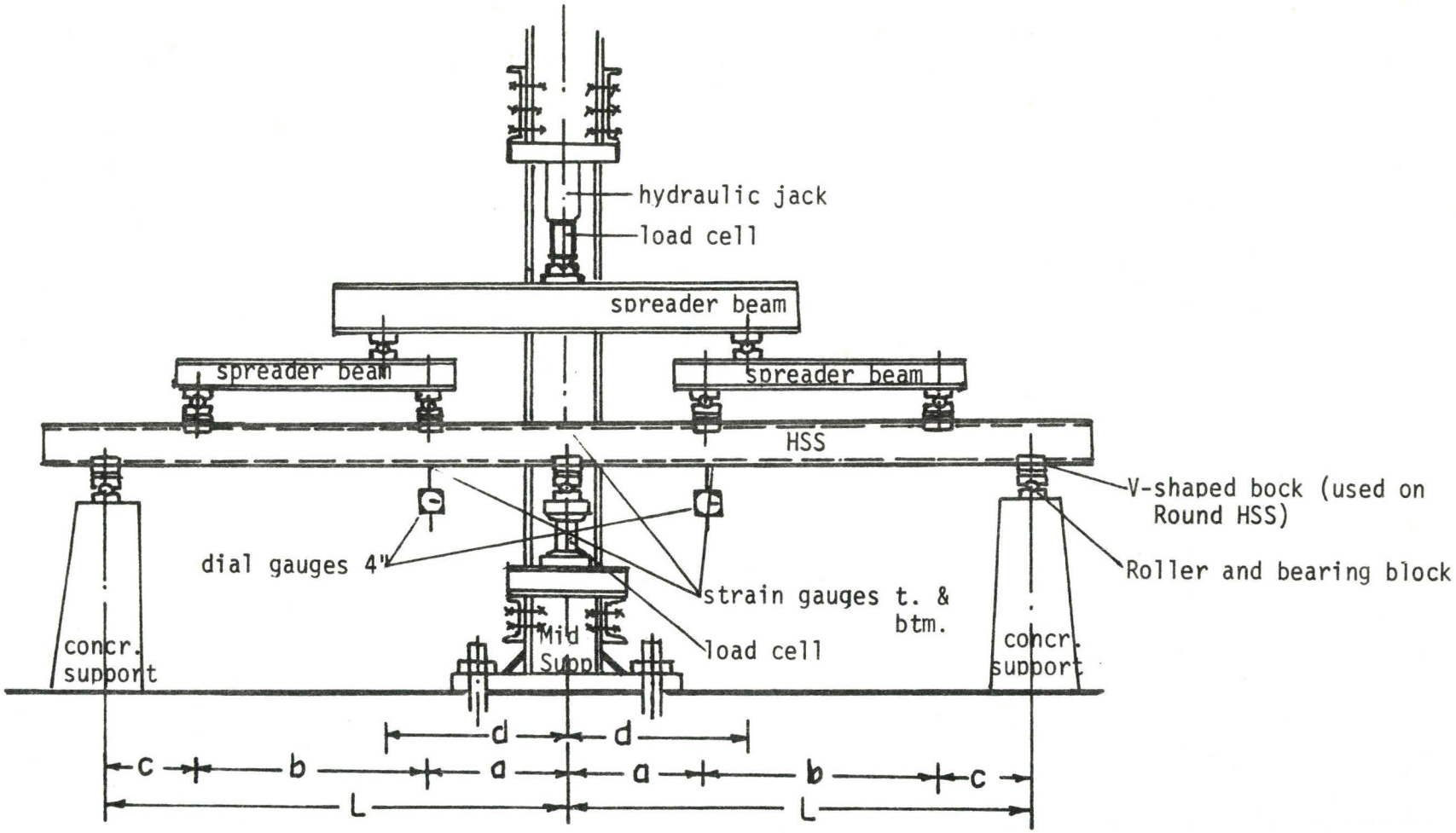

a ≃ 0.3L
b ≃ 0.5L
c ≃ 0.2L
d ≃ 0.4L

FIGURE 3.6 Details of Loading - Two Span Beam

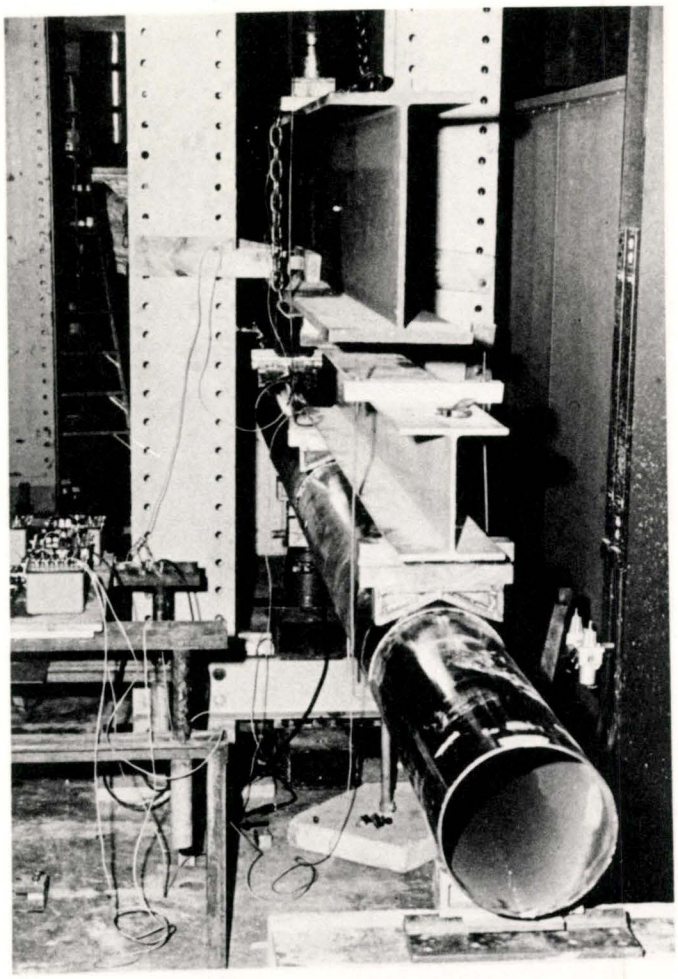

(a) Overall View

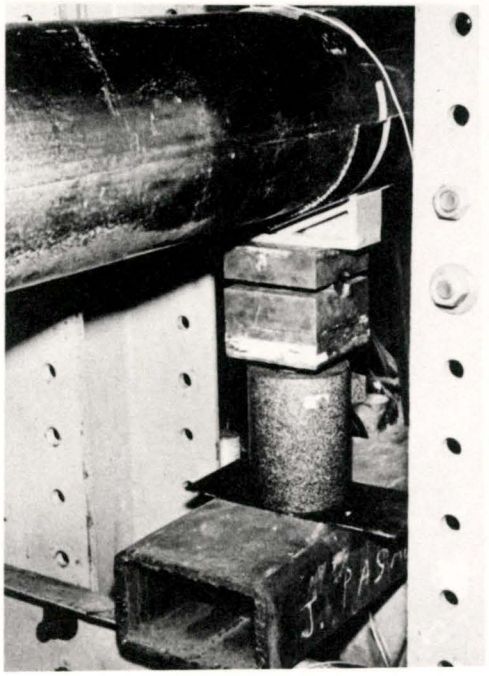

(b) Middle Support

Figure 3.7 Details of Test Arrangement - Two Span Beam

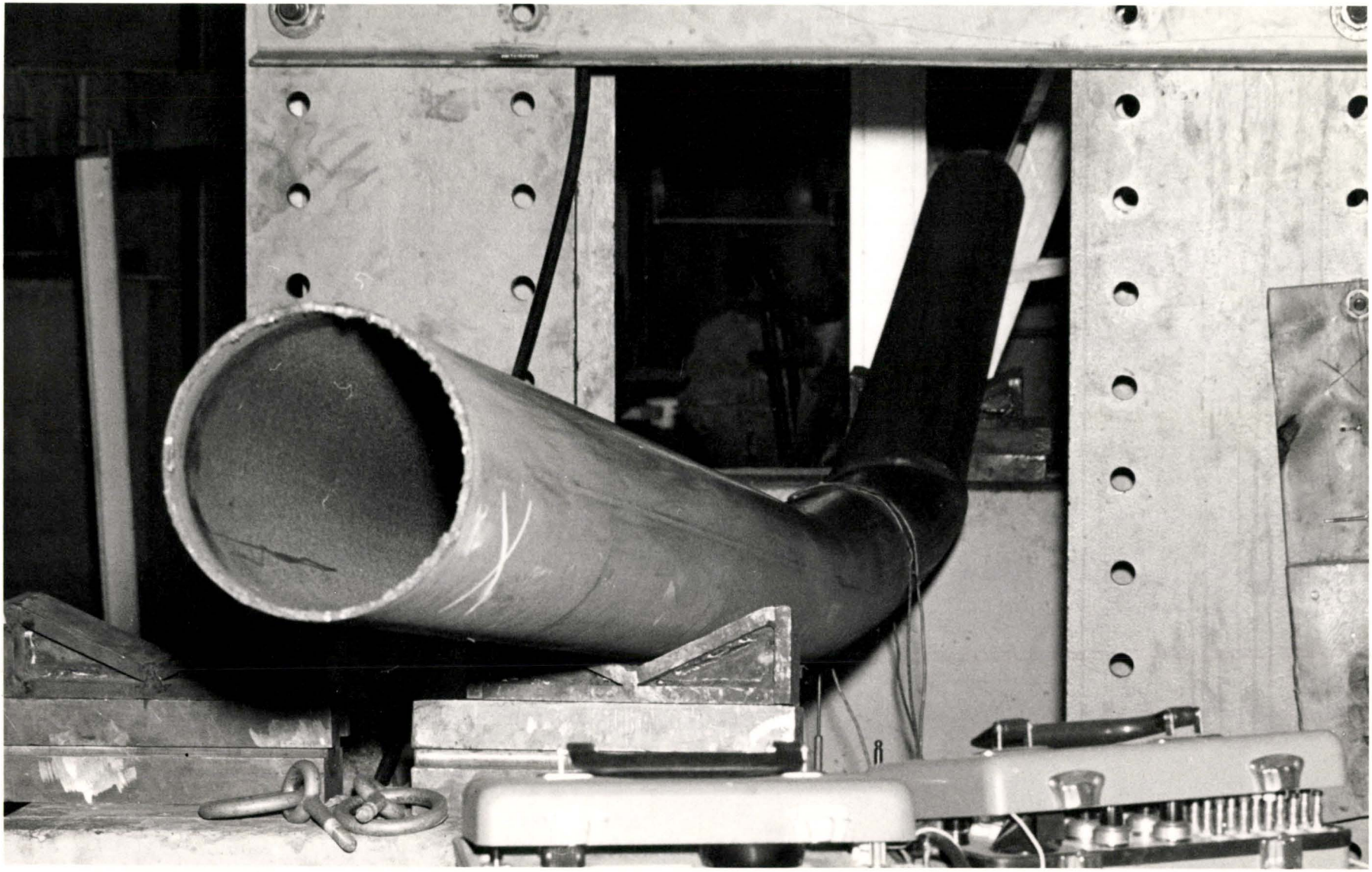

(a) Overall View of Deformations

FIGURE 3.8 Simple Span Test - HSS 6.625 O.D. X 0.156

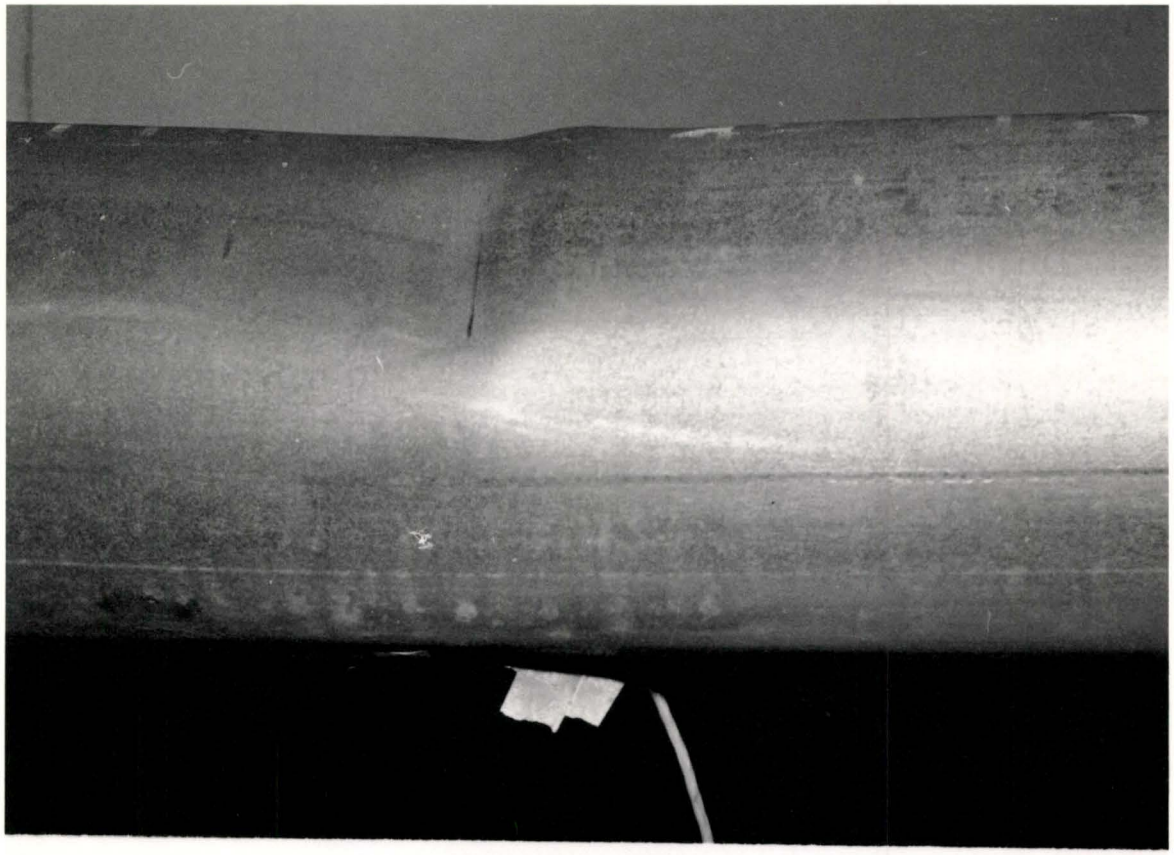

(b) Minor Buckle

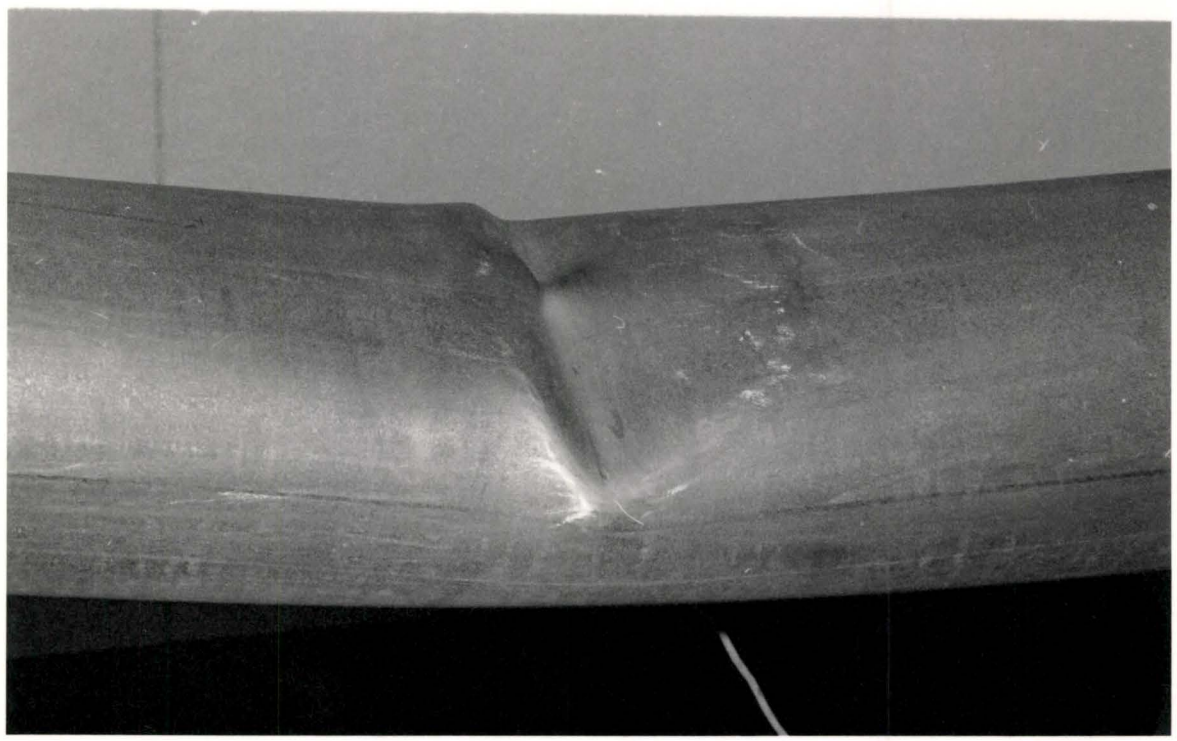

(c) Major Buckle

FIGURE 3.8 Simple Span Test - HSS 6.625 O.D. X 0.156

(a) Overall View of Deformations

FIGURE 3.9 Simple Span Test – HSS 10.75 O.D. X 0.219

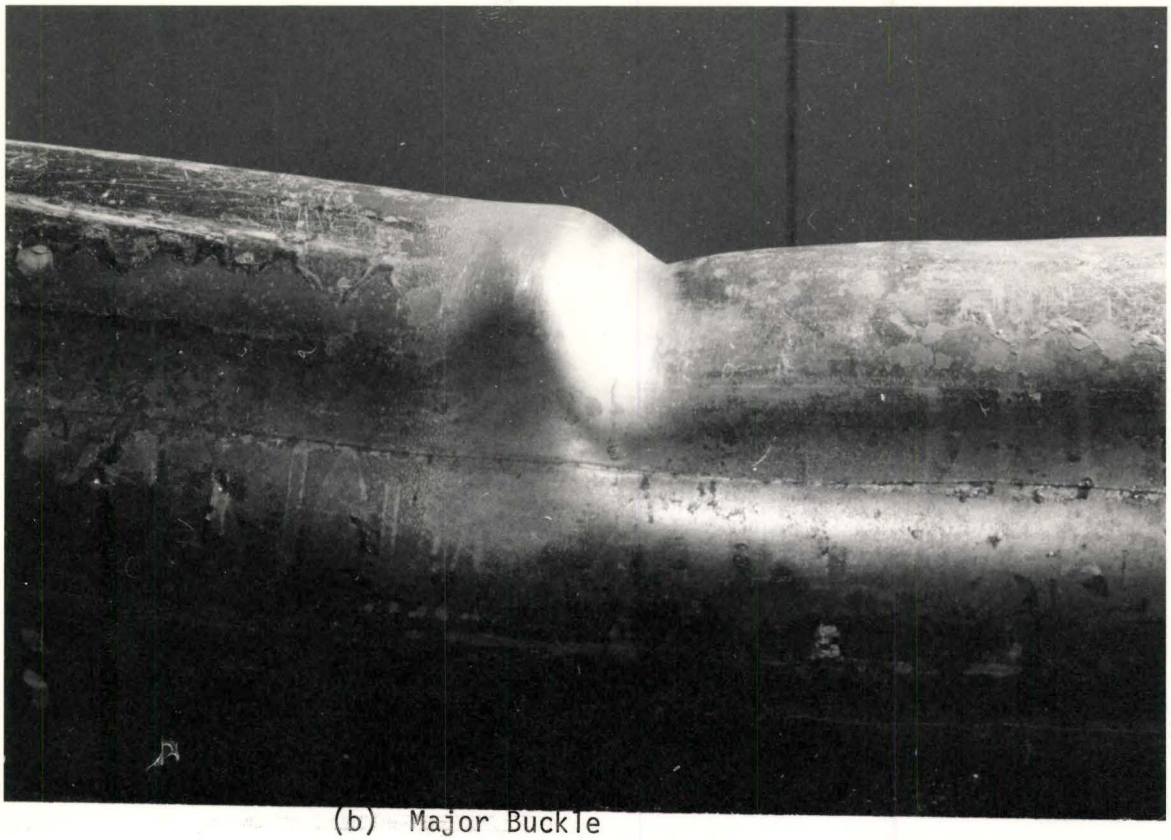

(b) Major Buckle

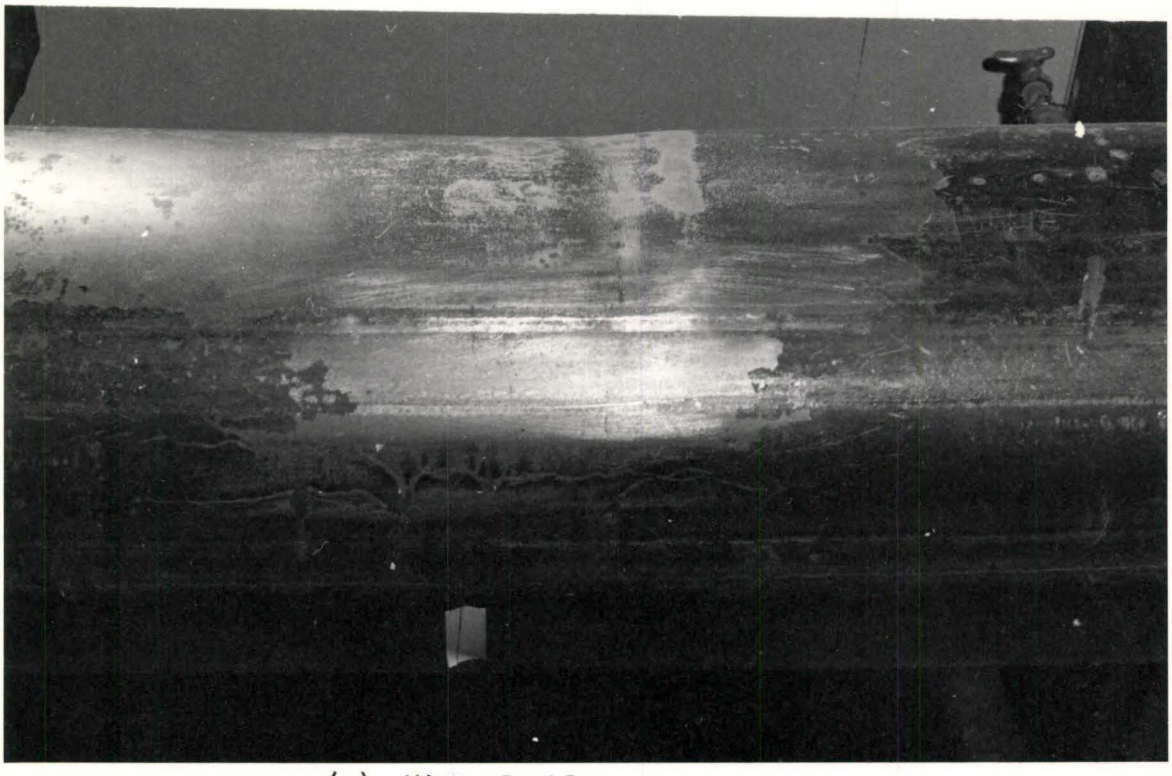

(c) Minor Buckle

FIGURE 3.9 Simple Span Test – HSS 10.75 O.D. X 0.219

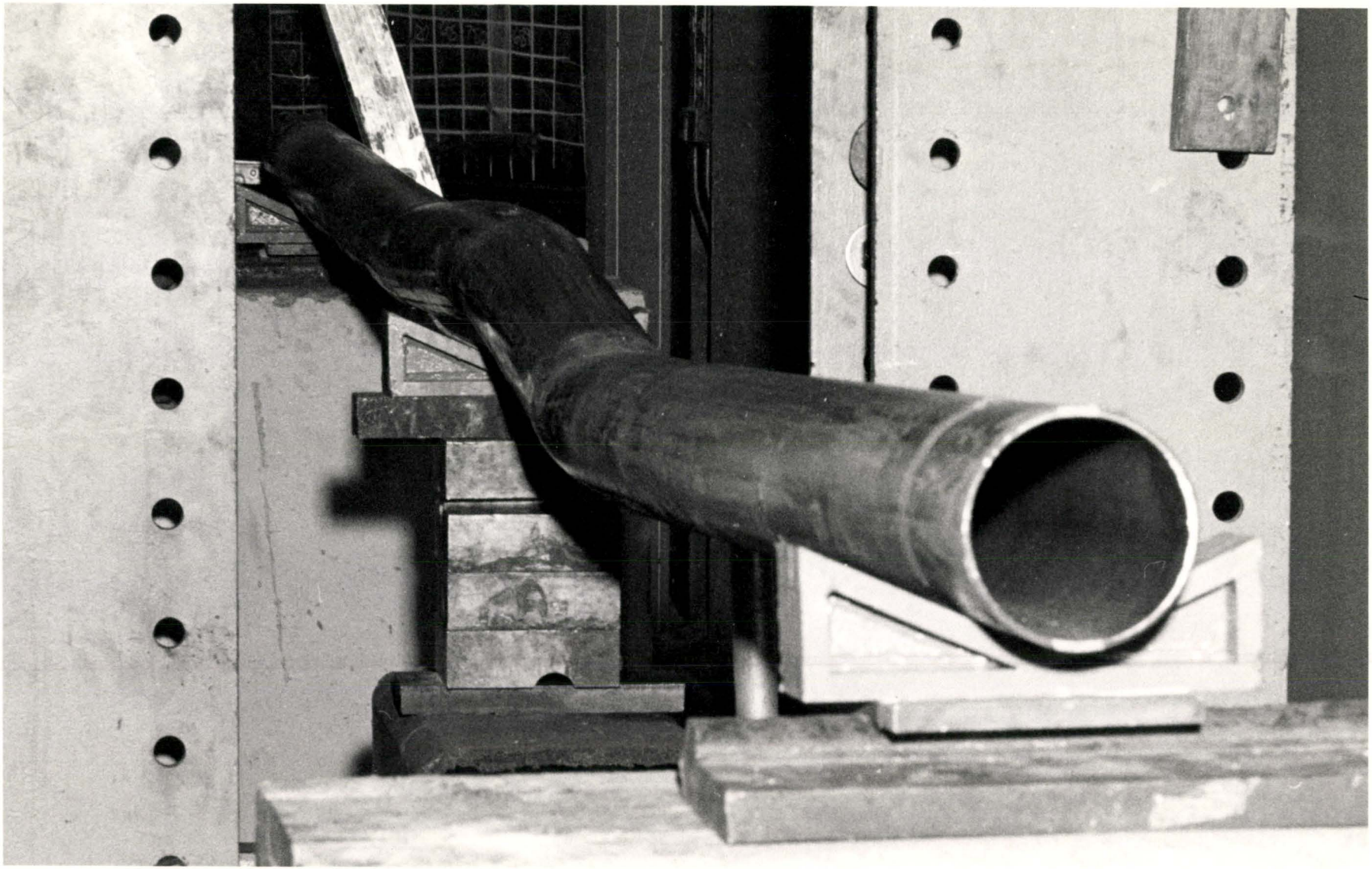

(a) Overall View of Deformations

FIGURE 3.10 Two Span Test - HSS 4.5 O.D. X 0.156

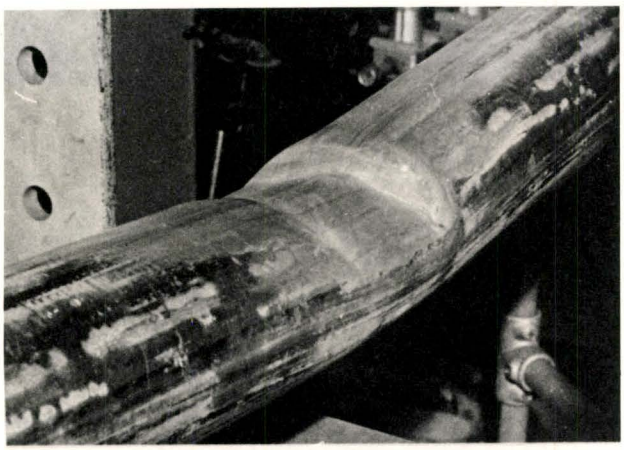

(a) Buckling at Middle Support

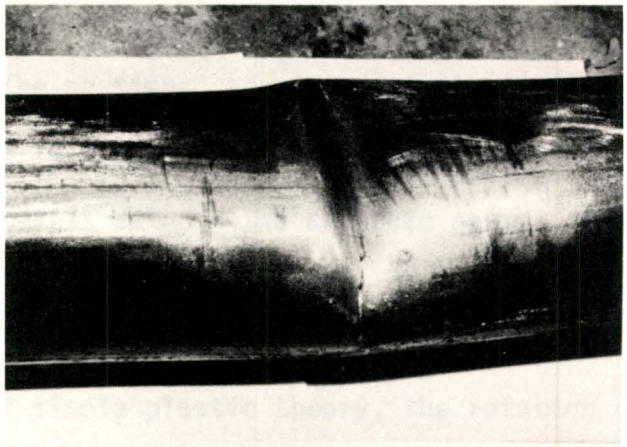

(b) Major Buckle in the Span

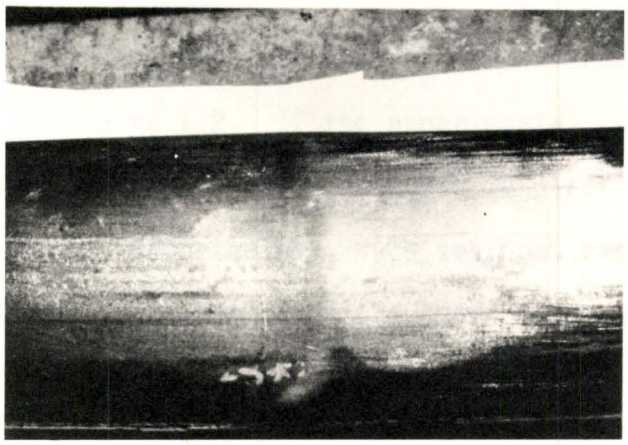

(c) Minor Buckle in the Span

Figure 3.10 Two Span Test - HSS 4.50 O.D. X 0.156

CHAPTER 4

EXPERIMENTAL RESULTS AND DISCUSSION

4.1 Preliminaries

An attempt is made in this chapter to compare the experimental results of HSS with those predicted by analysis. On this basis, a design criterion to categorise the sections, according to plastic and allowable stress methods of design, is established and compared with available design standards. This work is dealt with in two separate parts:

(a) Performance of rectangular HSS, and

(b) Performance of round HSS.

On the basis of simple plastic theory, the rotation capacity Θ is given by:

$$\Theta = K_L/K_p - 1$$

where K_L is the curvature at the intersection of the experimental curve at the level of M_p as shown in Figure 1.2. If the experimental curve does not reach the level of M_p, the section cannot be employed in plastic design at the designated yield strength. Nevertheless, such sections can be used in plastic design at a lower yield strength than the guaranteed value.

4.2 Performance of Rectangular Sections

The moment - curvature and load - deflection curves, on the basis of the actual strength of the sections are shown in Figure 4.1 to 4.8. These tests were performed on simple span beams with simulated two-point loading, in the order of increasing flange slenderness ratio and are numbered accordingly.

The behaviour predicted by analysis (on the assumption that local buckling does not take place), is shown as the full ine while the experimental behaviour is given by the full line with starts. Each star represents a stage at which data was recorded.

The following observations are noted:

(a) There is good correlation between the test results and analytical predictions for those sections in which local buckling did not occur until well into the plastic range (Figures 4.1 and 4.2).

(b) The rate of unloading, after local buckling has occurred, increases with increasing flange slenderness ratio. This result is due in part to the increased effect of bearing stresses applied at the load and support points (Figure 4.3 to 4.8).

(c) Sections (4a) and (7a) were also tested by Hudoba[3]. The present results indicate more load carrying capacity due to reduced shear stress intensity at the load points and supports, since the spans of the beams in the current work are longer than those in Hudoba's programme.

Before establishing design criteria for the bending of rectangular HSS some discussion concerning the results from this study and that of Hudoba in relation to practice is in order. The basic difference between the two test programmes of single span beams was in the span lengths. Hudoba's beams were considerably shorter than those reported herein (12 ft. vs. 24 ft. approximately) and hence the shear forces and bearing stresses were reduced in the current work. Consequently moment and rotation capacities were higher in the latter programme.

In relation to design, some mention will be made of test versus field conditions. For example, it is unlikely that major load points in the field would result in concentrating the load over a 3" length (along the beam).

Auxiliary framing and the physical dimensions of gravity loads are such that a more distributed load application would occur. Consequently, it is thought to be sufficiently conservative to recommend sections for design based on the aggregate data of the two programmes.

4.2.1 Design Criteria

Table 4.1 lists the rotation capacities Θ, and the ratio of ultimate moments to corresponding computed yield and plastic moments, M_u/M_0 and M_u/M_p respectively. These moment ratios are important in allowable stress design in order to establish whether a section is compact or non-compact. This data can be plotted against an effective flange slenderness ratio such as

$$\frac{b}{t}\Big/\sqrt{\frac{\sigma_0}{55}} .$$

This operation is performed in Figure 4.9. The value of 55 KSI was used to normalize the effective slenderness ratio because of the inherent differences in yield stresses of various sections tested. In addition, this value simplifies comparison with the earlier work of Hudoba. The points represented by squares are obtained from the present test data whereas those represented by circles are reproduced from earlier work[3]. On the basis of these points a curve was drawn to approximately represent the overall test data. Although the present work tends to bias the data towards greater load carrying capacity than for Hudoba, the overall impact is not significantly different. The boundaries used to categorise the sections are obtained in Figure 4.9. Plastic design sections are obtained from Figure 4.9(a) by using a rotation capacity of 4. The associated effective flange slenderness ratio designates limiting value for plastic design. Figure 4.9(b) is used to delineate compact and

non-compact sections in allowable stress design (assuming f = 1.17). Further comment will be made prior to establishing recommendations for design.

4.2.2 Design Supplement on the basis of Minimum Guaranteed Strength

The experimental moment-curvature relationships, (Figures 4.1 to 4.8) which are based on the actual yield strength of the sections can be translated to a common level of yield strength such as 55, 50, and 42 KSI by scaling down these curves in accordance with appropriate ratios $55/\sigma_0$, $50/\sigma_0$, etc.[3] This process is only valid for sufficiently stocky sections that possible buckling can occur only in the plastic range. Consequently, by using simple plastic theory, sections with a relatively large flange slenderness ratio can also be employed in plastic design at a lower design yield stress than the guaranteed value σ_{0G}. This operation is performed in Figure 4.10 and the corresponding increased rotation capacities are designated as $\Theta_i (i = 1, 2, \ldots, 5)$. In a similar way, the corresponding value of M_u/M_p are listed in Table 4.2. The data is incorporated to plot the design curves with σ_{0G} = 55 and 50 KSI respectively as shown in Figures 4.11 and 4.12, represented by dark squares, triangles, circles, etc. The light symbols are reproduced from Hudoba's work, on the same plot. Finally design curves are plotted on the basis of both sets of data and the boundaries to categorise the sections are marked.

4.3 Performance of Round Sections

The moment curvature and load-deflection curves for round sections on the basis of observed strengths are shown in Figures 4.14 to 4.23, and are numbered according to the chronological order of testing. The behaviour predicted by analysis (as if there were no buckling), is shown by a full line while the experimental behaviour is given by the full line with stars (or with triangles and rectangles where applicable). Each of these symbols represents a stage during the test at which data was recorded. The sections

numbered (1b) to (8b) were tested as simple span beams with simulated two-point loading whereas sections numbered (1c) and (2c) were tested as two span beams with symmetrical loading about the middle support.

Sections numbered (1b) to (4b) were tested using just V-shaped blocks for bearing load distribution to help to reduce local buckling. During the first test it was observed that the use of the V-shaped blocks alone did not avoid imposing a high stress concentration relative to bending stresses. This was due to the section's large tube slenderness ratio (d/t = 80). The loading was followed by a substantial deterioration of the bearing surface at the supports and the loading points. The result was a subsequent drop-off in bending moment resistance well below the yield moment. The other three sections showed less serious deterioration because of this effect. The reason for the difference in behaviour is due to smaller tube slenderness ratios. In the next 6 tests 3" to 6" wide saddle plates were cut from the sections themselves and were used between the V-shaped blocks and the section profile to distribute bearing load. It is obvious from the tests numbered (5b) to (8b) that the use of these plates contributed to improving the moment resistance of the sections. The two-span test section numbered (1c) was subjected to loading using 3" wide saddle plates. The experimental moment-curvature relationship at the support as well as at the loading point indicates higher strength than that observed in the simple span test without saddle plates numbered (5b), for the same section.

Since the carrying capacity of the 4.5" O.D. section was influenced by the bearing plates, the test numbered (1b) will not be taken as a representative measure of moment resistance. The conclusions will be based on the other 9 tests.

The following observations are to be noted:

(a) There is good correlation between test results and analytical predictions for those sections in which local buckling did not occur until well into the plastic range.

(b) The rate of unloading, after local buckling had occurred, increases considerably with an increase in tube slenderness ratio. This effect is very obvious in tests numbered (5b) to (8b).

(c) The two span tests (1c) and (2c) show the development of fully plastic moment in a statically indeterminate structure. Sections with intermediate and lower tube slenderness ratios for the normal yield strength described earlier are capable of undergoing plastic deformation and formation of mechanisms.

Table 4.4 lists various parameters in relation to the experimental data.

4.3.1 Comparison Between Theoretical and Experimental Buckling

The actual yield strengths of the test sections vary broadly in two ranges:

(a) $\sigma_{0G} \simeq 42$ ksi (tests no. 2b, 4b, 5b, 7b and 8b)

(b) $\sigma_{0G} \simeq 52$ ksi (tests no. 3b and 6b)

An effective slenderness ratio can be applied to each section to account for the difference in yield strengths. A factor of $\sqrt{\sigma_0 / \sigma_{0G}}$ multiplied by the actual slenderness ratio is used to define the effective slenderness to allow a compilation of sections into appropriate ranges. On this basis an effort to compare the test results with analytical predictions can be made as follows:

(a) $\sigma_{0G} = 42$ ksi

Figure 4.23(a) shows a plot of rotation capacities Θ vs $(D/t)\sqrt{\sigma_0/42}$.

For those sections which were loaded with saddle plates there is a reasonable parity between the theoretical curve and the experimental data. Figure 4.23(b) is a similar plot of M_u/M_p vs $(D/t)\sqrt{\sigma_0/42}$.

(b) σ_{0G} = 52 ksi

Only two tests were conducted in the higher strength range. Figure 4.24 shows the corresponding analytical and experimental data for these tests. It is observed that there is good agreement for the test in which load was distributed through accessory plates on the bearing surface of the HSS*.

Figures 3.8 and 3.9 show the deformation pattern of sections (4b) (D/t = 42.5) and (5b) (D/t = 51) respectively after test. The former was loaded through V-shaped blocks only while saddle plates were used on the latter. Due to the loading device a combination of oval and multi-wave type deformation is apparent and is more likely in the D/t range of these sections if saddle plates are used. However, an oval shape of deformation in test no. (1b) was observed on nearly the entire length of the section. On the whole it can be assessed that small deflection theory represents (if not complete) some parity with the experimental behaviour in view of deformations, for plastic design and compact sections.

4.3.2 Limitations of the Theory

(a) The theoretical solution is based on an approximate method of analysis. Though, as mentioned above, the analytical results are fairly compatible with the experimental behaviour, it cannot be stated that

---

* The experimental rotation capacity takes into account the post-buckling strength until such time as the moment drops below M_p. On the other hand the analysis predicts only the critical buckling curvature. Hence the comparison neglects a post-buckling reserve curvature range in the analysis but includes it in the experimental results.

deformation patterns are predictable. Indeed one does not anticipate a close comparison in deflection patterns in general. There is justification to compare moment capacities and associated curvature limits, however, since these values are not overly sensitive to variations to the deformed configuration.

(b) The theory does not take into account the stress concentrations caused by loading on the bearing surface of HSS. Since this factor is of considerable importance for tubes of large slenderness ratio, it can be pointed out that the theory would predict markedly high values of critical buckling stresses for such sections.

4.3.3 Design Criteria

The analytical and test data is incorporated into the form presently being used in CSA-S16 (1969) for limitations on D/t ratios as follows:

(a) plastic design sections

(i) σ_{0G} = 42 ksi

$$\frac{D}{t}\sqrt{\frac{\sigma_0}{42}} \leq 46; \frac{D}{t} \leq \frac{300}{\sqrt{\sigma_0}}$$

ii) σ_{0G} = 52 ksi

$$\frac{D}{t}\sqrt{\frac{\sigma_0}{52}} \leq 37; \frac{D}{t} \leq \frac{267}{\sqrt{\sigma_0}}$$

(b) compact sections in allowable stress design

(i) σ_{0G} = 42 ksi

$$\frac{D}{t} \cdot \frac{\sigma_0}{42} \leq 56; \frac{D}{t} \leq \frac{2350}{\sigma_0}$$

(ii) $\sigma_{0G} = 52$ ksi

$$\frac{D}{t} \cdot \frac{\sigma_0}{52} \leqslant 52; \frac{D}{t} \leqslant \frac{2704}{\sigma_0}$$

Since the results for the two yield stress values do not provide a consistent constant in each category (i.e. 300 vs 267 and 2350 vs 2704), it is clear that the form of expression is not satisfactory. A suitable design criterion which may reasonably take into account these variations (due to difference in the yield strengths) needs to be established.

The above set of data indicates that for a plastic design section the limiting D/t ratio is approximately inversely proportional to the yield strength. This is also supported from the viewpoint that to reach a plastic rotation which is four times the hypothetical elastic rotation, the critical buckling strains may differ widely for materials with different yield strengths (with the same modulus of elasticity). Therefore, for plastic design sections the limiting D/t ratio may be determined as follows:

$$\sigma_{0G} = 42 \text{ ksi}, \frac{D}{t} \cdot \frac{\sigma_0}{42} \leqslant 46; \frac{D}{t} \leqslant \frac{1932}{\sigma_0}$$

$$\sigma_{0G} = 52 \text{ ksi}, \frac{D}{t} \cdot \frac{\sigma_0}{52} \leqslant 37; \frac{D}{t} \leqslant \frac{1924}{\sigma_0}$$

Thus a limiting D/t ratio of $1924/\sigma_0$ can be safety adopted.

For compact sections in allowable stress design, there is a comparatively small difference in the values of limiting D/t ratio to attain fully plastic moment M_p, although the yield strength may vary widely. This is supported, analytically, by the fact that the sections under investigation reach M_p at a total strain of 7000 - 7500 μin/in. In this case the limiting

D/t ratio can be assumed to vary inversely with the square-root of the yield strength, and can be determined as follows:

$$\sigma_0 = 42 \text{ ksi}, \frac{D}{t}\sqrt{\frac{\sigma_0}{42}} \leqslant 56; \frac{D}{t} \leqslant \frac{365}{\sqrt{\sigma_0}}$$

$$\sigma_0 = 52 \text{ ksi}, \frac{D}{t}\sqrt{\frac{\sigma_0}{52}} \leqslant 52; \frac{D}{t} \leqslant \frac{375}{\sqrt{\sigma_0}}$$

Thus a limiting D/t ratio of $365/\sqrt{\sigma_0}$ can be safely adopted.

For a non-compact section the theoretical predictions are made in Chapter 2. Further investigations of the experimental behaviour are needed to recommend a design criterion for such sections. As a matter of fact, CSA-S16 recommends a limiting value of $3300/\sigma_0$ for D/t. This value translates sections of 79 for σ_0 = 42 ksi and 66 for σ_0 = 52 ksi. Clearly, test no. (1b) (D/t = 80) fails to satisfy the non-compact requirement both by test and by the current specification.

4.3.4 Comparison with CSA Specifications

(a Plastic Design Sections

Canadian Standards Association specifies a limiting D/t ratio of $200/\sqrt{\sigma_0}$ for such sections. This is highly conservative as compared to the results of the present work which in that format specifies a range of values from $267/\sqrt{\sigma_0}$ to $300/\sqrt{\sigma_0}$ for approximate yield strengths of 52 to 42 ksi respectively. It has also been established that the above form of design criterion is not very rational and, in fact, a suitable expression appears to be of the form of some constant number divided by the yield strength. The constant 1924 would appear to be suitable.

(b) Compact Sections in Allowable Stress Design

The recommended limiting D/t ratio of $3300/\sigma_0$ seems to be excessively liberal. The present work specifies these values to be $2340/\sigma_0$ and $2704/\sigma_0$ for approximate yield strengths of 42 and 52 ksi respectively. It is, therefore, clear that the form of design criterion is not consistent with the current study. In fact, the form of the limiting D/t ratio appears to be a constant number divided by the square-root of the yield strength. The value consistent with this revised form is 360.

(c) Non-Compact Sections in Allowable Stress Design

Further research is needed to comment on such sections. However, the value of $3300/\sigma_0$ as the limiting D/t ratio specified by CSA seems reasonable based on our limited experience with high slenderness ratios.

4.3.5 Comparison with Other Relevant Work

Premature local buckling is related to geometrical parameters as described by Schilling[20] on the basis of experiments on yield point steel tubes performed by Khalig and Schilling[19]. Accordingly he proposes a limiting D/t ratio to attain the fully plastic moment to be given by:

$$\frac{D}{t} \leqslant 0.12E/\sigma_0$$

Substituting for E = 29500 ksi

$$\frac{D}{t} \leqslant \frac{3540}{\sigma_0}$$

Thus if

$$\sigma_0 = 42 \text{ ksi}, \quad D/t \leqslant 84$$

σ_0 = 52 ksi, D/t $\leq$ 67

These values are considerably higher than those observed in the current work. One reason for the difference is due to the type of loading applied during a test. Pure moment applied to a section (implicit in Schilling's recommendation) is not realistic for design without experimental support. The effect of shear and particularly bearing stresses is not negligible.

Although the form recommended from the current study is also in conflict with Schilling's expression, sound scientific evidence for equation (1) is lacking. In addition there appears to be a difference between the behaviour of a tube with a gradual change in tangent modulus as compared to one with a sharp yield point. The linear form is certainly valid for elastic material. However, this form has not been substantiated for a material exhibiting a non-linear stress-strain response to the author's knowledge.

	H.S.S.	S_3 (in^3)	Z_3 (in^3)	f	σ_0 (ksi)	E_{st} (ksi)	b/t
(1a)	12.0 X 8.0 X .375	46.51	56.46	1.214	62.5	360	17.3

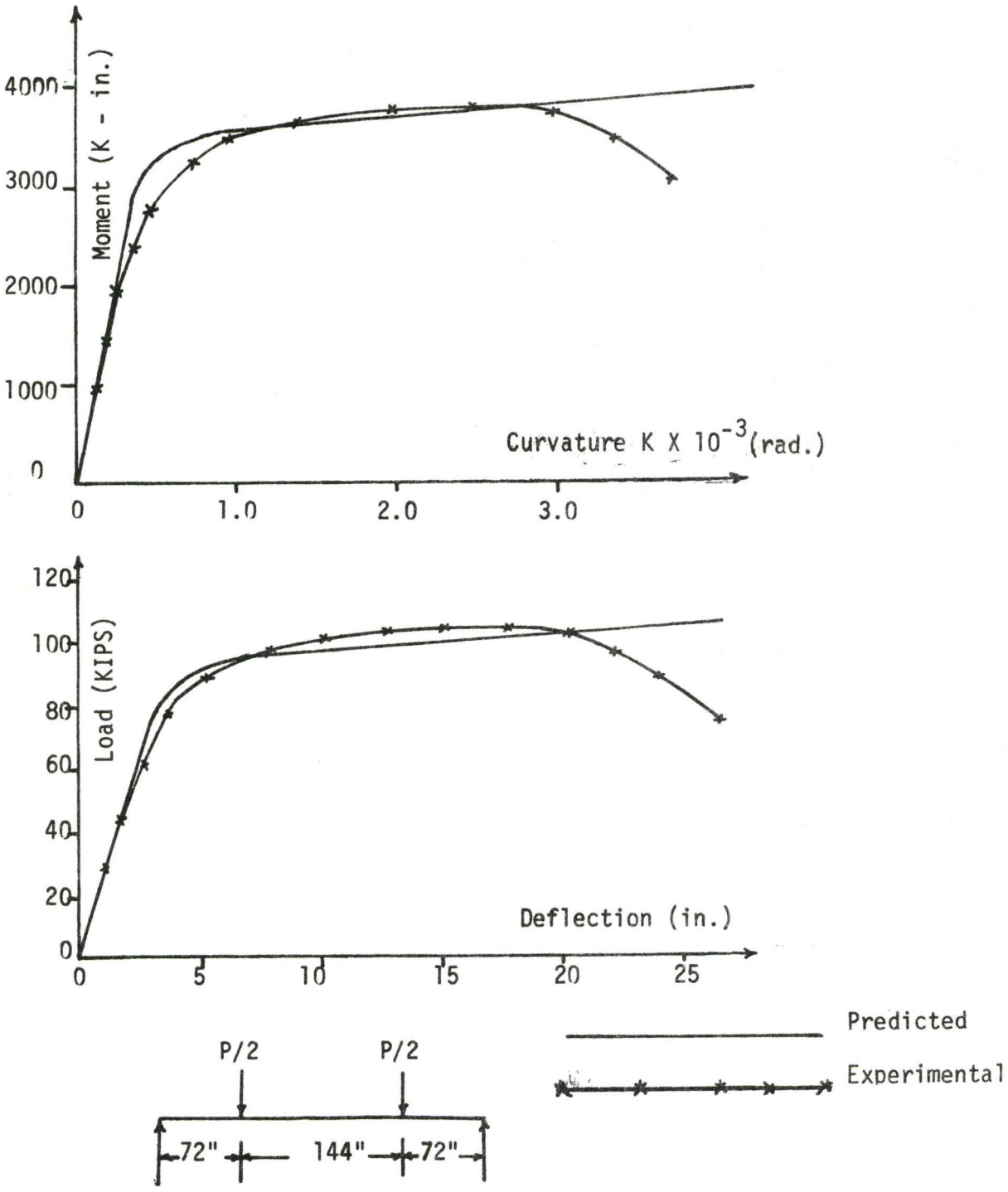

FIGURE 4.1 Results of Test No. (1a)

		S_3 (in^3)	Z_3 (in^3)	f	σ_0 (ksi)	E_{st} (ksi)	b/t
(2a)	H.S.S. 12.0 X 8.0 X .312	39.71	47.87	1.206	52.5	400	21.6

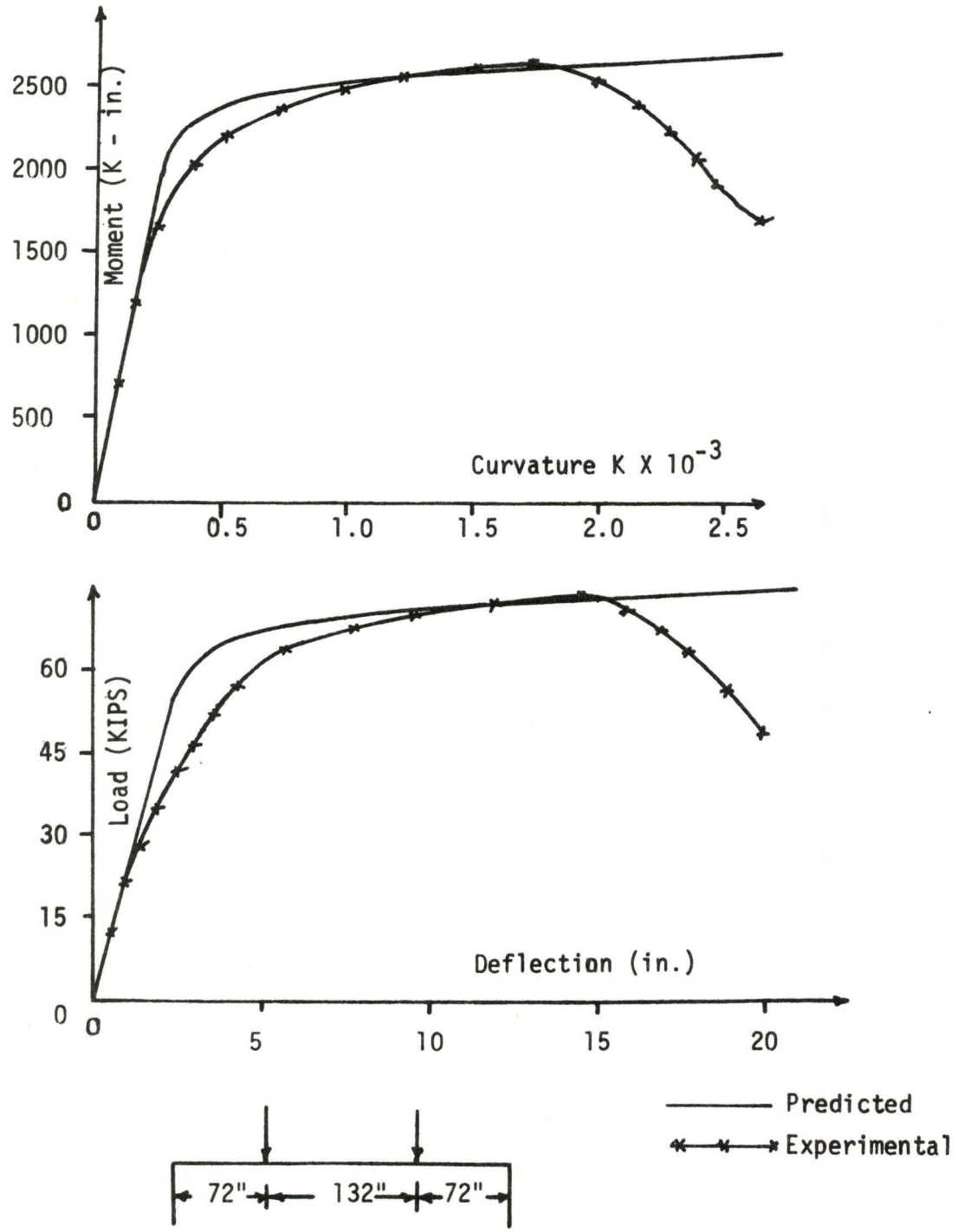

FIGURE 4.2 Results of Test No. (2a)

		S_3 (in^3)	Z_3 (in^3)	f	σ_0 (ksi)	E_{st} (ksi)	b/t
(3a)	H.S.S. 8.0 X 6.0 X .188	11.27	13.37	1.186	54.0	310	27.9

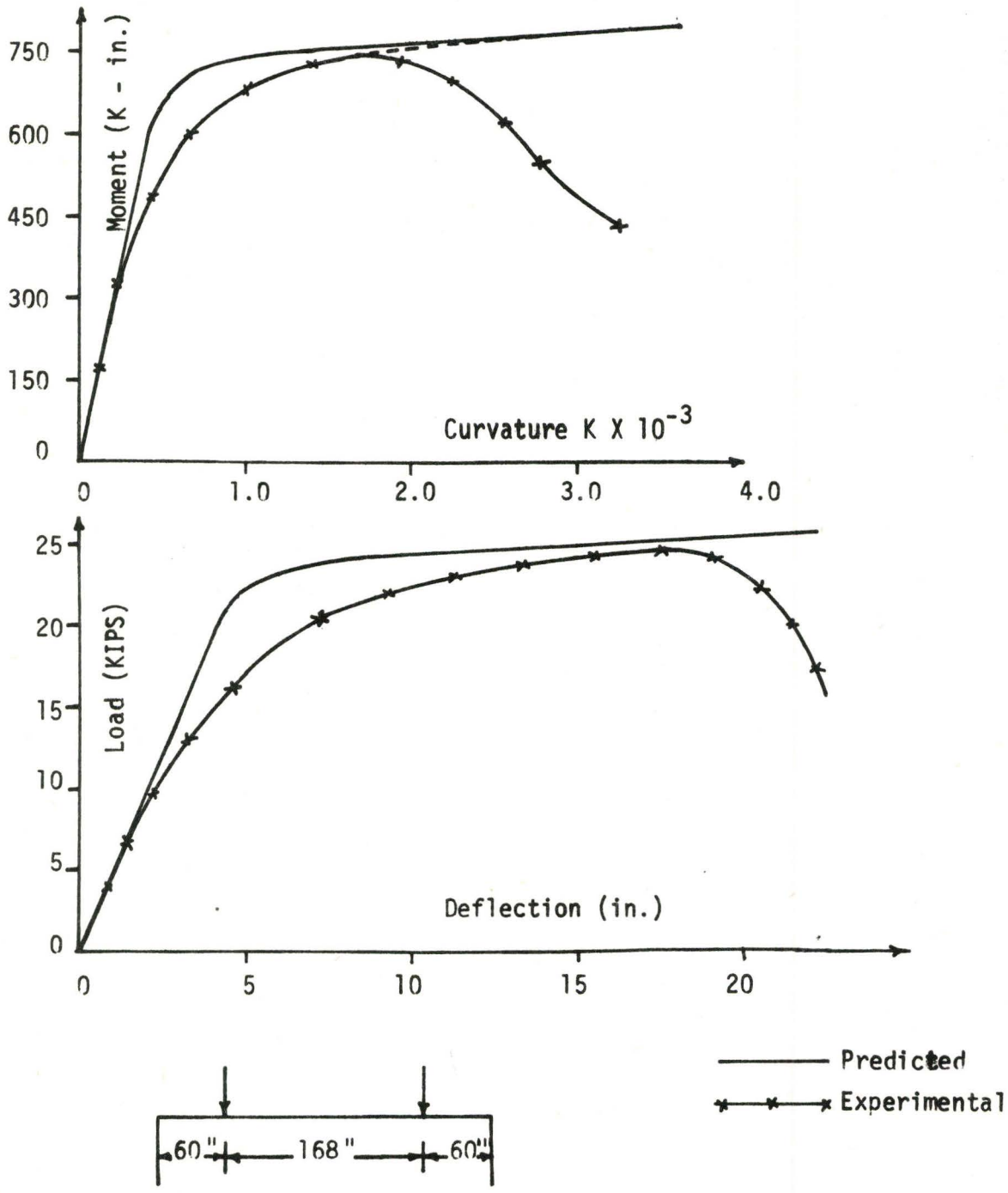

FIGURE 4.3 Results of Test No. (3a)

		S_3 (in^3)	Z_3 (in^3)	f	σ_η (ksi)	E_{st} (ksi)	b/t
(4a)	H.S.S. 6.0 X 6.0 X .188	7.94	9.26	1.166	55.3	420	27.9

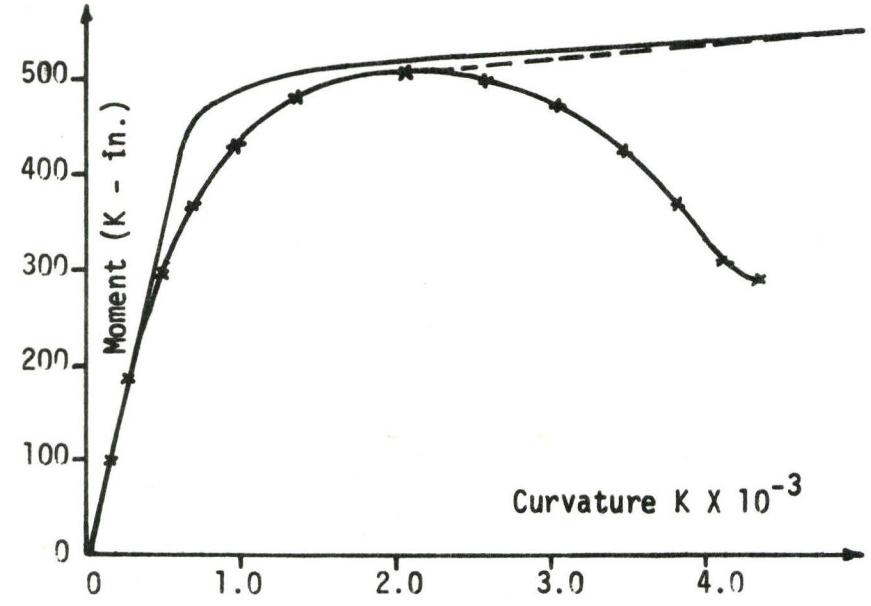

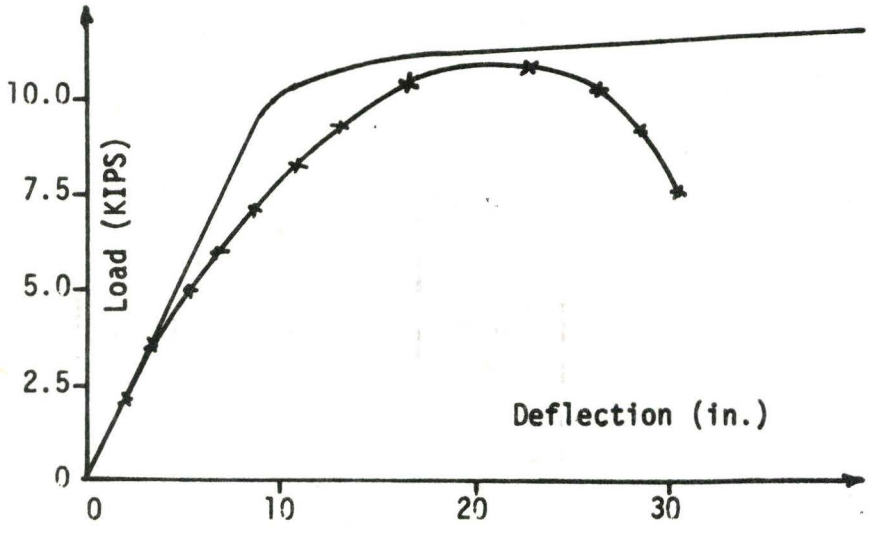

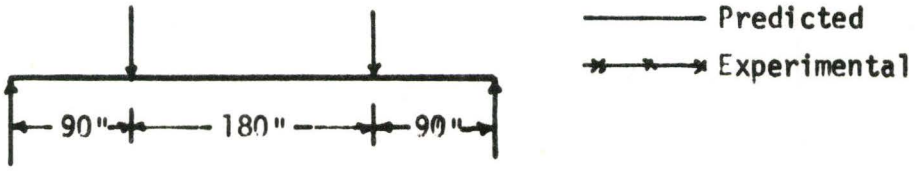

FIGURE 4.4 Results of Test No. (4a)

	S_3 (in^3)	Z_3 (in^3)	f	σ_0 (ksi)	E_{st} (ksi)	b/t
(5a) H.S.S. 8.0 X 8.0 X .250	18.79	21.90	1.165	58.0	420	28.0

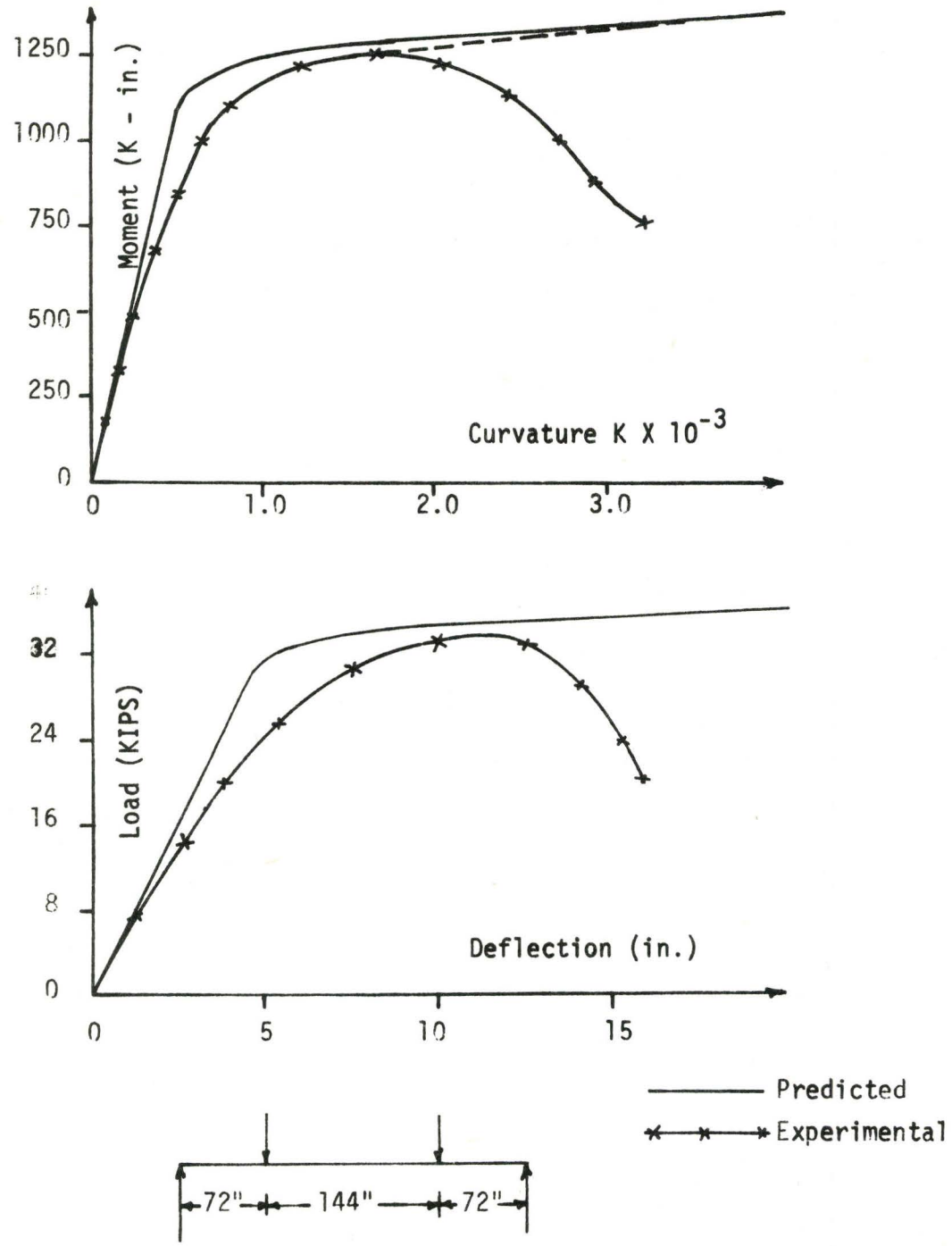

FIGURE 4.5 Results of Test No. (5a)

		S_3 (in^3)	Z_3 (in^3)	f	σ_0 (ksi)	E_{st} (ksi)	b/t
(6a)	H.S.S. 10.0 X 10.0 X .302	35.62	41.46	1.164	56.0	280	29.1

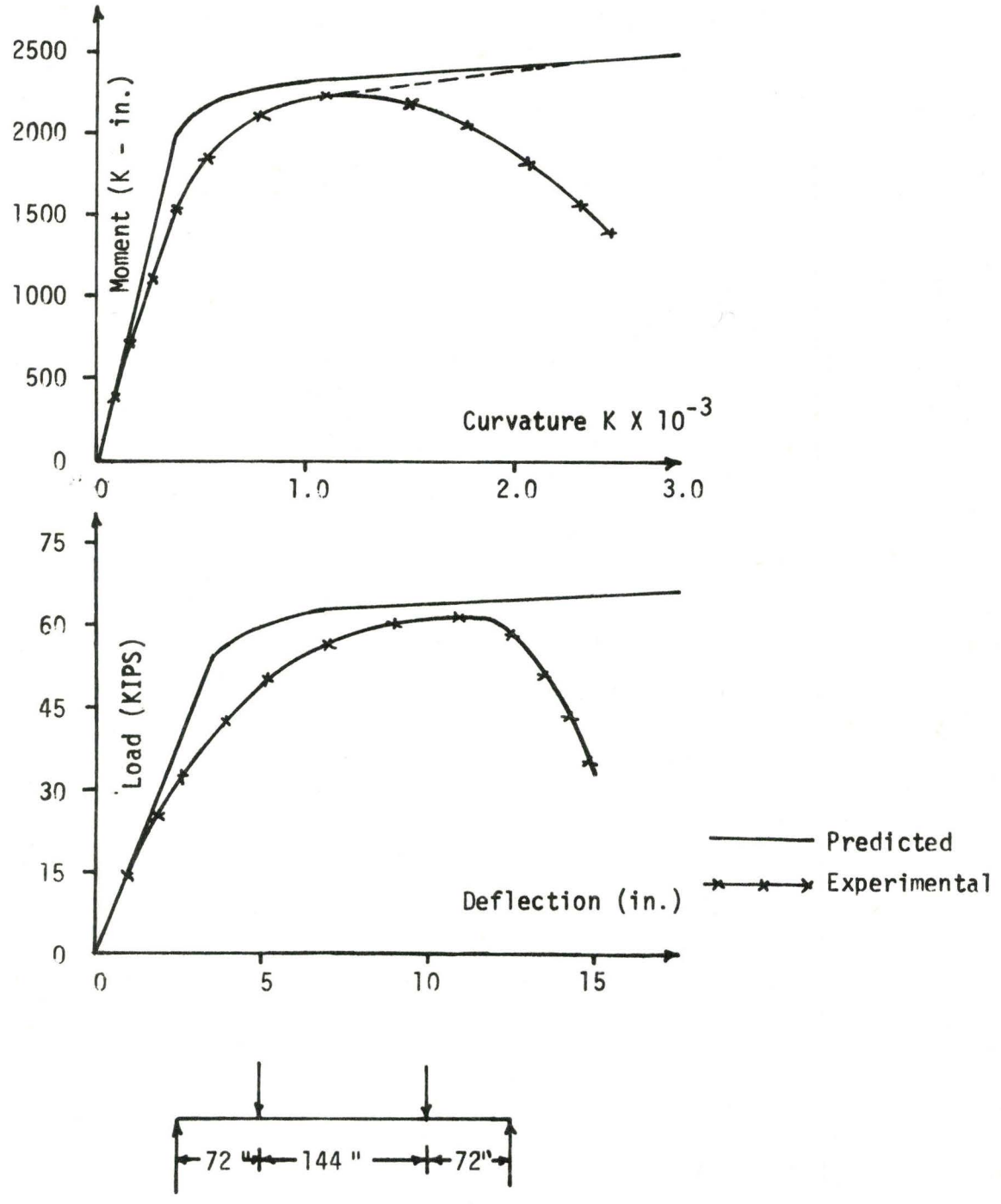

FIGURE 4.6 Results of Test No. (6a)

		S_3 (in^3)	Z_3 (in^3)	f.	σ_0 (ksi)	E_{st} (ksi	b/t
(7a)	H.S.S. 7.0 X 7.0 X .188	11.02	12.77	1.160	57.0	380	33.3

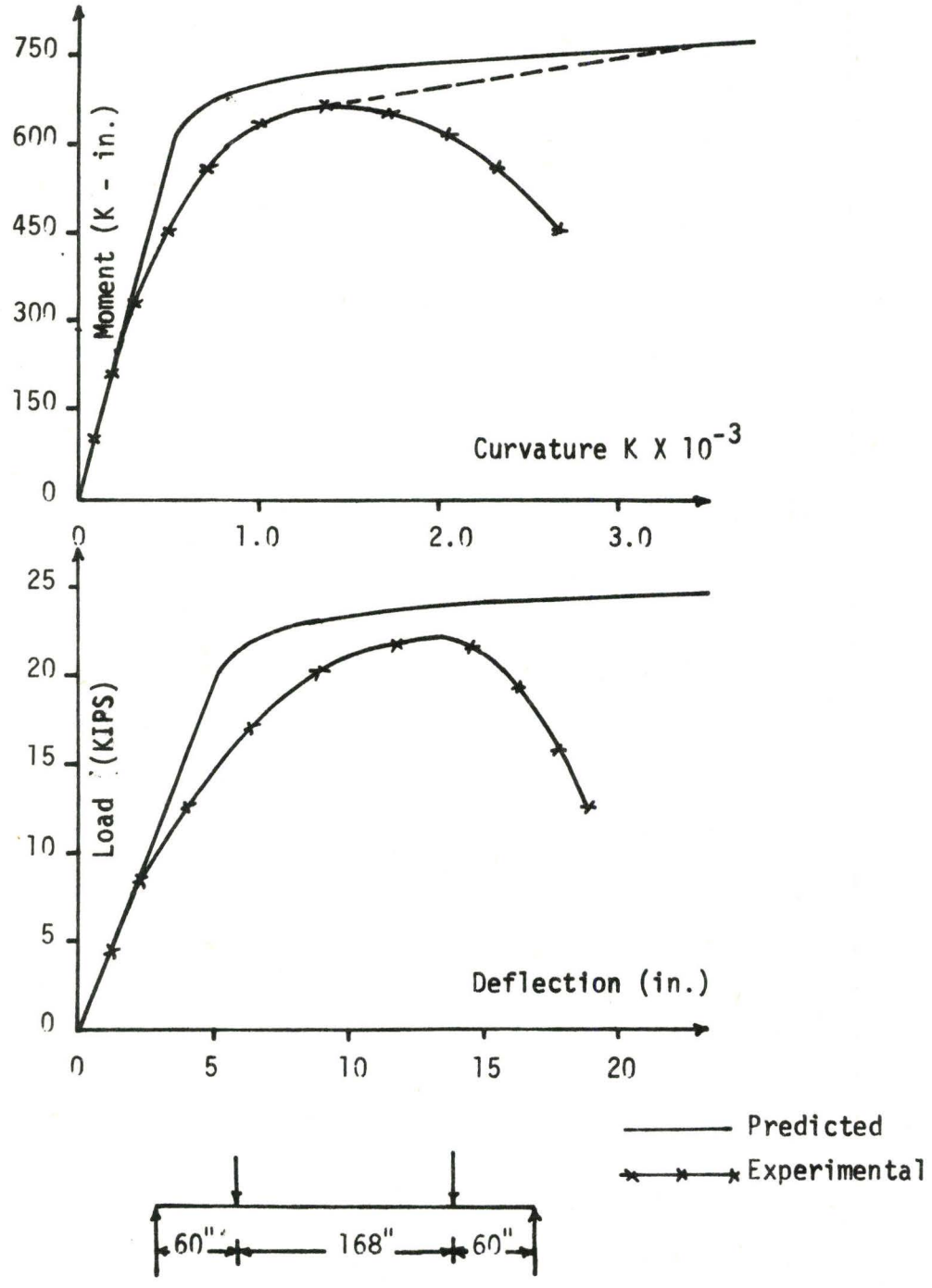

FIGURE 4.7 Results of Test No. (7a)

		S_3 (in^3)	Z_3 (in^3)	f	σ_0 (ksi)	E_{st} (ksi)	b/t
(8a)	H.S.S. 10.0 X 10.0 X .250	30.13	34.86	1.157	61.0	410	36.0

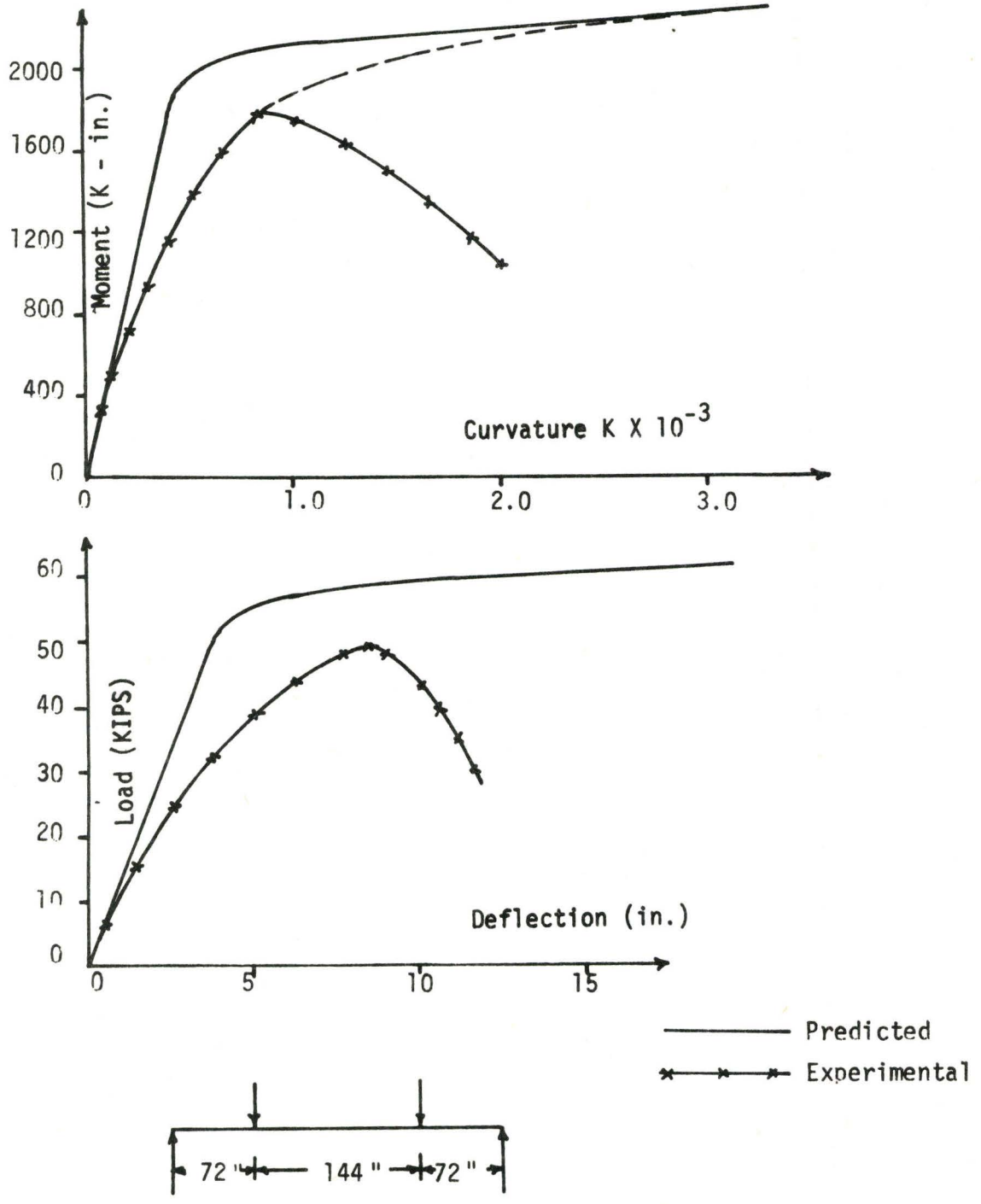

FIGURE 4.8 Results of Test No. (8a)

TABLE 4.1 Test Data - Rectangular Sections

No.	b/t	σ_0	$\frac{b}{t}\sqrt{\frac{\sigma_0}{55}}$	$\frac{M_u}{M_0}$	$\frac{M_u}{M_p}$	θ
1a	17.3	62.5	18.4	1.290	1.060	6.8
2a	21.6	52.5	21.1	1.270	1.054	5.2
3a	27.9	54.0	27.6	1.180	0.995	2.35
4a	27.9	53.5	28.0	1.160	0.990	2.25
5a	28.0	58.0	28.7	1.150	0.988	2.01
6a	29.1	56.0	29.4	1.120	0.962	1.70
7a	33.3	57.0	33.9	1.060	0.910	1.30
8a	36.0	61.0	37.8	0.940	0.810	0.82

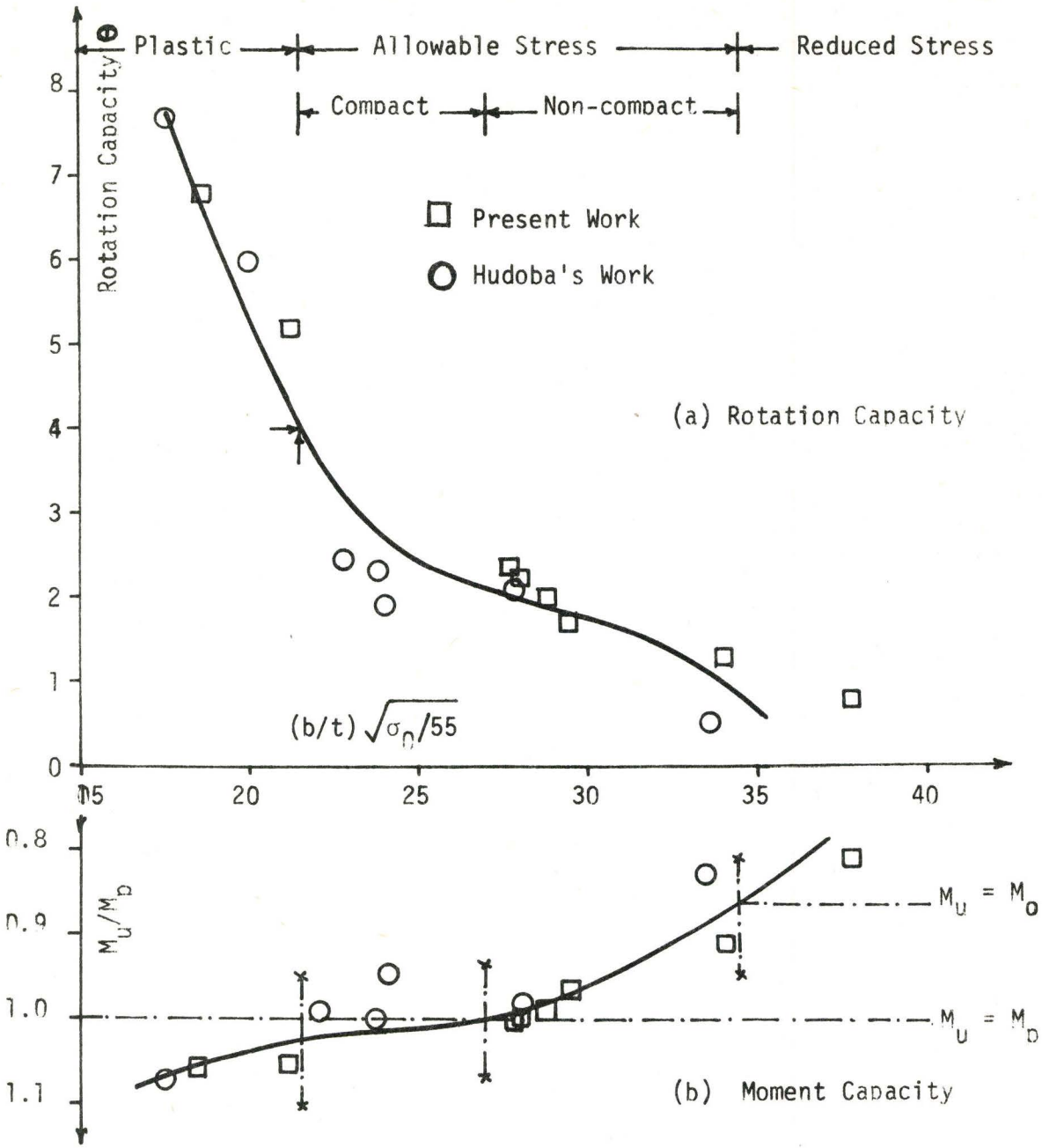

(a) Plastic Design Sections

$$\frac{b}{t}\Big/\sqrt{\frac{\sigma 0}{55}} \leq 21.5; \quad \frac{b}{t} \leq \frac{159}{\sqrt{\sigma_0}}$$

(b) Allowable Stress Design Sections

(i) Compact

$$\frac{b}{t}\Big/\sqrt{\frac{\sigma 0}{55}} \leq 27.0; \quad \frac{b}{t} \leq \frac{200}{\sqrt{\sigma_0}}$$

(ii) Non-compact

$$\frac{b}{t}\Big/\sqrt{\frac{\sigma 0}{55}} \leq 34.5; \quad \frac{b}{t} \leq \frac{255}{\sqrt{\sigma_0}}$$

FIGURE 4.9 Design Criteria

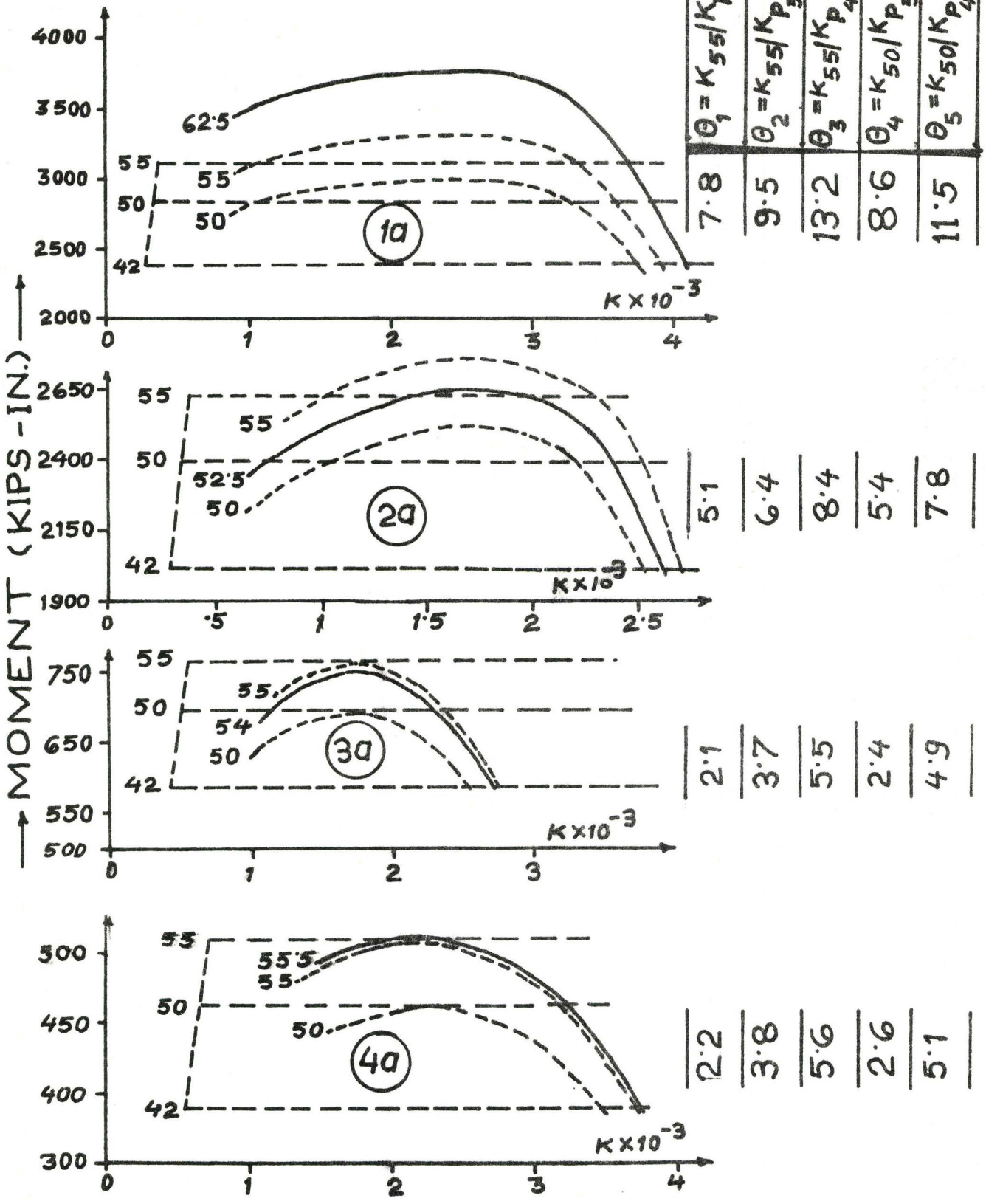

$\theta_1 = K_{55}/K_{P_{55}} - 1$	$\theta_2 = K_{55}/K_{P_{50}} - 1$	$\theta_3 = K_{55}/K_{P_{42}} - 1$	$\theta_4 = K_{50}/K_{P_{50}} - 1$	$\theta_5 = K_{50}/K_{P_{42}} - 1$
7·8	9·5	13·2	8·6	11·5
5·1	6·4	8·4	5·4	7·8
2·1	3·7	5·5	2·4	4·9
2·2	3·8	5·6	2·6	5·1

FIGURE 4.10 ROTATION CAPACITES
(CONTINUED)

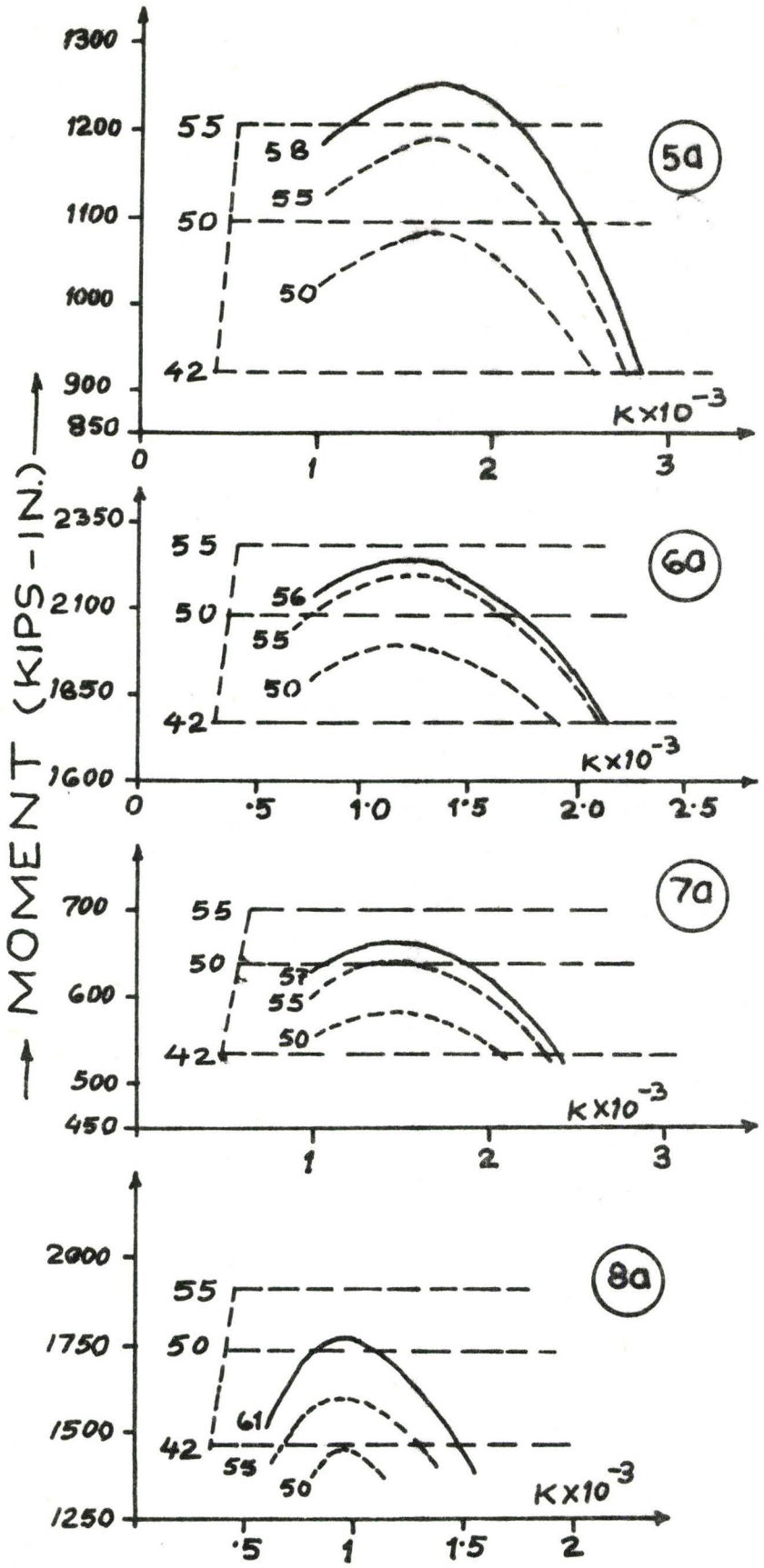

—	3·6	5·5	—	5·0
—	3·2	5·3	—	4·7
—	1·5	3·8	—	3·2
—	—	3·0	—	1·8

TABLE 4.2 Moment Ratios

No.	Ratio (Mu/Mp)				
	σ_{OG} = 55 KSI			σ_{OG} = 50 KSI	
	σ_0 = 55	σ_0 = 50	σ_0 = 42	σ_0 = 50	σ_0 = 42
1a	1.060	1.166	1.388	1.060	1.262
2a	1.054	1.159	1.380	1.054	1.255
3a	0.995	1.094	1.303	0.995	1.185
4a	0.990	1.090	1.300	0.990	1.180
5a	0.988	1.087	1.294	0.988	1.176
6a	0.962	1.058	1.260	0.962	1.145
7a	0.910	1.000	1.192	0.910	1.082
8a	0.810	0.893	1.067	0.810	0.968

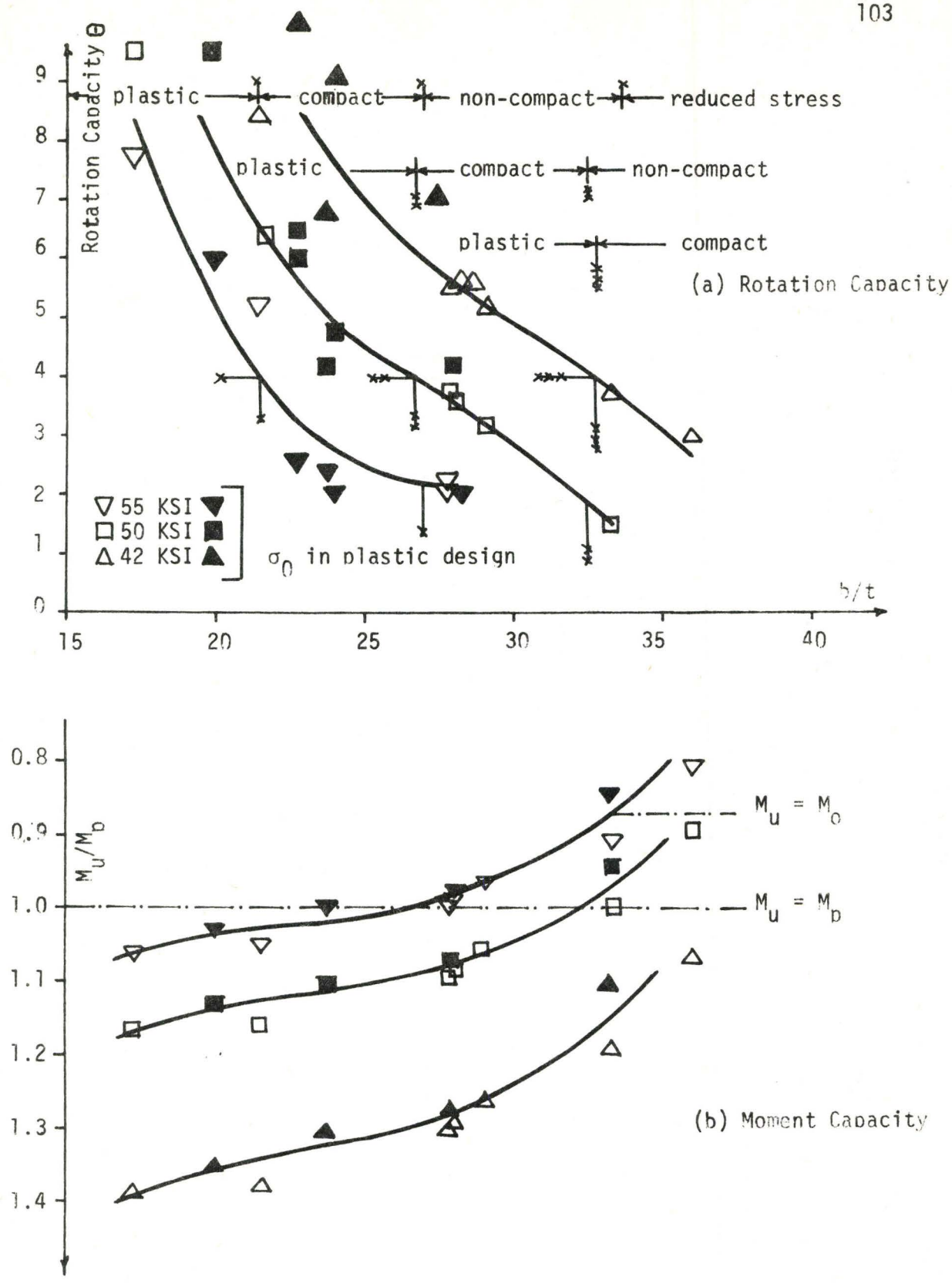

FIGURE 4.11 Design Curves; σ_{OG} = 55 KSI

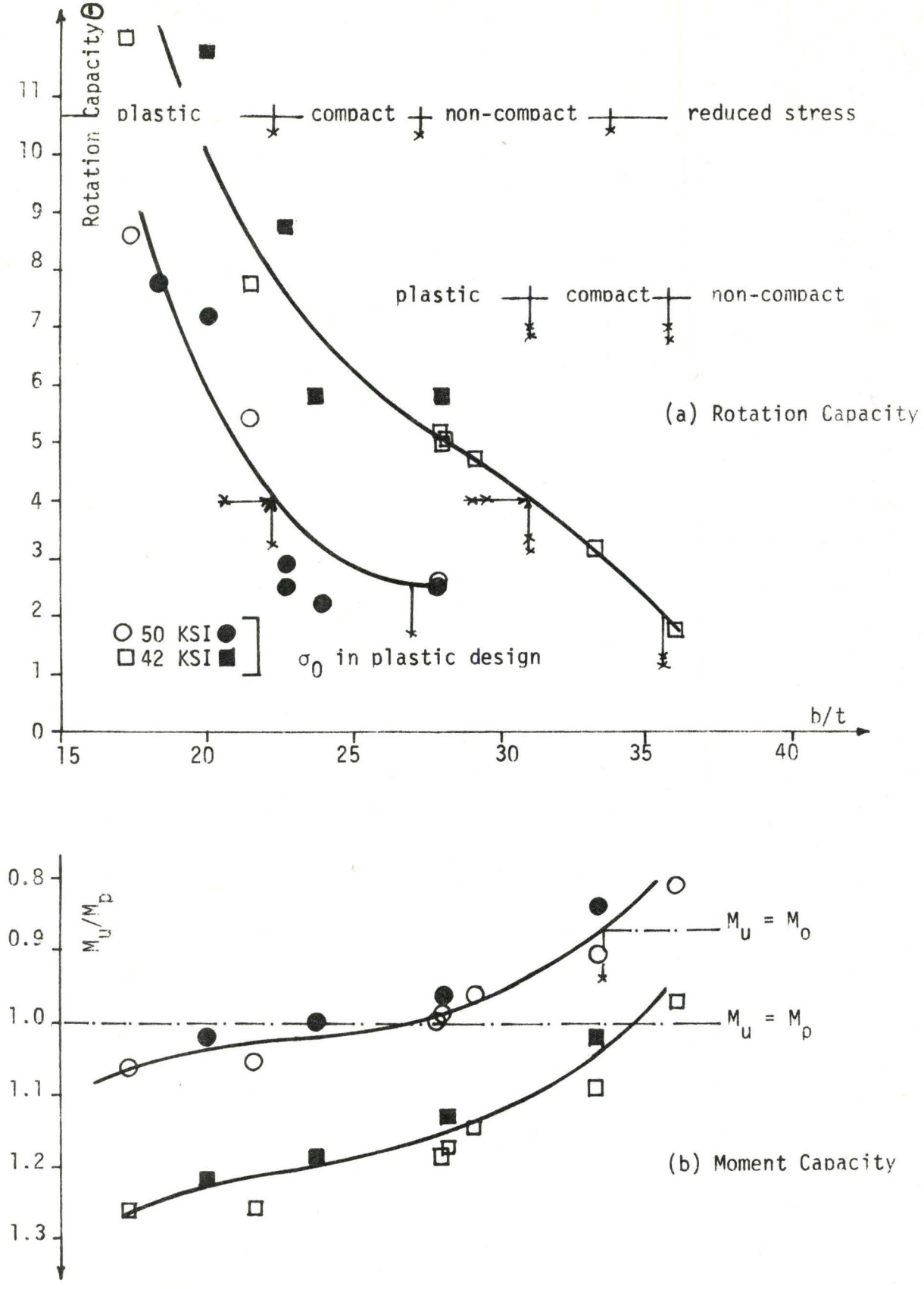

FIGURE 4.12 Design Curves; σ_{0G} = 50 KSI

		S_3 (in^3)	Z_3 (in^3)	f	σ_0 (ksi)	E_{st} (ksi)	D/t
(1b)	H.S.S. 20.0 O.D.X .250	75.61	97.47	1.289	54.4	290	80.0

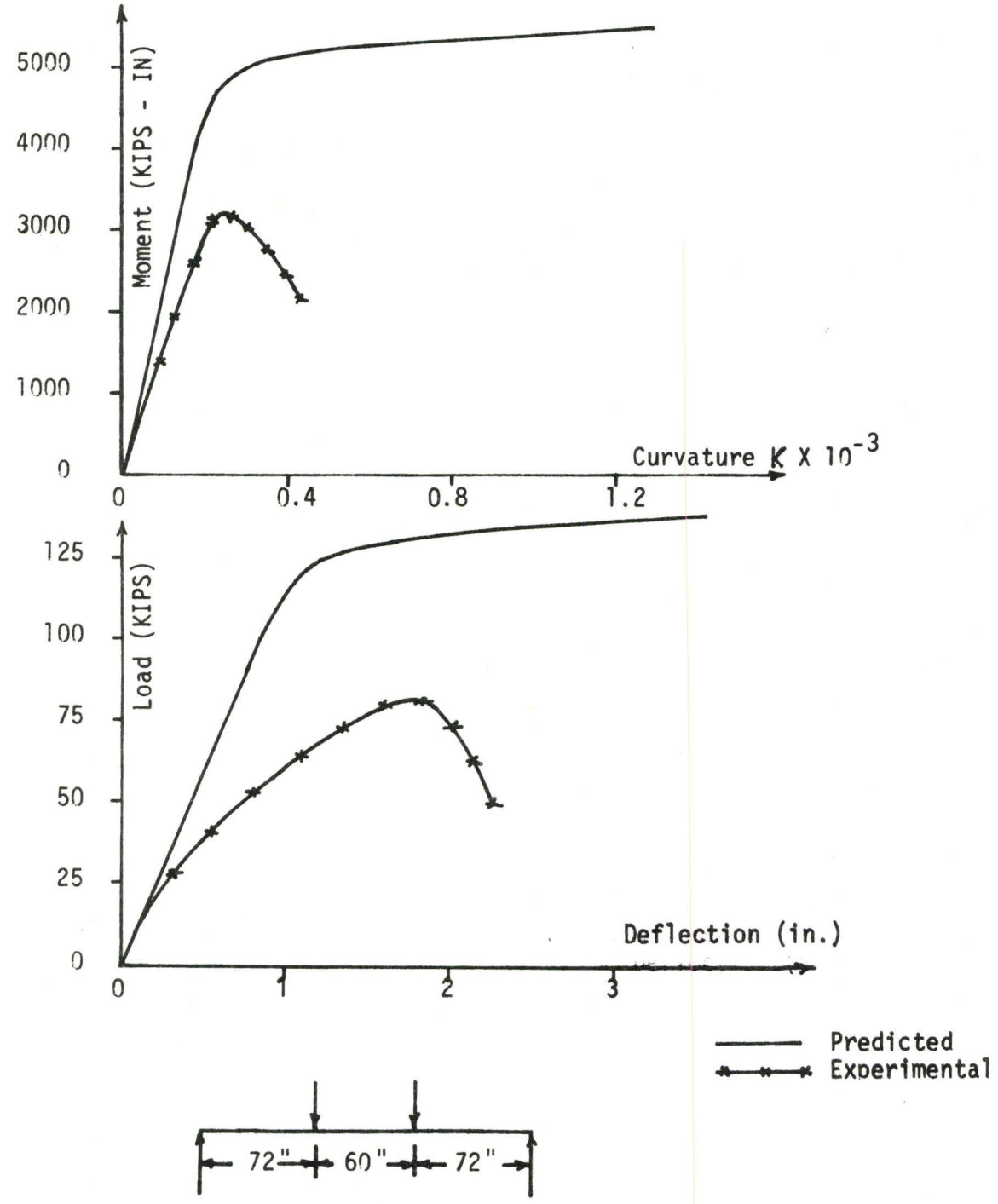

FIGURE 4.13 Results of Test No. (1b)

		S_3 (in^3)	Z_3 (in^3)	f	σ_0 (ksi)	E_{st} (ksi)	D/t
(2b)	H.S.S. 4.5 O.D.X .156	2.23	2.94	1.318	44.8	380	28.9

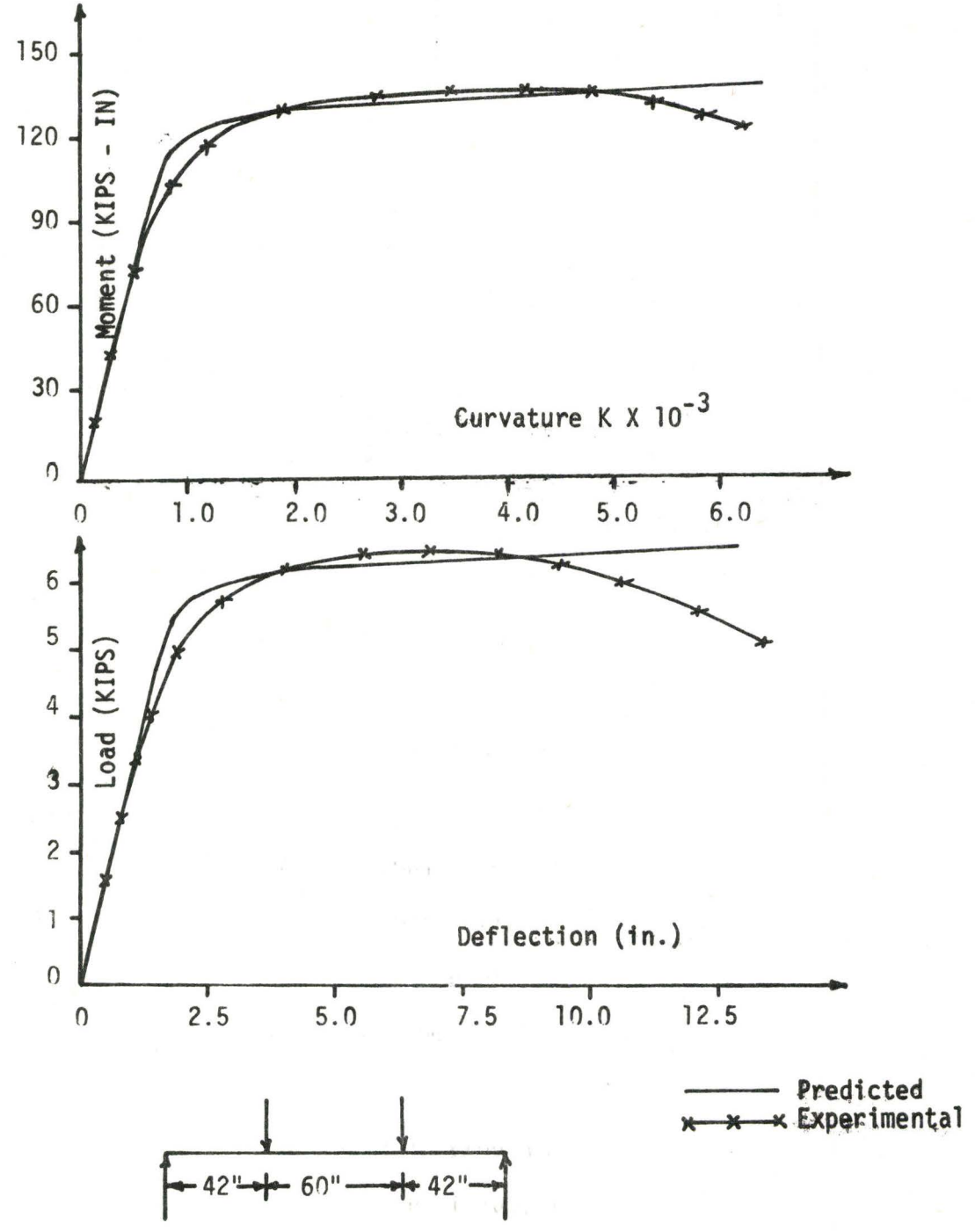

FIGURE 4.14 Results of Test No. (2b)

		S_3 (in^3)	Z_3 (in^3)	f	σ_0 (ksi)	E_{st} (ksi)	D/t
(3b)	H.S.S. 6.625 O.D.X .188	5.95	7.79	1.310	53.5	350	35.2

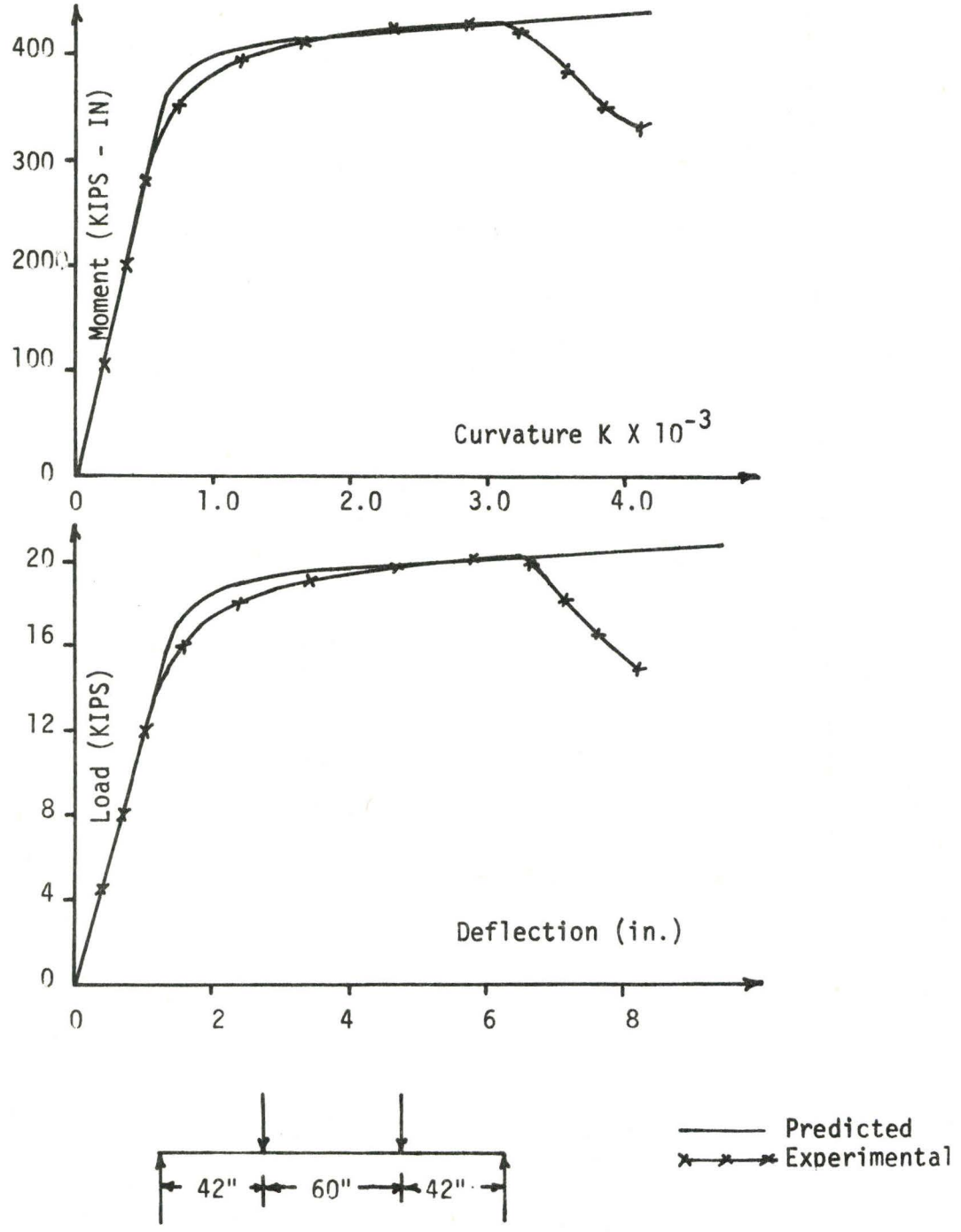

FIGURE 4.15 Results of Test No. (3b)

		S_3 (in^3)	Z_3 (in^3)	f	σ_0 (ksi)	E_{st} (ksi)	D/t
(4b)	H.S.S. 6.625 O.D.X .156	5.01	6.53	1.303	44.2	280	42.5

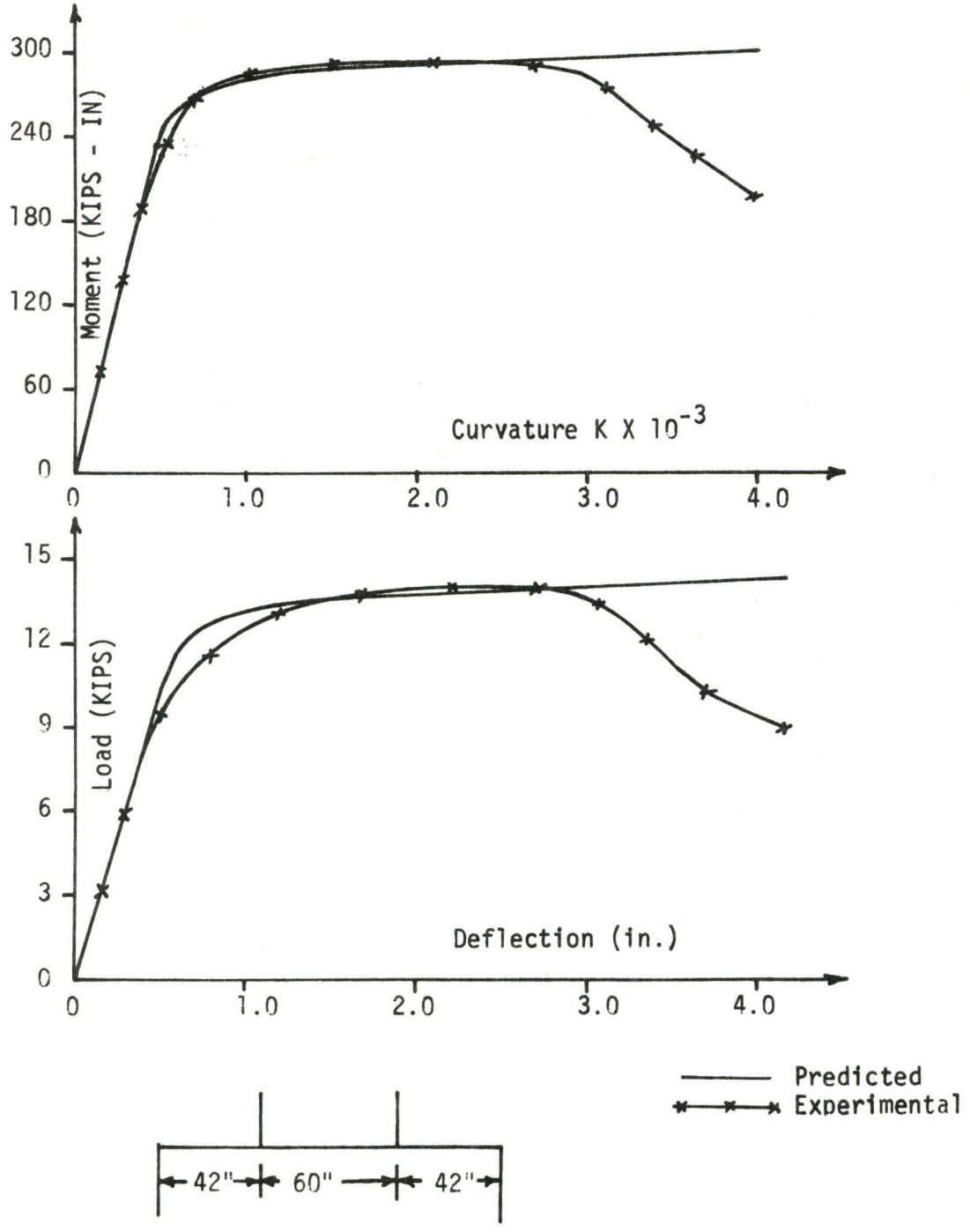

FIGURE 4.16 Results of Test No. (4b)

		S_3 (in^3)	Z_3 (in^3)	f	σ_0 (ksi)	E_{st} (ksi)	D/t
(5b)	H.S.S. 10.75 O.D.X 0.219	18.69	24.28	1.299	44.4	490	49.1

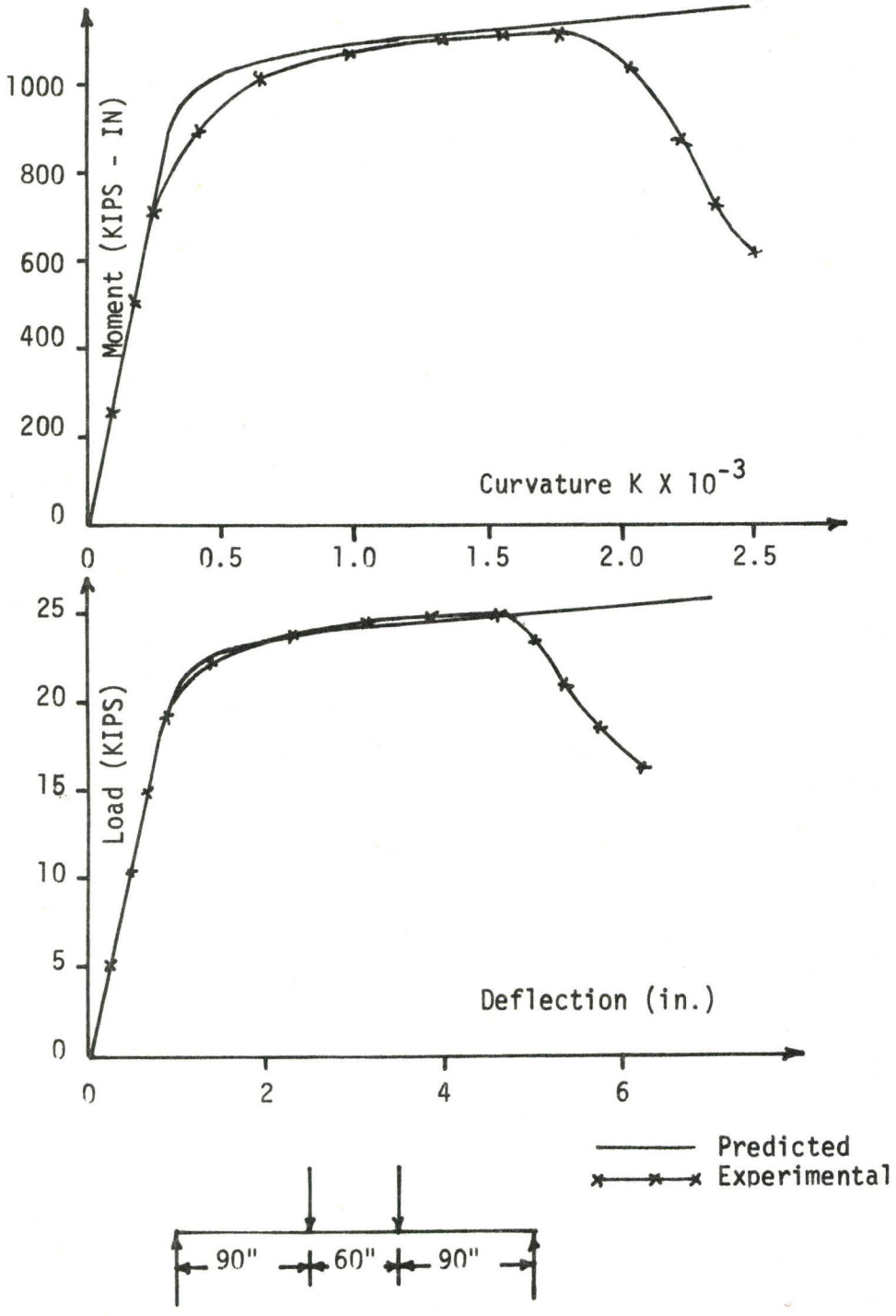

FIGURE 4.17 Results of Test No. (5b)

		S_3 (in^3)	Z_3 (in^3)	f	σ_0 (ksi)	E_{st} (ksi)	D/t
(6b)	H.S.S. 12.75 O.D.X .250	30.07	39.05	1.298	54.5	650	51.0

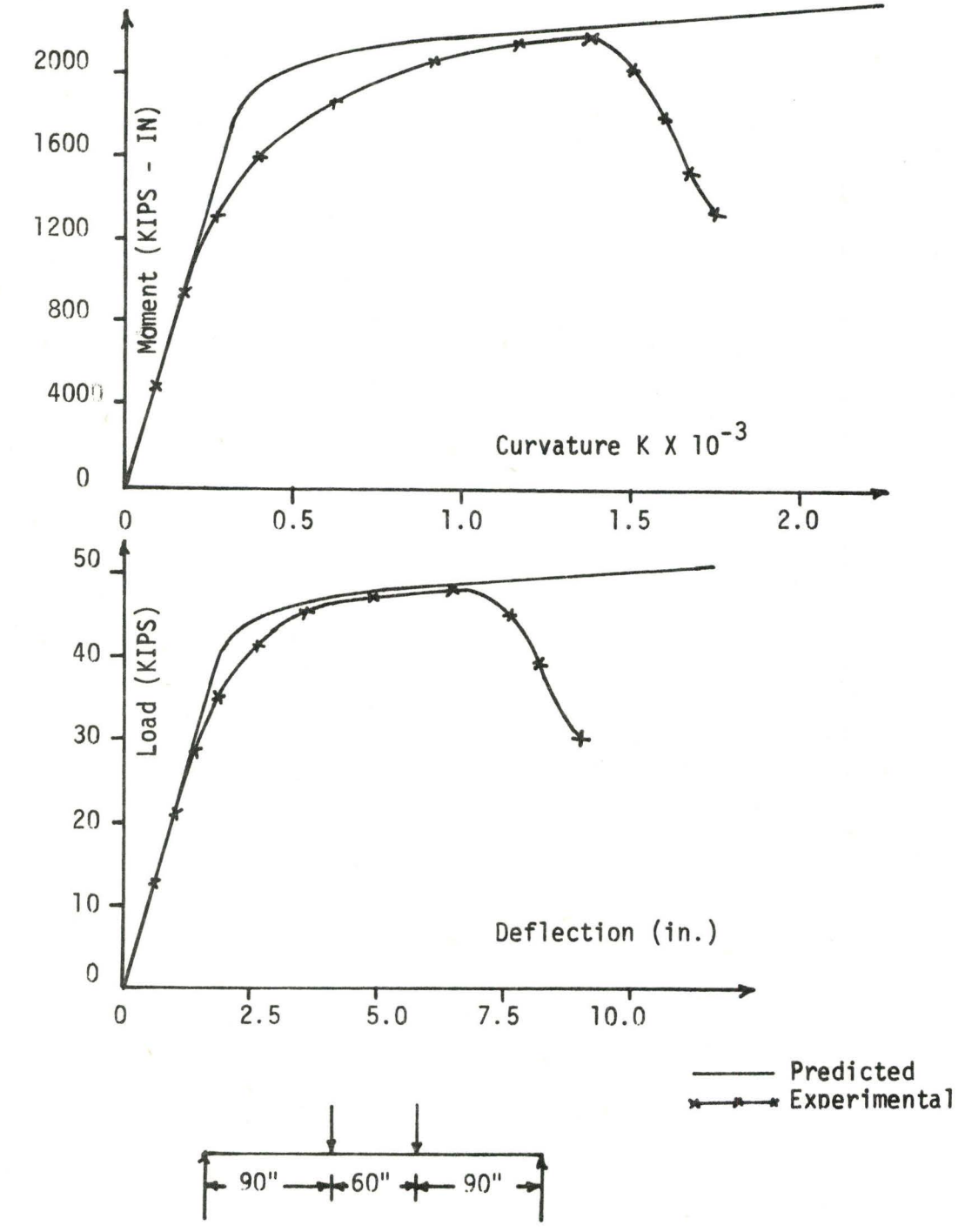

FIGURE 4.18 Results of Test No. (6b)

		S_3 (in^3)	Z_3 (in^3)	f	σ_0 (ksi)	E_{st} (ksi)	D/t
(7b)	H.S.S. 14.0 0 D X .250	36.45	47.25	1.296	43.2	400	56.0

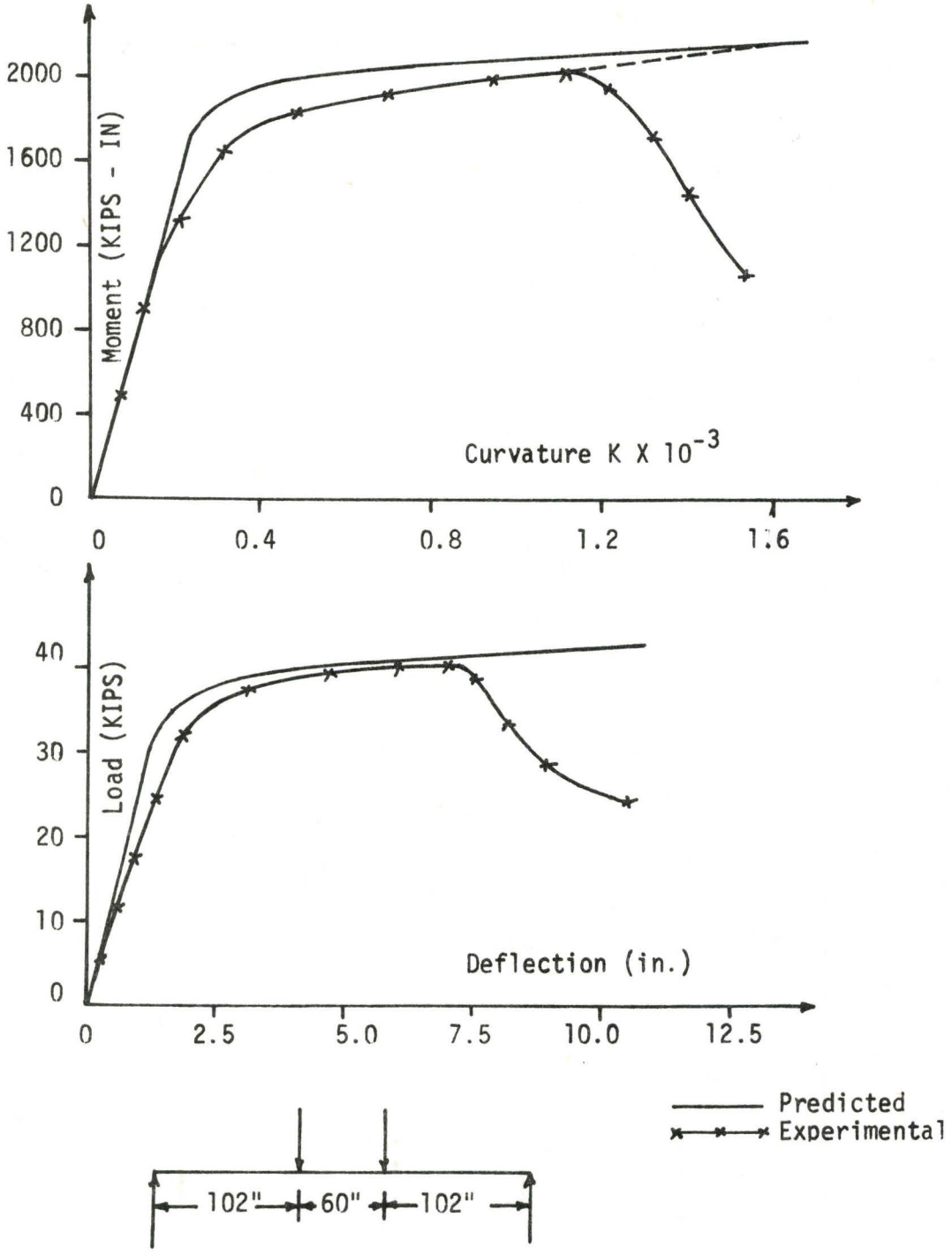

FIGURE 4.19 Results of Test No. (7b)

	S_3 (in^3)	Z_3 (in^3)	f	σ_0 (ksi)	E_{st} (ksi)	D/t
(8b) H.S.S. 16.0 O.D.X .250	47.93	61.99	1.293	44.8	255	64.0

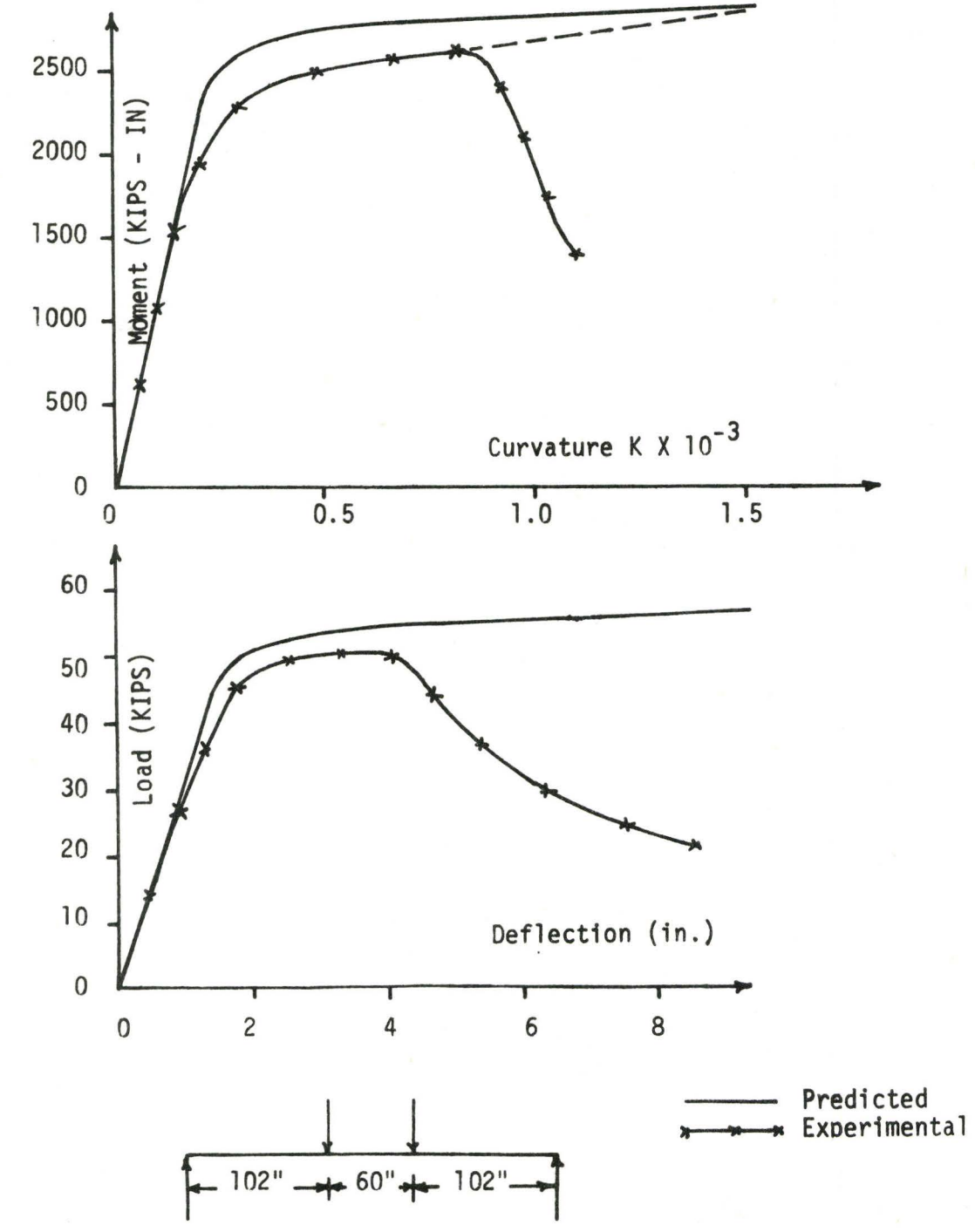

FIGURE 4.20 Results of Test No. (8b)

(1c) H.S.S.	S_3 (in^3)	Z_3 (in^3)	f	σ_0 (ksi)	E_{st} (ksi)	D/t
4.5 O.D.X .156	2.23	2.94	1.318	44.8	380	28.9

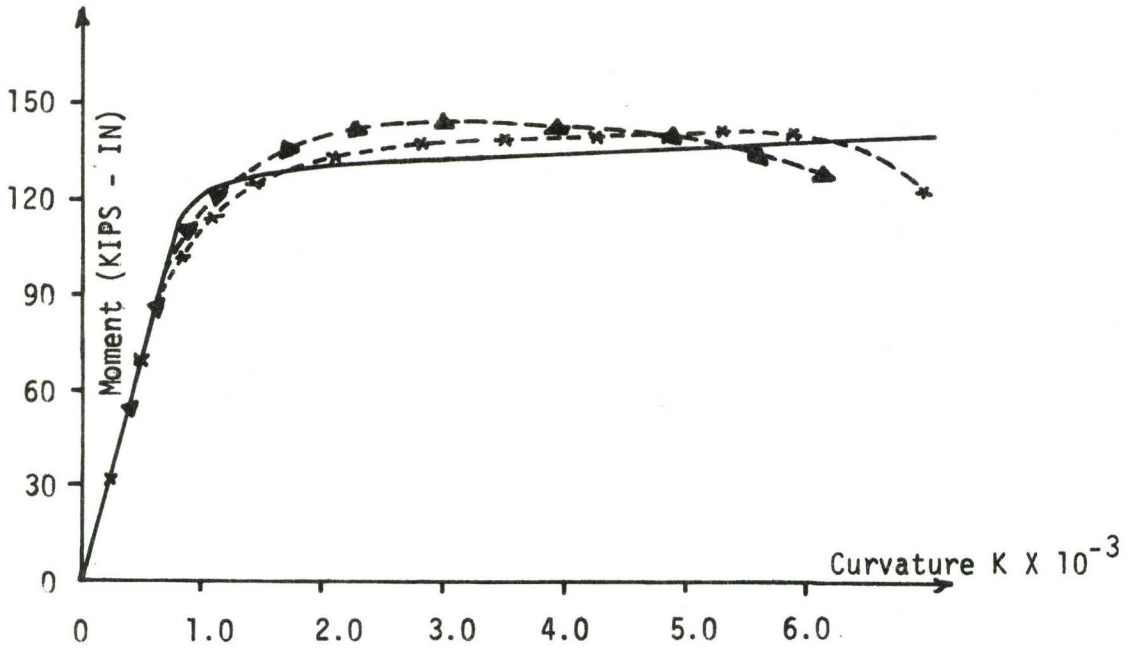

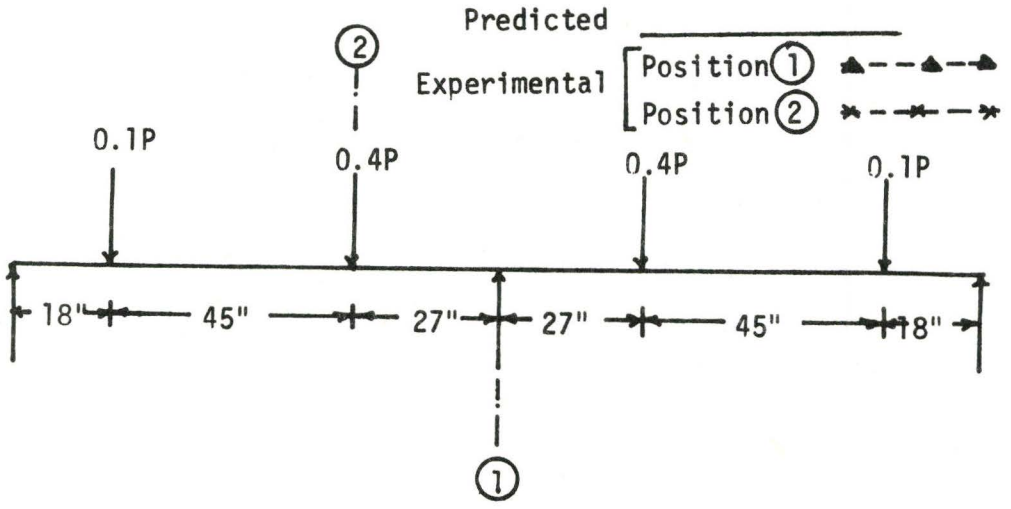

FIGURE 4.21 Two Span Beam - Test No. (1c)

	S_3 (in^3)	Z_3 (in^3)	f	σ_0 (ksi)	E_{st} (ksi)	D/t
(2c) H.S.S. 10.75 O.D.X 0.219	18.69	24.28	1.299	44.4	490	49.1

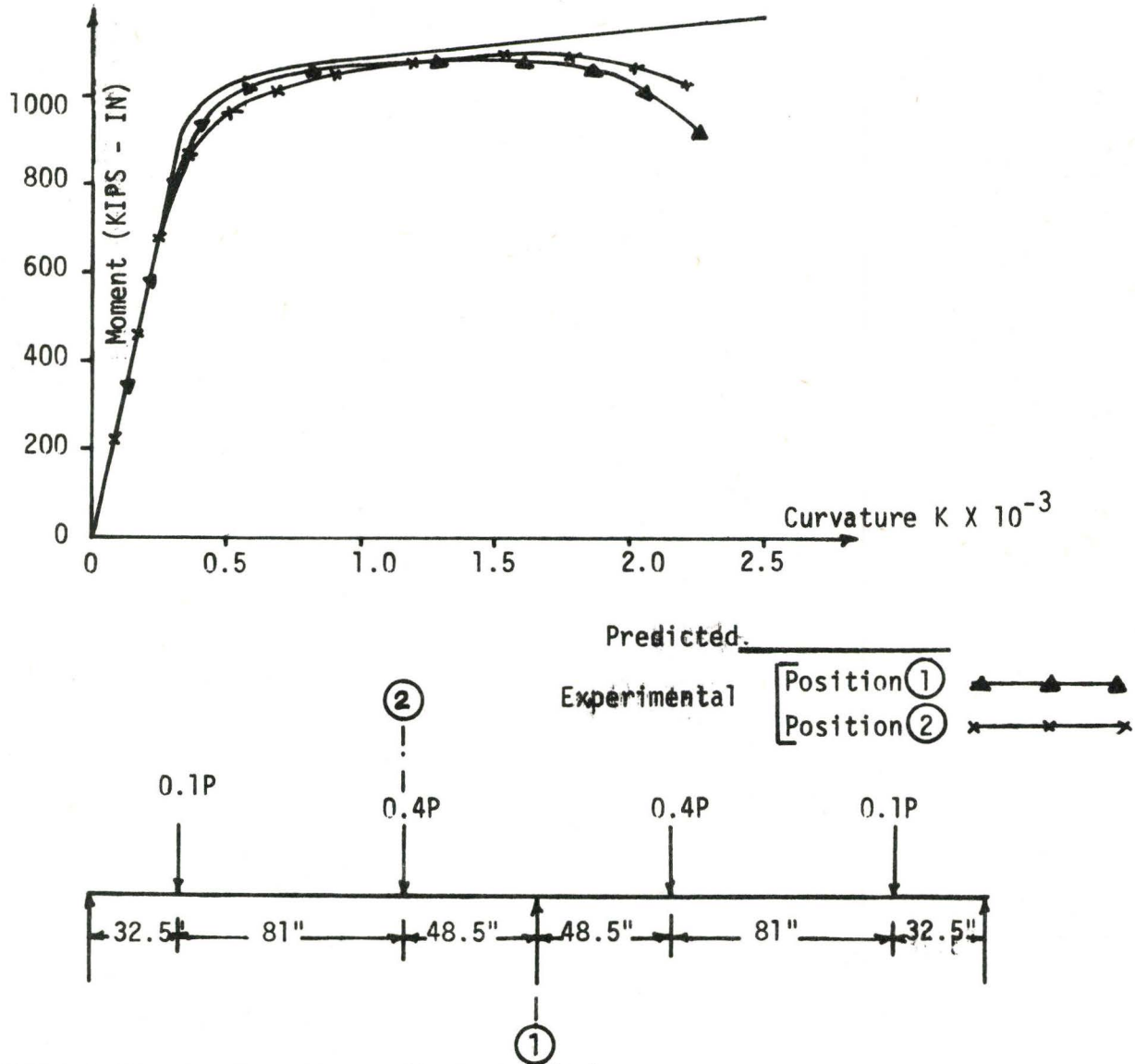

FIGURE 4.22 Two Span Beam - Test No. (2c)

TABLE 4.3 Test Data - Round Sections

(a) Simple Span Tests

(i) without bearing plates

No.	D/t	σ_0	M_u/M_o	M_u/M_p	Θ
(2b)	28.9	44.8	1.380	1.044	5.29
(3b)	35.2	53.5	1.352	1.032	3.54
(4b)	42.5	44.2	1.332	1.025	3.83

(ii) with bearing plates

No.	D/t	σ_0	M_u/M_o	M_u/M_p	Θ
(5b)	49.1	44.4	1.351	1.040	4.45
(6b)	51.0	54.5	1.338	1.030	2.84
(7b)	56.0	43.2	1.295	1.000	3.10
(8b)	64.0	44.8	1.213	0.947	2.35

(b) Two Span Tests

No.	D/t	σ_o	Middle Support			Major Load Point		
			M_u/M_o	M_u/M_p	Θ	M_u/M_o	M_u/M_p	Θ
(1c)	28.9	44.8	1.405	1.078	6.02	1.357	1.046	6.58
(2c)	49.1	44.4	1.316	1.011	3.82	1.310	1.005	4.56

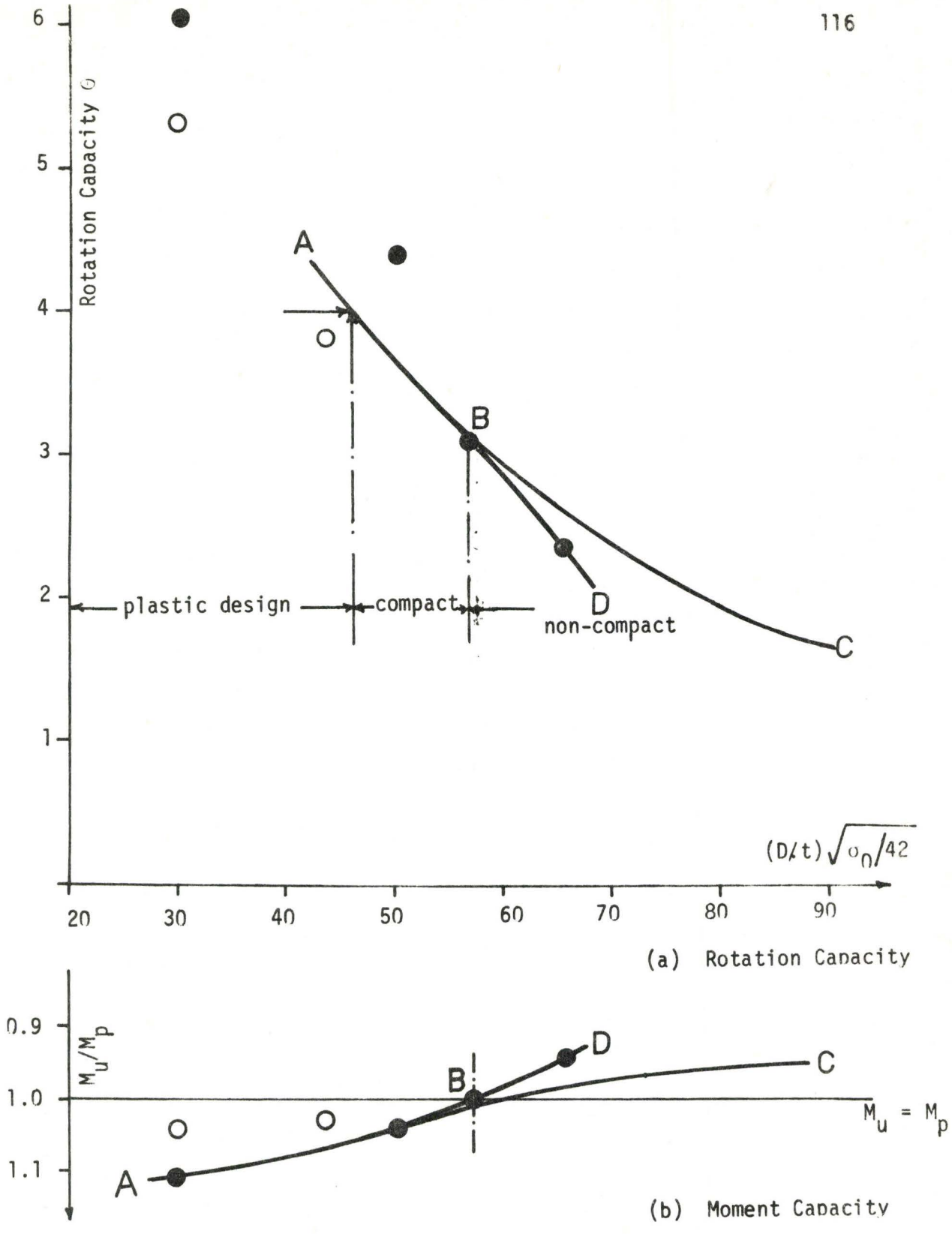

FIGURE 4.23 Design Criteria; σ_{0G} = 42 KSI

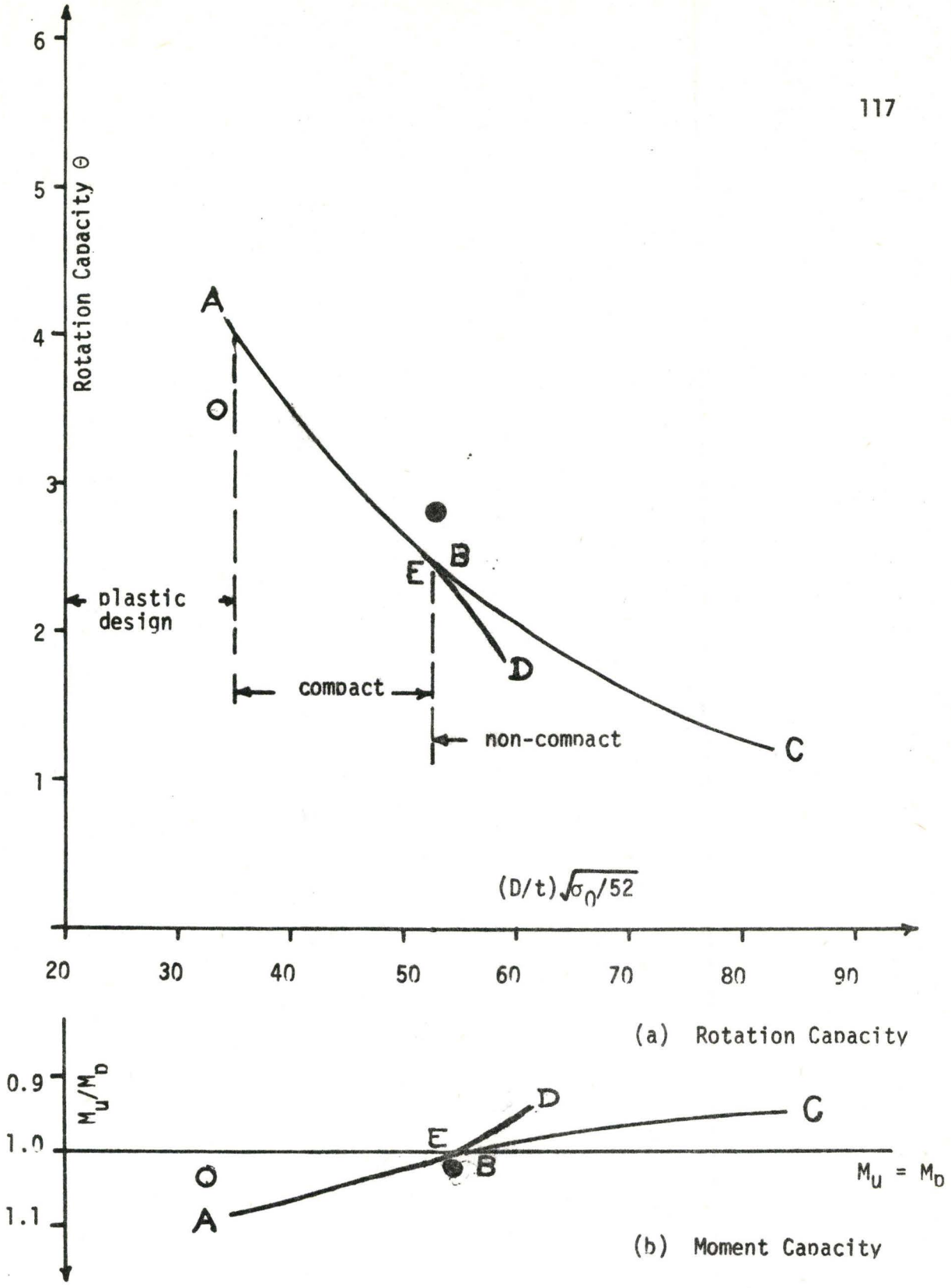

O Test without saddle plates
● Test with saddle plates
ABC: Theoretical curve
AED: Recommended design curve (extrapolated)

FIGURE 4.24 Design Criteria; σ_{0G} = 52 KSI

CHAPTER 5

CONCLUSIONS AND SUGGESTIONS FOR FURTHER RESEARCH

5.1 Rectangular Sections

The present series of experiments was meant to more firmly establish design criteria for rectangular HSS. The design recommendations were incorporated on the basis of the present test data as well as from the results of Hudoba[3]. Table 5.1 lists the limiting b/t ratios for design obtained from the overall data together with those specified by Hudoba and CSA-S16. The following remarks are made based on the two research programmes:

(a) For plastic design sections, the value of limiting flange slenderness ratio, b/t, specified by CSA-S16 is too liberal. The limiting value of b/t recommended is $159/\sqrt{\sigma_0}$ as compared to $200/\sqrt{\sigma_0}$ as is currently prescribed by CSA. This value is based upon a need for sufficient ductility of the sections to maintain the fully plastic moment at the first hinge to form before developing a mechanism in statically indeterminate structure. A plastic rotation capacity of 4 is decided to be adequate.

(b) In structures designed by the allowable stress method, the values of limiting b/t ratio recommended on the basis of aggregate data compare very well with the design specifications prescribed by CSA. For compact sections the specified value of $200/\sqrt{\sigma_0}$ is supported by the current work.

For non-compact sections the value recommended is $255/\sqrt{\sigma_0}$ which is slightly more than the value of $250/\sqrt{\sigma_0}$ as specified by CSA.

5.2 Round Sections

The design criterion for Round HSS has been established and discussed in the preceeding chapter. The limiting D/t ratios for round sections

in the preceding Chapter. On the basis of the theoretical study and test data the following remarks are made:

(a) For plastic design sections the maximum tube slenderness ratio D/t is limited to $200/\sqrt{\sigma_0}$ as specified by CSA. From the viewpoint of present work this value seems to be highly conservative. The limiting value recommended here varies from $300/\sqrt{\sigma_0}$ to $267/\sqrt{\sigma_0}$ for round HSS with yield strengths varying from 42 to 52 respectively. Also it was pointed out earlier that the form $A/\sqrt{\sigma_0}$ is not very rational and should be replaced by the form A/σ_0, where A is a constant. On this basis the limiting value of slenderness of rounds recommended in plastic design is $1924/\sigma_0$.

(b) For sections to be designed by the allowable stress method CSA recommends a limiting D/t ratio of $3300/\sigma_0$ and does not provide a distinction between compact and non-compact categories.

For compact sections this value is too liberal and is indicated to vary from $2350/\sigma_0$ to $2704/\sigma_0$ for σ_0 varying from 42 to 52 KSI respectively. A similar observation as indicated for the plastic design sections is apparent. Consequently it is proposed to alter the expression to a more consistent form with the results. The recommended limitation for D/t is, therefore, $365/\sqrt{\sigma_0}$.

For non-compact sections, experimental data is not available. However, the value of limiting D/t ratio for such sections, $3300/\sigma_0$, as prescribed by CSA seems to be reasonable and tends to be supported by our limited experience with tubes of large slenderness.

The beams tested in this programme were provided with saddle plates, approximately 3" to 6" wide at the load points and supports. In practice,

loads will normally be distributed to a much greater extent than was the case in the tests reported herein. Also bearing support surfaces will either be of at least an equivalent length and contact area as compared with the test series. Consequently the limiting D/t ratios as recommended above will be adequate except possibly in exceptional circumstances.

5.3 Suggestions for Further Research

The theoretical work dealt in Chapter 2 is believed to be adequate for predicting the buckling or ultimate moment with its associated curvature. To improve predictions of limiting D/t ratio in plastic design, however, large deflection theory incorporating non-linear material behaviour would have to be used since post-buckling response is required. Considerable complexity would be anticipated, however, due to the non-linear nature of the basic differential equation.

It has been observed that stress concentrations have severe effects on the bending moment resistance of the HSS generally and for tubes with large D/t ratio in particular. A better provision to avoid stress concentration on load points and supports is strongly recommended for such sections. Increased moment resistance can be attained by properly stiffening the section at the critical points. In addition, applying the load to the tension fibres or distributing it around the circumference by flexible straps would improve the carrying capacity. However, in practice, stress concentrations cannot be avoided completely. They can only be reduced in accordance with sound design principles.

Further research is necessary to establish the limiting D/t ratio for non-compact sections designed by the allowable stress method.

Category		Limiting b/t ratio		
		CSA-S16	Hudoba	Overall Data
Plastic Design		$200/\sqrt{\sigma_0}$	$150/\sqrt{\sigma_0}$	$159/\sqrt{\sigma_0}$
Allowable Stress Design	Compact	$200/\sqrt{\sigma_0}$	$210/\sqrt{\sigma_0}$	$200/\sqrt{\sigma_0}$
	Non-compact	$250/\sqrt{\sigma_0}$	$245/\sqrt{\sigma_0}$	$255/\sqrt{\sigma_0}$

TABLE 5.1 Limiting b/t Ratios for Rectangular Sections

Category		CSA S-16	Present Work	
			in the form as in CSA S-16	suggested expression
Plastic Design		$\frac{200}{\sqrt{\sigma_0}}$	$\frac{300}{\sqrt{\sigma_0}^*}$ to $\frac{267}{\sqrt{\sigma_0}^{**}}$	$\frac{1924}{\sigma_0}$
Allowable Stress Design	Compact	$\frac{3300}{\sigma_0}$	$\frac{2350}{\sigma_0^*}$ to $\frac{2704}{\sigma_0^{**}}$	$\frac{365}{\sqrt{\sigma_0}}$
	Non-compact	$\frac{3300}{\sigma_0}$	sufficient data not available	

Table 5.2 Limiting D/t Ratios for Round Sections

* $\sigma_0 \approx 42$ ksi

** $\sigma_0 \approx 52$ ksi

APPENDIX 1

DISPLACEMENT EQUATIONS

This Appendix is intended to solve the expression for longitudinal, circumferential and radial displacements in terms of critical buckling strain, material properties and geometrical parameters of the thin cylindrical shell. For convenience equations (10a), (10b), and (10c) of Chapter 2 can be re-written as follows:

$$A_1 \frac{\partial^2 u}{\partial x^2} + \frac{1}{4R^2} \frac{\partial^2 u}{\partial \theta^2} + \frac{3}{4R} \frac{\partial^2 v}{\partial x \partial \theta} + \frac{1}{2R} \frac{\partial w}{\partial x} = 0 \qquad (10a)$$

$$\frac{1}{R^2} \frac{\partial^2 v}{\partial \theta^2} + \frac{1}{4} \frac{\partial^2 v}{\partial x^2} + \frac{3}{4R} \frac{\partial^2 u}{\partial x \partial \theta} + \frac{1}{R^2} \frac{\partial w}{\partial \theta} = 0 \qquad (10b)$$

$$Y + \frac{1}{2} \frac{\partial u}{\partial x} + \frac{1}{R} \frac{\partial v}{\partial \theta} + \frac{w}{R} = 0 \qquad (10c)$$

where $Y = Y_1 + Y_2$ and

$$Y_1 = \frac{Rt^2}{12} \left[A_1 \frac{\partial^4 w}{\partial x^4} + \frac{2}{R^2} \frac{\partial^4 w}{\partial x^2 \partial \theta^2} + \frac{1}{R^4} \frac{\partial^4 w}{\partial \theta^4} \right]$$

$$Y_2 = \frac{3}{4} \varepsilon_c R \cos\theta \frac{\partial^2 w}{\partial x^2}$$

Differential Equation in x, y, u and w

$$A_1 \frac{\partial^3 u}{\partial x^3} + \frac{1}{4R^2} \frac{\partial^3 u}{\partial \theta^2 \partial x} + \frac{3}{4R} \frac{\partial^3 v}{\partial x^2 \partial \theta} + \frac{1}{2R} \frac{\partial^2 w}{\partial x^2} = 0 \qquad (A\text{-}1)$$

Differentiating equation (10b) w.r.t. θ and multiplying by 3/R,

$$\frac{3}{R^3}\frac{\partial^3 v}{\partial\theta^3} + \frac{3}{4R}\frac{\partial^3 v}{\partial x^2\partial\theta} + \frac{9}{4R^2}\frac{\partial^3 u}{\partial x\partial\theta^2} + \frac{3}{R^3}\frac{\partial^2 w}{\partial\theta^2} = 0 \qquad \text{(A-2)}$$

Eliminating $\frac{\partial^3 v}{\partial x^2\partial\theta}$ between equations (A-1) and (A-2),

$$A_1\frac{\partial^3 u}{\partial x^3} - \frac{2}{R^2}\frac{\partial^3 u}{\partial x\,\partial\theta^2} - \frac{3}{R^3}\frac{\partial^3 v}{\partial\theta^3} + \frac{1}{2R}\frac{\partial^2 w}{\partial x^2} - \frac{3}{R^3}\frac{\partial^2 w}{\partial\theta^2} = 0 \qquad \text{(A-3)}$$

Differentiating equation (A-3) w.r.t. x,

$$A_1\frac{\partial^4 u}{\partial x^4} - \frac{2}{R^2}\frac{\partial^4 u}{\partial x^2\partial\theta^2} - \frac{3}{R^3}\frac{\partial^4 v}{\partial x\partial\theta^3} + \frac{1}{2R}\frac{\partial^3 w}{\partial x^3} - \frac{3}{R^3}\frac{\partial^3 w}{\partial x\partial\theta^2} = 0 \qquad \text{(A-4)}$$

Differentiating equation (10a) w.r.t. θ twice,

$$\frac{A_1}{R^2}\frac{\partial^4 u}{\partial x^2\partial\theta^2} + \frac{2}{R^2}\frac{\partial A_1}{\partial\theta}\frac{\partial^3 u}{\partial x^2\partial\theta} + \frac{1}{R^2}\frac{\partial^2 A_1}{\partial\theta^2}\frac{\partial^2 u}{\partial x^2}$$

$$+ \frac{1}{4R^4}\frac{\partial^4 u}{\partial\theta^4} + \frac{3}{4R^3}\frac{\partial^4 v}{\partial x\partial\theta^3} + \frac{1}{2R^3}\frac{\partial^3 w}{\partial x\partial\theta^2} = 0 \qquad \text{(A-5)}$$

Eliminating $\frac{\partial^4 v}{\partial x\partial\theta^3}$ between equations (A-4) and (A-5),

$$\frac{A_1}{4}\frac{\partial^4 u}{\partial x^4} + \frac{(A_1 - \frac{1}{2})}{R^2}\frac{\partial^4 u}{\partial x^2\partial\theta^2} + \frac{2}{R^2}\frac{\partial A_1}{\partial\theta}\frac{\partial^3 u}{\partial x^2\partial\theta} + \frac{1}{R^2}\frac{\partial^2 A_1}{\partial\theta^2}\frac{\partial^2 u}{\partial x^2}$$

$$+\frac{1}{4R^4}\frac{\partial^4 u}{\partial\theta^4}+\frac{1}{8R}\frac{\partial^3 w}{\partial x^3}-\frac{1}{4R^3}\frac{\partial^3 w}{\partial x\partial\theta^2}=0 \qquad \text{(A-6)}$$

Differential Equation in x, y, v and w

Eliminating

$$\frac{\partial^3 u}{\partial x\partial\theta^2}$$

between equations (A-1) and (A-2),

$$\frac{1}{R^3}\frac{\partial^3 v}{\partial\theta^3}-\frac{2}{R}\frac{\partial^3 v}{\partial x^2\partial\theta}-3A_1\frac{\partial^3 u}{\partial x^3}+\frac{1}{R^3}\frac{\partial^2 w}{\partial\theta^2}-\frac{3}{2R}\frac{\partial^2 w}{\partial x^2}=0 \qquad \text{(A-7)}$$

Differentiating equation (A-7) w.r.t θ,

$$\frac{1}{R^4}\frac{\partial^4 v}{\partial\theta^4}-\frac{2}{R^2}\frac{\partial^4 v}{\partial x^2\partial\theta^2}-\frac{3A_1}{R}\frac{\partial^4 u}{\partial x^3\partial\theta}-\frac{3}{R}\frac{\partial A_1}{\partial\theta}\frac{\partial^3 u}{\partial x^3}$$

$$+\frac{1}{R^4}\frac{\partial^3 w}{\partial\theta^3}-\frac{3}{2R^2}\frac{\partial^3 w}{\partial x^2\partial\theta}=0 \qquad \text{(A-8)}$$

Differentiating equation (10b) w.r.t. x twice,

$$\frac{1}{R^2}\frac{\partial^4 v}{\partial x^2\partial\theta^2}+\frac{1}{4}\frac{\partial^4 v}{\partial x^4}+\frac{3}{4R}\frac{\partial^4 u}{\partial x^3\partial\theta}+\frac{1}{R^2}\frac{\partial^3 w}{\partial x^3\partial\theta}=0 \qquad \text{(A-9)}$$

Eliminating $\frac{\partial^4 u}{\partial x^3\partial\theta}$ between equations (A-8) and (A-9),

$$A_1 \frac{\partial^4 v}{\partial x^4} + \frac{1}{R^4} \frac{\partial^4 v}{\partial \theta^4} + \frac{(4A_1 - 2)}{R^2} \frac{\partial^4 v}{\partial x^2 \partial \theta^2} - \frac{3}{R} \frac{\partial A_1}{\partial \theta} \frac{\partial^3 u}{\partial x^3}$$

$$+ \frac{1}{R^4} \frac{\partial^3 w}{\partial \theta^3} + \frac{(4A_1 - 3/2)}{R^2} \frac{\partial^3 w}{\partial x^2 \partial \theta} = 0 \qquad \text{(A-10)}$$

where

$$\frac{\partial^3 u}{\partial x^3} = \frac{1}{A_1} \left[\frac{2}{R^2} \frac{\partial^3 u}{\partial x \partial \theta^2} + \frac{3}{R^3} \frac{\partial^3 v}{\partial \theta^3} - \frac{1}{2R} \frac{\partial^2 w}{\partial x^2} + \frac{3}{R^3} \frac{\partial^2 w}{\partial \theta^2}\right]$$

from equation (A-3), and

$$\frac{1}{R^2} \frac{\partial^3 u}{\partial x \partial \theta^2} = -\frac{4}{3} \left[\frac{1}{R^3} \frac{\partial^3 v}{\partial \theta^3} + \frac{1}{4R} \frac{\partial^3 v}{\partial x^2 \partial \theta} + \frac{1}{R^3} \frac{\partial^2 w}{\partial \theta^2}\right]$$

from equation (A-2).

Differential Equation between x,y and w

Differentiating equation (10c) w.r.t. x,

$$\frac{\partial Y}{\partial x} + \frac{1}{2} \frac{\partial^2 u}{\partial x^2} + \frac{1}{R} \frac{\partial^2 v}{\partial x \partial \theta} + \frac{1}{R} \frac{\partial w}{\partial x} = 0 \qquad \text{(A-11)}$$

Eliminating $\frac{\partial^2 v}{\partial x \partial \theta}$ between equations (10a) and (A-11),

$$\frac{\partial Y}{\partial x} + \left(\frac{1}{2} - \frac{4}{3} A_1\right) \frac{\partial^2 u}{\partial x^2} - \frac{1}{3R^2} \frac{\partial^2 u}{\partial \theta^2} + \frac{1}{3R} \frac{\partial w}{\partial x} = 0 \qquad \text{(A-12)}$$

Differentiating equation (10c) w.r.t. θ,

$$\frac{1}{R} \frac{\partial Y}{\partial \theta} + \frac{1}{2R} \frac{\partial^2 u}{\partial x \partial \theta} + \frac{1}{R^2} \frac{\partial^2 v}{\partial \theta^2} + \frac{1}{R^2} \frac{\partial w}{\partial \theta} = 0 \qquad \text{(A-13)}$$

Eliminating $\frac{\partial^2 v}{\partial x \partial \theta}$ between equations (10b) and (A-13),

$$\frac{1}{R}\frac{\partial \gamma}{\partial \theta} - \frac{1}{4R}\frac{\partial^2 u}{\partial x \partial \theta} - \frac{1}{4}\frac{\partial^2 v}{\partial x^2} = 0 \qquad \text{(A-14)}$$

Differentiating equation (A-14) w.r.t. θ,

$$\frac{1}{R}\frac{\partial^2 \gamma}{\partial \theta^2} - \frac{1}{4R}\frac{\partial^3 u}{\partial x \partial \theta^2} - \frac{1}{4}\frac{\partial^3 v}{\partial x^2 \partial \theta} = 0 \qquad \text{(A-15)}$$

Eliminating $\frac{\partial^3 v}{\partial x^2 \partial \theta}$ between equations (A-1) and (A-15),

$$\frac{3}{R^2}\frac{\partial^2 \gamma}{\partial \theta^2} + A_1\frac{\partial^3 u}{\partial x^3} - \frac{1}{2R^2}\frac{\partial^3 u}{\partial x \partial \theta^2} + \frac{1}{2R}\frac{\partial^2 w}{\partial x^2} = 0 \qquad \text{(A-16)}$$

Differentiating equation (A-12) w.r.t. x,

$$\frac{\partial^2 \gamma}{\partial x^2} + \left(\frac{1}{2} - \frac{4}{3}A_1\right)\frac{\partial^3 u}{\partial x^3} - \frac{1}{3R^2}\frac{\partial^3 u}{\partial x \partial \theta^2} + \frac{1}{3R}\frac{\partial^2 w}{\partial x^2} = 0 \qquad \text{(A-17)}$$

Eliminating $\frac{\partial^3 u}{\partial x \partial \theta^2}$ between equations (A-16) and (A-17),

$$\frac{1}{R^2}\frac{\partial^2 \gamma}{\partial \theta^2} - \frac{1}{2}\frac{\partial^2 \gamma}{\partial x^2} + (A_1 - 1/4)\frac{\partial^3 u}{\partial x^3} = 0 \qquad \text{(A-18)}$$

Eliminating $\frac{\partial^3 u}{\partial x^3}$ between equations (A-16) and (A-18),

$$\frac{(2A_1 - 3/4)}{R^2}\frac{\partial^2 \gamma}{\partial \theta^2} + \frac{A_1}{2}\frac{\partial^2 \gamma}{\partial x^2} + \frac{(A_1 - 1/4)}{2R^2}\frac{\partial^3 u}{\partial x \partial \theta^2}$$

$$+ \frac{(A_1 - 1/4)}{2R} \frac{\partial^2 w}{\partial x^2} = 0 \qquad \text{(A-19)}$$

Differentiating equations (A-18) w.r.t. θ twice,

$$\frac{1}{R^4} \frac{\partial^4 \gamma}{\partial \theta^4} - \frac{1}{2R^2} \frac{\partial^4 \gamma}{\partial x^2 \partial \theta^2} + \frac{(A_1 - 1/4)}{R^2} \frac{\partial^5 u}{\partial x^3 \partial \theta^2}$$

$$+ \frac{2}{R^2} \frac{\partial A_1}{\partial \theta} \frac{\partial^4 u}{\partial x^3 \partial \theta} + \frac{1}{R^2} \frac{\partial^2 A_1}{\partial \theta^2} \frac{\partial^3 u}{\partial x^3} = 0 \qquad \text{(A-20)}$$

Differentiating equation (A-19) w.r.t. x twice,

$$\frac{(2A_1 - 3/4)}{R^2} \frac{\partial^4 \gamma}{\partial \theta^2 \partial x^2} + \frac{A_1}{2} \frac{\partial^4 \gamma}{\partial x^4} - \frac{(A_1 - 1/4)}{2R^2} \frac{\partial^5 u}{\partial x^3 \partial \theta^2}$$

$$+ \frac{(A_1 - 1/4)}{2R} \frac{\partial^4 w}{\partial x^4} = 0 \qquad \text{(A-21)}$$

Eliminating $\frac{\partial^5 u}{\partial x^3 \partial \theta^2}$ between equations (A-20) and (A-21),

$$\frac{(4A_1 - 2)}{R^2} \frac{\partial^4 \gamma}{\partial x^2 \partial \theta^2} + A_1 \frac{\partial^4 \gamma}{\partial x^4} + \frac{1}{R^4} \frac{\partial^4 \gamma}{\partial \theta^4} + \frac{(A_1 - 1/4)}{R} \frac{\partial^4 w}{\partial x^4}$$

$$+ \frac{2}{R^2} \frac{\partial A_1}{\partial \theta} \frac{\partial^4 u}{\partial x^3 \partial \theta} + \frac{1}{R^2} \frac{\partial^2 A_1}{\partial \theta^2} \frac{\partial^3 u}{\partial x^3} = 0 \qquad \text{(A-22)}$$

where $$\frac{\partial^3 u}{\partial x^3} = \frac{1}{(A_1 - 1/4)} \left[\frac{1}{2} \frac{\partial^2 \gamma}{\partial x^2} - \frac{1}{R^2} \frac{\partial^2 \gamma}{\partial \theta^2}\right]$$

and $$\frac{1}{R}\frac{\partial^4 u}{\partial x^3 \partial \theta} = \left[-\frac{1}{(A_1 - 1/4)R}\frac{\partial A_1}{\partial \theta}\right.\quad \frac{1}{2}\frac{\partial^2 Y}{\partial \theta^2} - \frac{1}{R^2}\frac{\partial^2 Y}{\partial \theta^2}$$

$$\left. + \frac{1}{2R}\frac{\partial^3 Y}{\partial x^2 \partial \theta} - \frac{1}{R^3}\frac{\partial^3 Y}{\partial \theta^3}\right] \frac{1}{(A_1 - 1/4)}$$

from equation (A-18).

Thus equation (A-22) forms an eighth-order partial differential equation in w when derivatives of Y are substituted. The result is given as equation (11) in Chapter 2.

APPENDIX 2

DESCRIPTION OF COMPUTER PROGRAM FOR EVALUATION OF LIMITING D/t RATIOS

A.2.1 Introduction

A special computer program to evaluate the value of limiting D/t ratio for a preassigned value of critical buckling strain was developed using the technique of finite elements. Reference is made to equations (16) to (22) of Chapter 2.

The input data consists of the following:

(i) the material properties of the tube (Ramberg-Osgood stress-strain relationship),

(ii) the number of terms considered in equation (16), i.e., 'p',

(iii) the preassigned value of critical buckling strain, i.e., ε_c,

(iv) the number of elements into which the circumference of the tube is divided, i.e., N, and,

(v) the trial values of D/t and $\frac{m\pi R}{L}$.

For each trial value of D/t and (mπR/L) the resulting determinant given by equation (22) is calculated. The resulting grid of determinants is used to estimate the limiting D/t ratio for the preassigned value of critical buckling strain as discussed in Chapter 2.

Each of the coefficients q_j given by equations (19a) to (19s) consists of 'p' terms and can be expressed as follows:

$$q_j = q'_{j1}\, a_0 + q'_{j2}\, a_1 + q'_{j3}\, a_2 + \ldots\ldots\ldots\ldots$$

$$+ q'_{j(p-1)}\, a_{(p-2)} + q'_{jp}\, a_{(p-1)}$$

where q'_{j1}, q'_{j2} etc. are functions of m, R, L and θ. The expressions for the elements of the determinant given by equation (22), then, can be simplified as follows:

$$\beta_{nq} = \int_0^{2\pi} \left[\sum_{j=1}^{19} \alpha_j \, q'_{jn} \right] \cos (q - 1)\theta d\theta$$

This formulation was utilized to simplify the program.

The Fortran program consists of the following:

(a) A Main Program which computes the coefficients α_j, q'_{jn} etc. for each elements of the circumference of the tube and finally evaluates the elements (β_{11}, β_{21} etc.) of the determinant by numerical integration over the circumference. Finally the determinant is calculated by using subroutine MINV from McMaster Library of Subroutines.

(b) A Subroutine DELTA which iterates the value of stress for the given strain on an element (since direct computation of stress distribution is not possible) to the given degree of accuracy. The tangent and secant modulii are then calculated at the level of each element to find the plasticity coefficient A_1 and its higher derivatives w.r.t.θ.

A.2.2 Designations

The meaning of the variables used in the Fortran program are as given below. The details of operations are shown in the program by comment cards and in the flow-charts drawn in section A.2.3.

E = E

SO = $\sigma_{0.7}$

YS = σ_0

K = k

T = t

NEL = N

STNC = ε_c

KLK = p

JR = number of trial values of D/t ratio

JX = number of trial values of ($m\pi R/L$)

RAT = D/t

XL = ($m\pi R/L$)

DELANG = $d\theta = 2\pi/N$

ANGLE = θ

ET = E_T

ES = E_s

KJ = the accuracy of stress-strain distribution iterations in decimal places

SR = σ_x'

SN = ε_x

DELSR = $\delta\sigma_x'$

DELE = $\delta\sigma_x'/E_T$

SND = ε_x'

A_1, B_1 = A_1

$$A_2,\ B_2 = \frac{\partial A_1}{\partial \theta}$$

$$A_3,\ B_3 = \frac{\partial^2 A_1}{\partial \theta^2}$$

$$A_4,\ B_4 = \frac{\partial^3 A_1}{\partial \theta^3}$$

A_5, $B_5 = \dfrac{\partial^4 A_1}{\partial \theta^4}$

ALP (J) = the value of α_j

ALPHA (I, JJ) = the value of α_j

PQ (J) = the value of $q'_{j(n+1)}$

BBB (NN, NQ) = $\beta_{(q+1)(n+1)}$

D, DETT = Δ

] at an angle θ specified by Fortran variable ANGLE (I)

Other are works variables only.

A.2.3 Flow-Charts

(a) Main Program

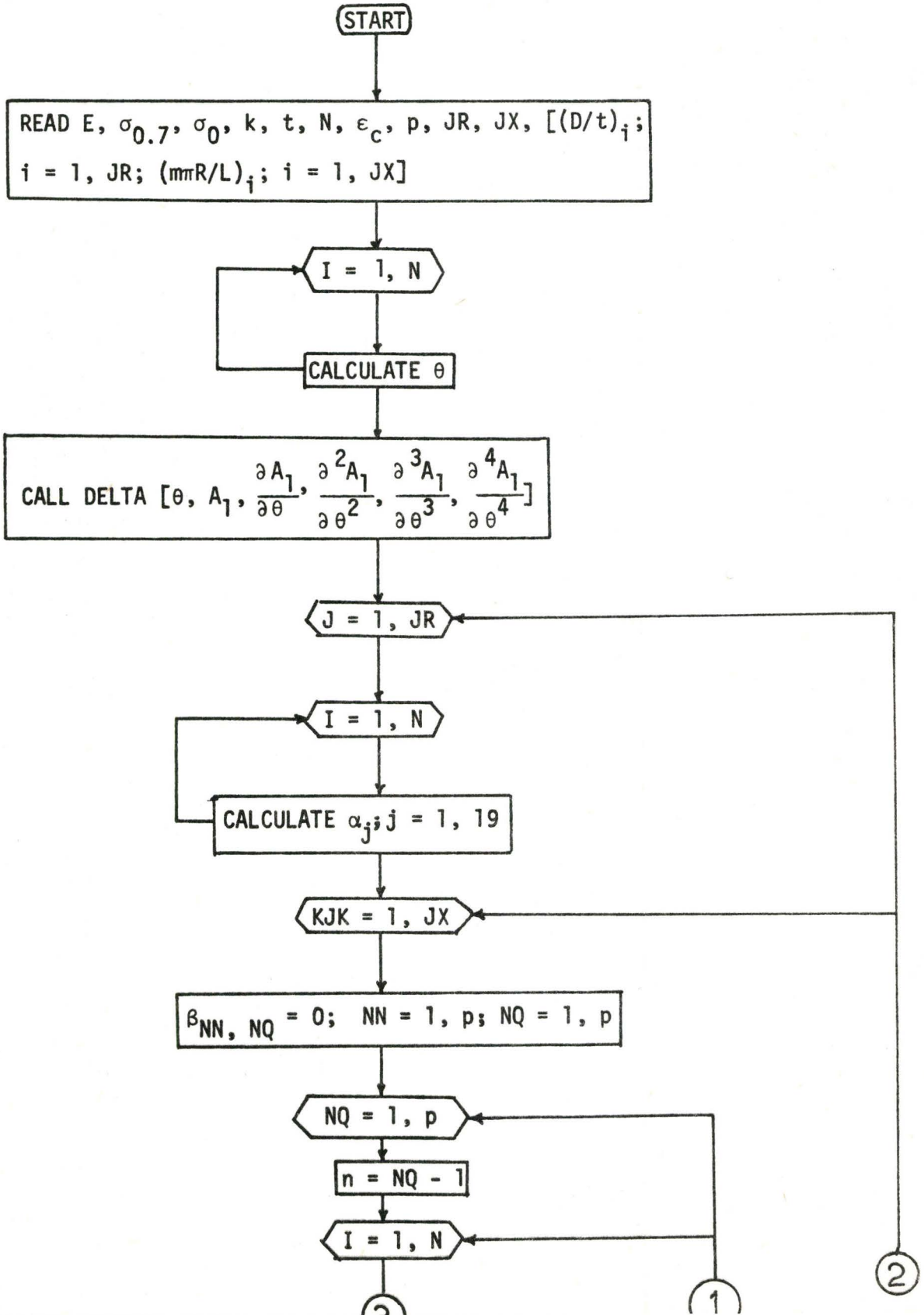

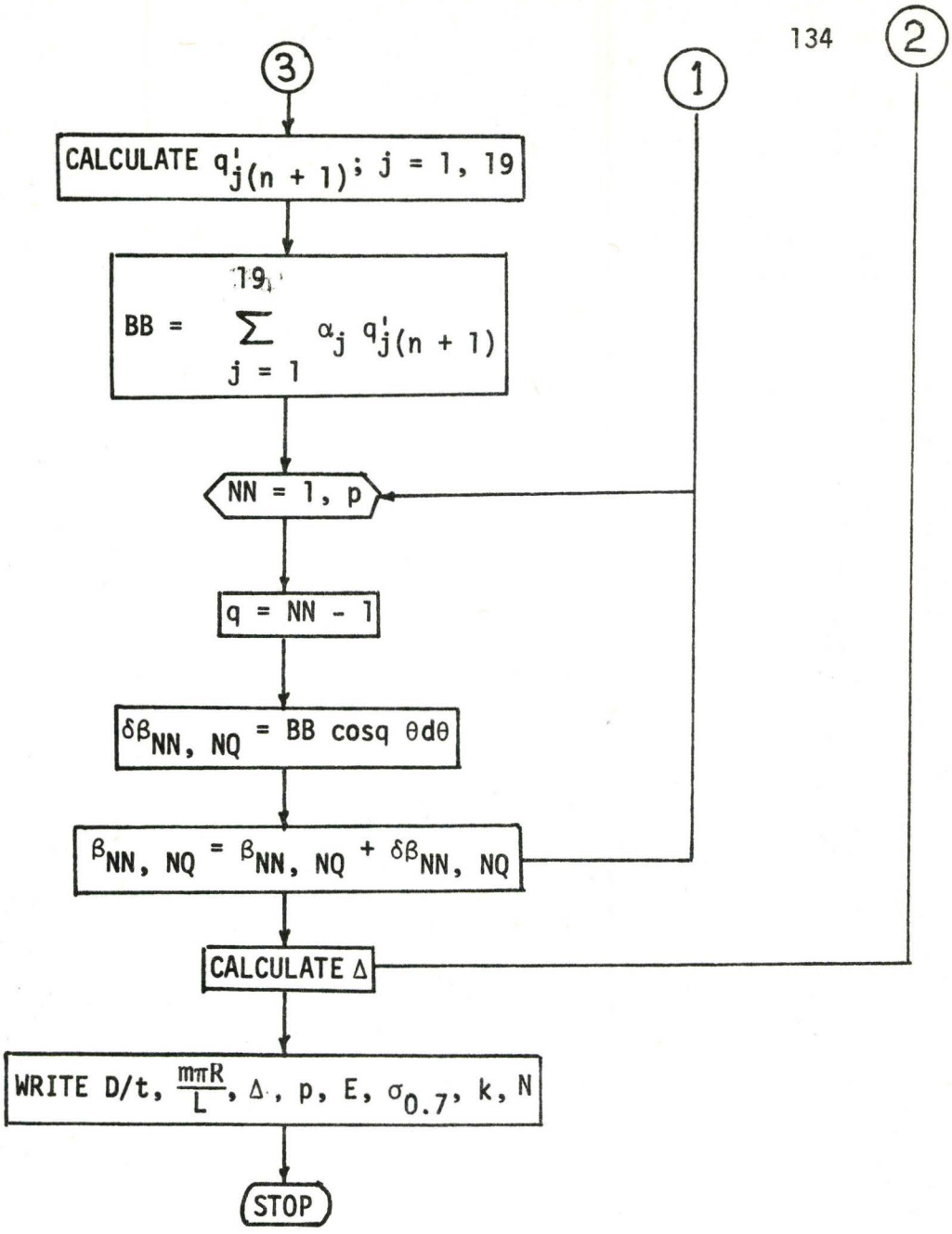
3
1
2
CALCULATE $q'_{j(n+1)}$; j = 1, 19
$BB = \sum_{j=1}^{19} \alpha_j \, q'_{j(n+1)}$
NN = 1, p
q = NN - 1
$\delta\beta_{NN, NQ} = BB \cos q \, \theta d\theta$
$\beta_{NN, NQ} = \beta_{NN, NQ} + \delta\beta_{NN, NQ}$
CALCULATE Δ
WRITE D/t, $\frac{m\pi R}{L}$, Δ, p, E, $\sigma_{0.7}$, k, N
STOP

(b) Subroutine DELTA

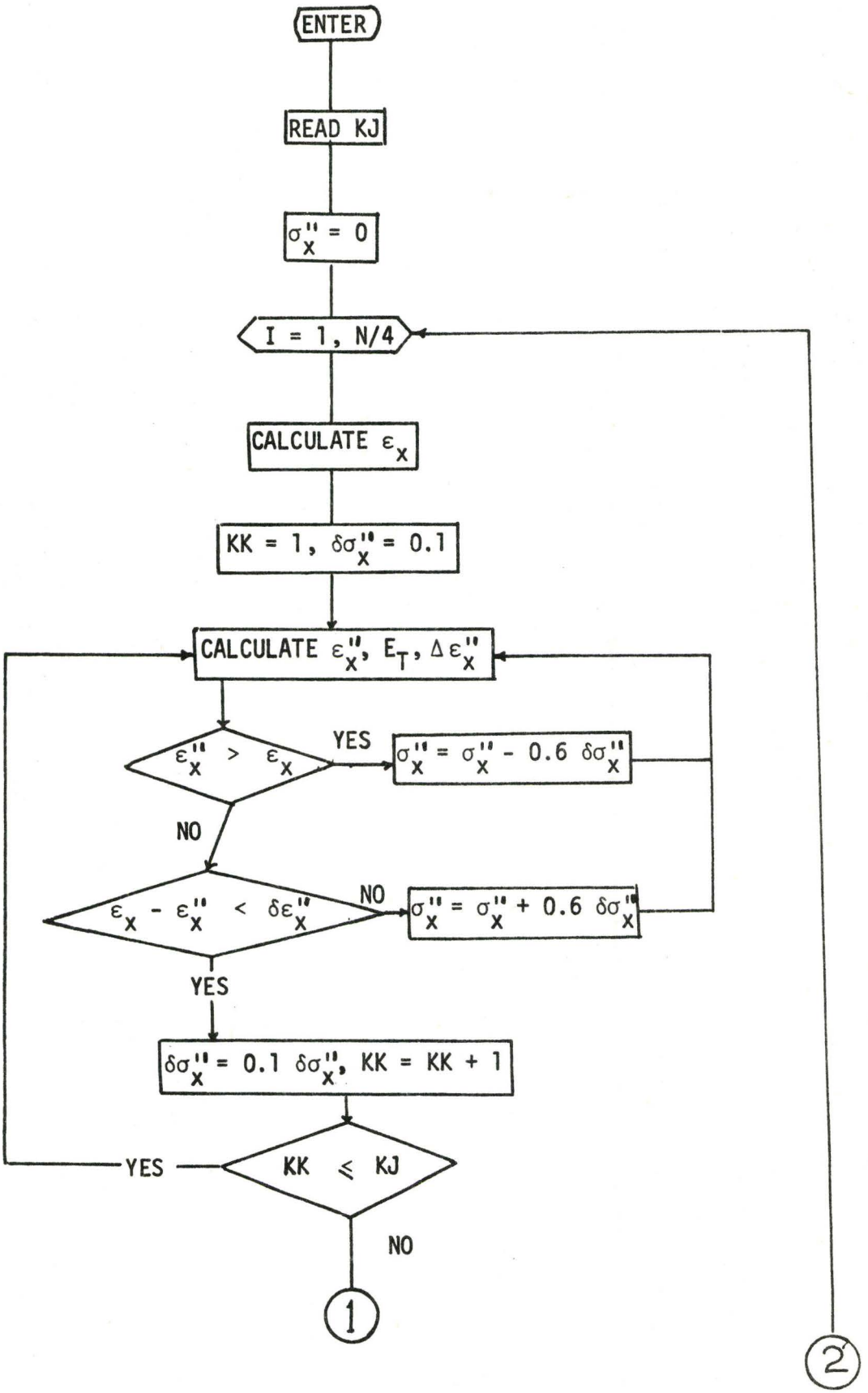

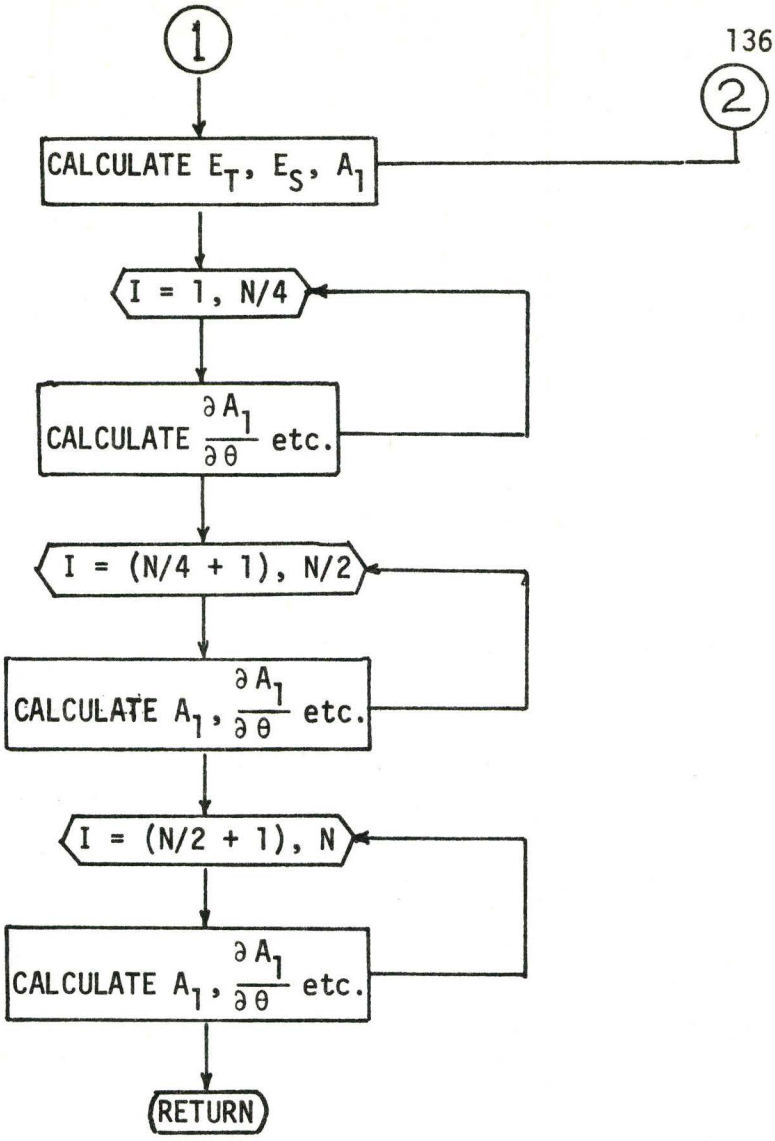
1
2
CALCULATE E_T, E_S, A_1
I = 1, N/4
CALCULATE $\frac{\partial A_1}{\partial \theta}$ etc.
I = (N/4 + 1), N/2
CALCULATE A_1, $\frac{\partial A_1}{\partial \theta}$ etc.
I = (N/2 + 1), N
CALCULATE A_1, $\frac{\partial A_1}{\partial \theta}$ etc.
RETURN

A.2.4 COMPUTER PROGRAM

```
HRK6,CM50000,T400.                                                    PRASAD
RUN(S)
SETINDF.
REDUCF.
LGO.
'        6400 END OF RECORD
      PROGRAM TST (INPUT,OUTPUT,TAPE5=INPUT,TAPE6=OUTPUT)
C     THE VARIABLES ARE DEFINED IN SECTION A.2.2.
      DIMENSION ANGLE(360),B1(360),B2(360),B3(360),B4(360),B5(360),
     1RAT(10),RZ(10),L(12),M(12),ALP(19),Q(19),P(19),XL(15),DETT(8,15),
     2PO(19),C(19),ALPHA(360,19),BBB(12,12),B(144),DETT(8,15),XL(15)
      COMMON NEL,K,SO,STNC
      REAL LX
      READ(5,49)E,SO,YS,K,T,NEL
      READ(5,51)STNC,KLK,JR,JX
      READ(5,52)(RAT(J),J=1,JR)
      READ(5,53)(XL(KJK),KJK=1,JX)
      PI=4.*ATAN(1.)
      DELANG=2.*PI/FLOAT(NEL)
C     DIVIDE THE CIRCUMFERENCE OF THE TUBE INTO THE SPECIFIED NUMBER OF
     *ELEMENTS
      DO 100  I=1,NEL
      ANGLE(I)=(FLOAT(I)-0.5)*DELANG
 100  CONTINUE
C     CALL SUBROUTINE DELTA TO OBTAIN THE VALUES OF PLASTICITY COEFFICIENT
     *AND ITS HIGHER DERIVATIVES ALONG THE CIRCUMFERENCE FOR EACH ELEMENT
      CALL DELTA(ANGLE,B1,B2,B3,B4,B5)
C     FIX THE TRIAL VALUE OF D/T RATIO
      DO  42  J=1,JR
      RZ(J)=T*(RAT(J)-1.)/2.
      R=RZ(J)
C     CALCULATE THE VALUES OF COEFFICIENTS ALP(1), ALP(2),.......,ALP(19)
     *ETC. FOR EACH ELEMENT
      DO 95  I=1,360
      A1=B1(I)
      A2=B2(I)
      A3=B3(I)
      A4=B4(I)
      A5=B5(I)
      X=COS(ANGLE(I))
      Y=SIN(ANGLE(I))
      AO=A1-0.25
      ALP(1)=A1**2
      ALP(2)=4.*A1**2
      ALP(3)=10.*A1-4.
      ALP(4)=4.*A1
      ALP(5)=1.
      ALPA=A2*A1/AO/R
      ALP(6)=2.*(4.*A1-2.)*A2/R+ALPA
      ALP(7)=A2/R/AO*(2.*A1+1.)
      ALP(8)=-3.*A2/AO/R
```

```
      ALP(9)=-2.*A2/A0/R
      ALPA=4.*A1-2.+A1/(2.*A0)
      ALPB=0.25*A2**2/A0**2
      ALPC=A1*9.*STNC/T**2*X
      ALP(10)=(A3*ALPA-ALPB)/R**2+ALPC
      ALPA=(4.*A1-2.)*9.*STNC/T**2*X
      ALPB=A3*(6.+(1.-A1)/A0)/R**2
      ALPC=A2**2/A0*(6.+2.*(1.-A1)/A0)/R**2
      ALP(11)=ALPA+ALPB-ALPC
      ALPA=9.*STNC/T**2*X
      ALPB=1./R**2/A0
      ALPC=3.*A2**2/A0-1.5*A3
      ALP(12)=ALPA+ALPB*ALPC
      ALP(13)=-1./R**2/A0*(A3-2./A0*A2**2)
      ALPA=4.*A4
      ALPB=2.*A2/A0
      ALPC=2./A0*A2**2-4.*A3
      ALPD=A2/A0*X-4.*(2.*A1-1.)*Y
      ALP(14)=(ALPA+ALPB*ALPC)/R**3+9.*STNC/T**2/R*ALPD
      ALPA=4.*Y+2.*A2/A0*X
      ALP(15)=-9.*STNC/R/T**2*ALPA
      ALPA=-(4.*A1-2.)*9.*STNC/(R*T)**2*X
      ALPB=A5/R**4
      ALPC=1./R**2/A0
      ALPD=A3-2./A0*A2**2
      ALPE=4.5*STNC/T**2*X-A3/R**2
      ALPF=2./R**2*A2/A0
      ALPG=-4.5*STNC/T**2*Y-A4/R**2
      ALPH=A0*12./(R*T)**2
      ALP(16)=ALPA+ALPB+ALPC*ALPD*ALPF+ALPF*ALPG+ALPH
      ALPA=54.*STNC/(R*T)**2*X
      ALPB=1./6.*ALPA/A0
      ALPC=2.*A2**2/A0-A3
      ALPD=54.*A2/A0*STNC/(R*T)**2*Y
      ALP(17)=-ALPA+ALPB*ALPC+ALPD
      ALPA=2.*Y*(A3-2.*A2**2/A0)+6.*A2*X
      ALP(18)=9.*STNC/(R**3*T**2)*(4.*Y+1./A0*ALPA)
      ALPA=X*(A3-2.*A2**2/A0)-2.*A2*Y
      ALP(19)=9.*STNC/(R**4*T**2)*(X+ALPA/A0)
      DO 95 JJ=1,19
      ALPHA(I,JJ)=ALP(JJ)
   95 CONTINUE
C     FIX THE TRIAL VALUE OF BUCKLE HALF-WAVE-LENGTH PARAMETER
      DO  42  KJK=1,JX
      WRITE(6,71)XL(KJK),RAT(J)
      LX=XL(KJK)/R
      Q(1)=LX**8
      Q(2)=LX**6
      Q(3)=LX**4
      Q(4)=LX**2
      Q(5)=1.
      Q(6)=LX**6
      Q(7)=LX**4
      Q(8)=LX**2
      Q(9)=1.
      Q(10)=-LX**6
      Q(11)=-LX**4
```

```
      Q(12)=-LX**2
      Q(13)=-1.
      Q(14)=-LX**4
      Q(15)=-LX**2
      Q(16)=LX**4
      Q(17)=LX**2
      Q(18)=LX**2
      Q(19)=-LX**2
C     SET THE ELEMENTS OF THE DETERMINANT TO BE ZERO INITIALLY
      DO  222  NN=1,KLK
      DO  222  NQ=1,KLK
      BBB(NN,NQ)=0.
 222  CONTINUE
C     FIX THE VALUE OF NQ
      DO  41  NQ=1,KLK
      RR=FLOAT(NQ-1)
      RN=RR/R
      P(1)=Q(1)
      P(2)=Q(2)*RN**2
      P(3)=Q(3)*RN**4
      P(4)=Q(4)*RN**6
      P(5)=Q(5)*RN**8
      P(6)=Q(6)*RN
      P(7)=Q(7)*RN**3
      P(8)=Q(8)*RN**5
      P(9)=Q(9)*RN**7
      P(10)=Q(10)
      P(11)=Q(11)*RN**2
      P(12)=Q(12)*RN**4
      P(13)=Q(13)*RN**6
      P(14)=Q(14)*RN
      P(15)=Q(15)*RN**3
      P(16)=Q(16)
      P(17)=Q(17)*RN**2
      P(18)=Q(18)*RN
      P(19)=Q(19)
C     CALCULATE THE VALUES OF COEFFICIENTS Q(1), Q(2),.......,Q(19) ETC.
     *FOR EACH ELEMENT
      DO  41  I=1,360
      ANGR=RR*ANGLE(I)
      XX=COS(ANGR)
      YY=SIN(ANGR)
      PQ(1)=P(1)*XX
      PQ(2)=P(2)*XX
      PQ(3)=P(3)*XX
      PQ(4)=P(4)*XX
      PQ(5)=P(5)*XX
      PQ(6)=P(6)*YY
      PQ(7)=P(7)*YY
      PQ(8)=P(8)*YY
      PQ(9)=P(9)*YY
      PQ(10)=P(10)*XX
      PQ(11)=P(11)*XX
      PQ(12)=P(12)*XX
      PQ(13)=P(13)*XX
      PQ(14)=P(14)*YY
      PQ(15)=P(15)*YY
```

```
      PQ(16)=P(16)*XX
      PQ(17)=P(17)*XX
      PQ(18)=P(18)*YY
      PQ(19)=P(19)*XX
C     CALCULATE THE VALUES OF PARAMETER BB FOR EACH ELEMENT
      BB=0.
      DO  97  JK=1,19
      C(JK)=ALPHA(I,JK)*PQ(JK)
      BB=BB+C(JK)
   97 CONTINUE
C     FIX THE VALUE OF NN
      DO  41  NN=1,KLK
C     COMPUTE THE VALUES OF THE ELEMENTS OF THE DETERMINANT
      QQ=FLOAT(NN-1)
      ANGQ=QQ*ANGLE(I)
      XYX=COS(ANGQ)*DELANG
      CB=BB*XYX
      BBB(NN,NQ)=BBB(NN,NQ)+CB
   41 CONTINUE
C     STORE THE ELEMENTS OF THE DETERMINANT IN THE FORM SPECIFIED BY THE
     *SUBROUTINE MINV WHICH IS AVAILABLE IN MCMASTER LIBRARY OF SUBROUTINES
      DO  39  NN=1,KLK
      DO  39  NQ=1,KLK
      IJK=NN+(NQ-1)*KLK
      B(IJK)=BBB(NN,NQ)
   39 CONTINUE
      WRITE(6,69)
      WRITE(6,72)((BBB(NN,NQ),NQ=1,KLK),NN=1,KLK)
C     CALL SUBROUTINE MINV TO COMPUTE THE VALUE OF THE DETERMINANT
      CALL MINV (B,KLK,D,L,M)
      WRITE(6,73)D
      DETT(J,KJK)=D
   42 CONTINUE
      WRITE(6,75)
      WRITE(6,77) E,SO,K,KLK
      WRITE(6,76)  STNC,YS
      WRITE(6,501)(RAT(J),J=1,JR)
      WRITE(6,601) ((XL(KJK),(DETT(J,KJK),J=1,JR)),KJK=1,JX)
      STOP
   49 FORMAT(3F10.0,I2)
   69 FORMAT(30X,*ELEMENTS   OF   DETERMINANT*//)
   53 FORMAT(12F5.0)
   52 FORMAT(8F10.0)
   51 FORMAT(F10.0,3I3)
   71 FORMAT(1H1,20X,*HALF   WAVE-LENGTH=*,F6.2,10X,*D/T  =*,F10.4//)
   73 FORMAT(30X,*DETERMINANT=*,E25.8//)
   72 FORMAT(8E15.5//)
   76 FORMAT(20X,*MAXIMUM   STRAIN =*,F10.6, 15X,*YS =*,F6.2//)
   75 FORMAT(1H1,30X,*COMPARISION*/////)
   77 FORMAT(10X,*E=*,F10.1,5X,*STRESS(0.7)=*,F10.3,5X,*INDEX K=*,I3,
     15X,*DETERMINANT  SIZE=*,I2//)
  501 FORMAT(16X,7F15.1//)
  601 FORMAT(F20.2,7F15.1//)
      END
      SUBROUTINE DELTA(ANGLE,B1,B2,B3,B4,B5)
      DIMENSION ANGLE(1),B1(1),B2(1),B3(1),B4(1),B5(1),AA2(91),AA4(91)
      COMMON NEL,K,SO,STNC
```

```
      NEL1=NEL/4
      NEL11=NEL1+1
      NEL2=NEL/2
      NEL22=NEL2+1
      READ(5,14) KJ
   14 FORMAT(2I)
C     ITERATE THE VALUE OF STRESS TO THE SPECIFIED DEGREE OF ACCURACY
     *FOR THE PREASSIGNED STRAIN ON EACH ELEMENT IN THE FIRST QUADRANT
     *OF THE CIRCUMFERENCE
      SR=0.
      DO 101  I=1,NEL1
      SN=STNC*SIN(ANGLE(I))
      DELSR=0.1
      KK=1
   15 CONTINUE
      SND=(1.+3./7.*(SR/SO)**(K-1))/E*SR
      ET=E/(1.+3./7.*FLOAT(K)*(SR/SO)**(K-1.))
      DELE=DELSR/ET
      IF((SN-SND).LE.(-1.E-9))GO TO 16
      IF((SN-SND).LE.DELE)GO TO 17
      SR=SR+0.6*DELSR
      GO TO 15
   16 CONTINUE
      SR=SR-0.6*DELSR
      GO TO 15
   17 CONTINUE
      DELSR=0.1*DELSR
      KK=KK+1
      IF(KK.LE.KJ)GO TO 15
      PK=FLOAT(K)
      PKP=3./7.*(SR/SO)**(K-1)*PK
      ET=E/(PKP+1.)
      ES=E/(PKP/PK+1.)
C     CALCULATE THE VALUE OF PLASTICITY COEFFICIENT
      B1(NEL1-I)=0.25+0.75*ET/ES
  101 CONTINUE
C     CALCULATE THE VALUES OF THE HIGHER DERIVATIVES
      AA2(1)=0.
      AA2(NEL11)=0.
      DO 91  I=2,NEL1
      AA2(I)=(B1(I)-B1(I-1))/DELANG
   91 CONTINUE
      DO 92  I=1,NEL1
      B2(I)=(AA2(I+1)+AA2(I))/2.
      B3(I)=(AA2(I+1)-AA2(I))/DELANG
   92 CONTINUE
      AA4(1)=0.
      AA4(NEL11)=0.
      DO 93  I=2,NEL1
      AA4(I)=(B3(I)-B3(I-1))/DELANG
   93 CONTINUE
      DO 94  I=1,NEL1
      B4(I)=(AA4(I+1)+AA4(I))/2.
      B5(I)=(AA4(I+1)-AA4(I))/DELANG
   94 CONTINUE
C     COMPUTE THE SET OF SIMILIAR DATA FOR THE REST THREE QUADRANTS OF
     *THE CIRCUMFERENCE USING THE PRINCIPLE OF SYMMETRY
```

```
      DO 103  I=NEL11,NEL2
      B1(I)=B1(NEL22-I)
      B2(I)=-B2(NEL22-I)
      B3(I)=B3(NEL22-I)
      B4(I)=-B4(NEL22-I)
      B5(I)=B5(NEL22-I)
 103  CONTINUE
      DO 104  I=NEL22,NEL
      B1(I)=B1(I-NEL2)
      B2(I)=B2(I-NEL2)
      B3(I)=B3(I-NEL2)
      B4(I)=B4(I-NEL2)
      B5(I)=B5(I-NEL2)
 104  CONTINUE
      RETURN
      END
'        6400 END OF RECORD
 29500.    37.75      42.15      17
0.011000      8  2  4
48.          50.
7.5  8.0  8.5  9.
 8
'           END OF FILE

                                CD TOT    0302
```